FOUR THEORIES OF THE MADDEN-JULIAN OSCILLATION

C. Zhang[1*], *Á.F. Adames*[2], *B. Khouider*[3], *B. Wang*[4], and *D. Yang*[5,6]

1. NOAA Pacific Marine Environmental Laboratory, Seattle, WA
2. University of Michigan, Ann Arbor, MI
3. University of Victoria, Victoria, BC
4. University of Hawaii, Honolulu, HI
5. University of California at Davis, Davis, CA
6. Lawrence Berkeley National Laboratory, Berkeley, CA

Key points:

1. A theory for the Madden-Julian Oscillation (MJO) must explain its most fundamental features of temporal-spatial scales and eastward propagation.
2. Four theories provide contrasting explanations for the MJO based on different assumptions and treatment of physical processes.
3. These MJO theories represent a general progress towards understanding the MJO and also the need to further advance such understanding.

This is the author manuscript accepted for publication and has undergone full peer review but has not been through the copyediting, typesetting, pagination and proofreading process, which may lead to differences between this version and the Version of Record. Please cite this article as doi: 10.1029/2019RG000685

* Corresponding Author: Chidong Zhang (Chiding.zhang@noaa.gov)

ABSTRACT

Studies of the Madden-Julian Oscillation (MJO) have progressed considerably during the past decades in observations, numerical modeling, and theoretical understanding. Many theoretical attempts have been made to identify the most essential processes responsible for the existence of the MJO. Criteria are proposed to separate a hypothesis from a theory (based on the first principles with quantitative and testable assumptions, able to predict quantitatively the fundamental scales and eastward propagation of the MJO). Four MJO theories are selected to be summarized and compared in this article: the skeleton theory, moisture-mode theory, gravity-wave theory, and trio-interaction theory of the MJO. These four MJO theories are distinct from each other in their key assumptions, parameterized processes, and particularly, selection mechanisms for the zonal spatial scale, time scale, and eastward propagation of the MJO. The comparison of the four theories and more recent development in MJO dynamical approaches lead to a realization that theoretical thinking of the MJO is diverse and understanding of MJO dynamics needs to be further advanced.

Plain Language Summary

The Madden-Julian Oscillation (MJO) is a tropical phenomenon that includes heavy rainfall and stiff wind over an area of roughly 1500 km in latitude and 4500 km in longitude. It starts over the Indian Ocean, moves eastward to the Pacific Ocean in about a month. As it moves eastward, it influences weather and climate phenomena in many parts of the world. Understanding the fundamental physics of the MJO forms the base for forecasting it and its global influences. This article reviews four theories of the MJO and compares their similarities and differences. Future studies needed to further our understanding of the MJO are recommended.

1. INTRODUCTION

The Madden-Julian Oscillation (MJO) is a planetary-scale phenomenon in the tropics characterized by its intraseasonal (30 – 90 days) timescale and eastward propagation (5 ms^{-1} on average) in precipitation and the associated atmospheric circulation

over the Indo-Pacific warm pool. The reason for its very existence has been puzzling since its first documentation by *Madden and Julian* [1971, 1972]. Many hypotheses have been proposed to explain the dynamics of the MJO [see summaries of *Zhang* 2005 and *Wang* 2012]. As will be discussed below, many of these ideas have failed to explain the most fundamental characteristics of the MJO. Others have evolved and have been merged to form modern theories that describe several fundamental aspects of the MJO.

The purpose of this article is to present and compare four current MJO theories. They are the skeleton theory [*Majda and Stechmann*, 2009], moisture-mode theory [*Adames and Kim*, 2016], gravity-wave theory [*Yang and Ingerso*ll, 2013], and trio-interaction theory [*Wang et al*., 2016]. The choice of the four MJO theories in this article was originally made at a workshop on the MJO [*Ling et al.*, 2017], at which the four MJO theories were jointly presented and discussed for the first time. This article was recommended by the workshop to assist the general research community to better appreciate and evaluate these theories. The four MJO theories compared in this article represent the diverse and distinct thinking of MJO dynamics up to date. The goal of this article is to help readers to appreciate such diverse and distinct theoretical thinking of the MJO. In this article, we do not judge which theory is correct or not. We leave that to the readers to decide. We want to help readers to understand to what extent the mechanisms proposed by these theories might be essential to the MJO and what the gaps are that need to be filled to advance our understanding of MJO dynamics.

The MJO has inspired research interests for both intellectual and practical reasons. The MJO is such a prominent phenomenon that it can be seen from raw data without statistical filtering [*Zhang* 2005]. Yet, its simulation by global numerical models has always been a challenge [*Hayashi & Golder*, 1986; *Lau & Lau*, 1986; *Slingo et al.*, 1996; *Sperber et al.*, 1997; *Zhang et al.*, 2006; *Kim et al.*, 2009; *Hung et al.*, 2013; *Jiang et al.*, 2015; *Ahn et al.*, 2017]. Because of its intraseasonal timescale and slow eastward propagation, the MJO serves as a major source of subseasonal predictability of the Earth System [*Waliser et al.*, 2003; *National Academies 2016*] with global impact on weather-climate [*Zhang* 2013]. Improved prediction of the MJO benefits weather prediction not just in the tropics, but in the extratropics as well [*Vitart & Molteni*, 2010]. However, there remains a large gap between current MJO prediction skill and its known predictability limit

[*Gottschalck et al.,* 2010; *Kim et al.,* 2014; *Neena et al.,* 2014; *Lee et al.,* 2015]. Understanding the key physical mechanisms that drive the MJO is the foundation for improving its prediction.

When documenting the MJO using dynamical and thermodynamical variables (zonal wind, pressure, temperature, and humidity), Madden and Julian immediately recognized the central role that atmospheric convection plays in it. The tandem eastward propagation of convection and the circulation depicted in the first MJO schematics by *Madden and Julian* [1972] firmly cemented the notion that the MJO is a convection-circulation coupled phenomenon. This concept is reinforced by the absence of an MJO mode as a dry wave solution to shallow-water equations on an equatorial β-plane [*Matsuno* 1966]. The biggest enigma of the MJO is its planetary and intraseasonal scales and its slow eastward propagation. Explaining its scale and propagation has been the primary target of most attempts to theoretically understand the MJO.

There have been many early studies that aimed to explain the key dynamical features of the MJO [see reviews by *Zhang* 2005; *Wang* 2012; *Wang et al.,* 2016]. These studies focused on certain aspects of the MJO, including some dynamical mechanisms. Even though they do not explain all dynamical essences of the MJO (its scale selection and eastward propagation), these efforts paved the road to the theories discussed here.

Chang [1977] made the first theoretical attempt of understanding the MJO. He addressed the issue of deep vertical mode that propagates much more slowly than what the *Matsuno* [1966] linear theory predicts. He demonstrated that effects of cumulus convection, in the form of dissipation, could slow down the propagation speed of a deep mode, but not enough to match the propagation speed of the MJO. Some studies aimed to explain the MJO as a dynamical disturbance radiating away from a stationary or low-frequency oscillatory forcing source [*Yamagata & Hayashi,* 1984; *Anderson & Stevens,* 1987]. They were unsuccessful because the disturbance propagated too fast and lacked the eastward moving vortex pair that is part of the observed MJO structure (see section 2). *Chao* [1987] considered the MJO as a moving Gill solution [*Gill* 1980] without explaining why MJO moves eastward. Explanations of the MJO as a response to stochastic forcing [*Salby & Garcia,* 1987; *Yu & Neelin,* 1994] did not provide a viable mechanism for the scale selection of the MJO. But the idea foreshadowed more sophisticated efforts of including

stochasticity in MJO theories (see section 4.3).

Attempts were made using the concept of wave-CISK [*Lindzen* 1974] to explain the MJO [*Lau & Peng*, 1987; *Chang & Lim*, 1988]. Even though these efforts gained substantial attention, they failed to explain the MJO's planetary scale without unrealistic assumptions on diabatic heating. To overcome the "instability catastrophe" [*Crum & Dunkerton*, 1992], namely, maximum growth rate occurs at the smallest scales, *Wang* [1988a] and *Wang and Chen* [1989] introduced a boundary layer (BL) convergence feedback mechanism to the wave-CISK model. They demonstrated how the BL convergence feedback can lead to a planetary scale selection. By integrating the mechanisms of convective interaction with dynamics, i.e., the wave-CISK and BL convergence feedback, *Wang and Rui* [1990] proposed a frictionally coupled Kelvin-Rossby wave theory. This theory has since been expanded to include moisture variability, forming a recent MJO theory (section 7).

Emanuel [1987] and *Neelin et al.*, [1987] independently suggested surface evaporation from the ocean as the main energy source to the MJO in a theory known as the wind-induced surface heat exchange (WISHE) or wind-evaporation feedback (WEF). This theory assumes mean surface easterlies in the region of main MJO activity, namely, the tropical Indian and western Pacific Oceans. This is in contrast to observations, which show that the mean surface winds are weak or westerly over this region [*Wang* 1988b]. Its predicted flux maximum leading (east of) MJO convection was proven incorrect by observations [*Zhang* 1996; *Lin & Johnson*, 1996; *Zhang & McPhaden*, 2000]. Even so, the possible role of surface evaporation in the MJO has been continuously explored [*Sobel et al.*, 2008; *Fuchs & Raymond*, 2017; *Khairotdinov & Emanuel*, 2018].

Hu and Randall [1994, 1995] proposed that interactions between cloud, radiation, and evaporation could give rise to intraseasonal oscillations at a fixed location. The role of radiation in this theory, which avoided addressing the issue of eastward propagation of the MJO, has been integrated as the main instability mechanism in a recent MJO theory (section 5).

Because of the central role of atmospheric convection in the MJO and the observed structural evolution of moisture through its life cycle [*Hendon & Liebmann*, 1990; *Jones & Weare*, 1996; *Lin & Johnson*, 1996; *Kemball-Cook & Weare*, 2001; *Myers & Waliser*,

2003; *Kiladis et al.*, 2005], the MJO has been perceived as a moisture mode. The concept of moisture mode implies that temporal variations in moisture are key to the MJO [*Raymond* 2001; *Fuchs & Raymond*, 2005; *Raymond & Fuchs*, 2007, 2009]. This perception has helped evolve the diagnostic metric of gross moist stability (GMS) [*Neelin & Held*, 1987; *Neelin & Yu*, 1994] into one known as normalized gross moist stability (NGMS) [*Raymond & Fuchs*, 2007; *Raymond et al*., 2009]. Based on the concepts of the moisture-mode MJO and NGMS, several attempts at theoretical treatment of the MJO were made [*Sobel et al*., 2001; *Fuchs & Raymond*, 2005, 2007; *Sugiyama,* 2009; *Sukhatme*, 2014]. These attempts laid the foundation of a recent MJO theory (section 5). The importance of moist dynamics has been central to two other MJO theories based on different dynamical frameworks (sections 4 and 7).

There are other theoretical studies on additional processes associated with the MJO. These include the effects of the mean state on the seasonality of the MJO [*Wang & Xie*, 1997], atmosphere-ocean coupling [*Wang & Xie*, 1998], and scale interactions [*Majda & Biello*, 2004; *Biello & Majda*, 2005; *Wang & Liu*, 2011; *Liu & Wang*, 2012, 2013]. These studies address more specific aspects of the MJO and are not discussed further in this review.

There are ideas and suggestions on the importance of other processes for the MJO. They include air-sea interaction [*Flatau et al.*, 1997; *Wang & Xie*, 1998], atmospheric energy discharge-recharge [*Blade & Hartmann*, 1993], and influences from extratropics [*Hsu et al.*, 1990; *Frederiksen*, 2002; *Ray et al.*, 2009]. For the reason explained in section 2, these ideas, however appealing, do not satisfy the criteria of an MJO theory.

In this article, we first propose a set of criteria that distinguish a theory from a hypothesis of the MJO (section 2). In this regard, we treat a theory as a mathematically formulated ideas, including assumptions. A theoretical model or framework is a set of equations used to quantify the ideas. An idea that cannot be expressed mathematically remains a hypothesis. In section 3, we describe the common mathematical framework (a set of simplified Navier–Stokes equations) for the four MJO theories reviewed here. Based on the common framework, the four MJO theories are described individually in sections 4 to 7. Each of these sections includes a brief history of the theory discussed, its essence, main assumptions, uniqueness, mathematical framework, other features, summary,

limitations and recommendations for further evaluation. These aspects of the theories are further compared directly to each other in section 8 and summarized in Tables 1 – 5. In section 9, we briefly introduce new theoretical studies on the MJO published during the writing of this article and recommend future studies to further our theoretical understanding of the MJO.

In sections 4 – 7, subsections 4 provide the most basic aspects of the mathematical formulation for these theories and subsections 5 briefly introduce other, often expanded features of these theories. Readers who are not interested in any mathematical details of the theories may skip these two subsections. Readers who wish to know the complete mathematical derivation of each theory and more details about their expansion are referred to the original papers cited in sections 4 - 7. A glossary is provided for technical terms used in this article that all readers may not be familiar with.

2. CRITERIA AND DESIRABLE FUNCTIONS OF MJO THEORIES

In this section, we lay the ground necessary to distinguish a theory from a hypothesis of the MJO, and specify what an MJO theory is expected to explain.

An MJO theory should satisfy the following criteria:

(A) Its framework must be established from the Navier–Stokes equations or their simplified versions.

(B) Its assumptions and approximations unique to the framework must be mathematically expressed. They should be testable against observations available currently or in the future.

(C) It must be able to predict or explain quantitatively the most fundamental scales of the MJO in time (intraseasonal) and space (planetary) and its eastward propagation.

This set of criteria distinguish theories from paradigms and hypotheses based purely on intuitions, observations or numerical simulations. There are many viable ideas about the mechanisms that drive the MJO. There are qualitative arguments without an explanation for the mechanism of scale selection of the MJO based on the first principles of atmospheric dynamics. These are hypotheses, not theories, despite whatever observational support they may have received. An example is the discharge-recharge paradigm [*Blade & Hartmann*, 1993]. Although this idea has received support from observations and numerical simulations, there has yet been a quantitative demonstration of how this process selects the

MJO scales in time and space and how this process would explain the slow eastward propagation of the MJO. Thus, it remains a hypothesis, not a theory of the MJO. However, the concept of discharge-recharge is implicitly included in three of the theories discussed here (sections 4, 5 and 7).

There is no consensus on whether the observed vertically tilted structure of the MJO is fundamental. There is agreement that the MJO has primarily a first baroclinic structure, with lower-level convergent zonal flow and upper-level divergent zonal flow near its convection center, as depicted by the first MJO schematic diagram by *Madden and Julian* [1972]. A westward tilt with height in thermodynamic and dynamic variables associated with the MJO has been repeatedly observed [*Sperber*, 2003; *Kiladis et al*., 2005; *Tian et al*., 2006; *Benedict & Randall*, 2007; *Houze et al.*, 2000; *Chen et al.*, 2016]. There is an argument that such a tilt is so robust in observations that it should be required for an MJO theory to explain. The counter-argument is that the tilt is not unique to the MJO and it is much weaker in the MJO than in other waves such as convectively-coupled Kelvin and inertia-gravity waves [*Kiladis et al. 2009, Inoue et al. 2020*], and thus can be neglected to first order.

It is undoubtedly desirable that an MJO theory is able to reproduce and explain these vertical structures and many other observed features of the MJO:

(a) Three-dimensional structure. There are pairs of low-level cyclonic (anticyclonic) vortices associated with the positive (negative) anomalies of MJO precipitation (reversed circulation at upper levels) [*Hendon & Salby*, 1994*; Kiladis et al*., 2005].

(b) Seasonal cycle. The MJO migrates in latitude and peaks in the summer hemisphere [*Salby & Hendon*, 1994; *Zhang & Dong*, 2004]. During boreal summer, the MJO propagates northeastward [*Wang & Rui*, 1990a]. This complication of the MJO propagation is likely related to the background state of the Asian summer monsoon.

(c) Irregularity. MJO events may occur in a group with one following another, known as successive MJO events [*Matthews*, 2000]. Based on a simple visual inspection, one would find that the number of MJO events in a boreal winter season (December – February) can be 0 – 3. The interval between two adjacent MJO events can be 30 – 160 days [*Zhang*, 2005].

(d) Multi-scale structure (e.g., embedded waves). Within the convection envelope of the

MJO, there is a rich spectrum of higher-frequency perturbations [*Nakazawa*, 1988; *Chen et al,* 1996; *Roundy*, 2008]. Some of these disturbances belong to the family of equatorial waves, others do not.

(e) Modulation by other phenomena (e.g., IOD, ENSO, QBO, extratropical perturbations). The number, strength, and longitudinal location of the MJO vary with lower-frequency climate variability [*Son et al*., 2017].

(f) Air-sea interaction. Through its strong surface wind, rainfall, and cloudiness, the MJO modulates the ocean mixed-layer structure and near surface current of the underneath ocean. Oceanic feedback to the MJO is subtle in observations, although its effects are evident in numerical simulation and prediction [*DeMott et al*., 2015]. It has been studied theoretically [*Wang & Xie*, 1998].

In addition, it would be of merit if an MJO theory helps explain and remedy the difficulty of reproduction of the MJO by numerical models. Currently, few global models produce statistical signatures of the MJO close to the observed [*Hung et al*., 2013; *Jiang et al.*, 2015; *Ahn et al.*, 2017]. Most others produce weak or no statistical MJO signals because they simulate much fewer MJO events than in observations [*Ling et al*., 2017]. This is an issue of both MJO initiation and propagation.

There are reasons for that these features discussed above are desirable but not considered as the most fundamental criteria for an MJO theory. The fundamental features of the MJO in criterion (C), namely, its planetary zonal scale, intraseasonal timescale, and eastward propagation, were identified by the original work of *Madden and Julian* [1972]. They serve as the simplest definition of the MJO. Even though there is a continuum between the MJO and other tropical disturbances, such as the Kelvin waves, without a clear boundary [*Roundy*, 2012; *Zhang & Ling*, 2017], these fundamental features are unique to the MJO, shared by no other tropical phenomena. Once these features are seen, you know you have an MJO event, nothing else. In contrast, other features of the MJO listed above are not unique to the MJO. For example, (a), (d), (e) and (f) can be found in many other tropical phenomena to different extents. It is arguable whether the Rossby-Kelvin couplet or the quadruple vortices should be considered as the fundamental horizontal structure of the MJO. Both are observed. But they are determined by the zonal distribution of diabatic

heating (monopole heating sources vs. dipole heating and cooling). Explaining all these interesting and important features of the MJO is hence desirable but not essential for an MJO theory.

3. COMMON FRAMEWORK OF MJO THEORIES

The first criterion we proposed in section 2 requires MJO theories to be based on the Navier–Stokes equations of fluid motions for the Earth's atmosphere. A reduced set of these equations for the free troposphere serves as a common framework for the four MJO theories reviewed here. On an equatorial beta-plane and in pressure coordinates, they read as follows

$$\frac{\partial u}{\partial t} - \beta y v = -\frac{\partial \phi}{\partial x} - \epsilon u \quad (1a)$$

$$\frac{\partial v}{\partial t} + \beta y u = -\frac{\partial \phi}{\partial y} - \epsilon v \quad (1b)$$

$$\alpha = -\frac{\partial \phi}{\partial p} \quad (1c)$$

$$\frac{\partial u}{\partial x} + \frac{\partial v}{\partial y} + \frac{\partial \omega}{\partial p} = 0 \quad (1d)$$

$$C_p \frac{\partial T}{\partial t} - \omega \left(C_P \frac{\partial T}{\partial p} - \alpha \right) = Q_1 \quad (1e)$$

$$\frac{Dq}{Dt} = -Q_2 \quad (1f)$$

where u, v, ω are zonal, meridional, and vertical wind components, respectively; ϕ is geopotential, T temperature, q specific humidity, ε the diffusivity coefficient, C_p the specific heat of air at constant pressure, L_v latent heat of evaporation; Q_1 is apparent heating due to phase change of water, radiation and vertical convergence of the eddy transport of sensible heat, and Q_2 measures the apparent moisture sink due to a combination of evaporation, condensation, deposition and sublimation [*Yanai et al*., 1973; *Johnson et al.*, 2015]; $\alpha = RT/p$ with R being the gas constant; ∂/∂t is the local time tendency and D/Dt the total or Lagrangian time derivative, which includes local time tendency and advection.

In this set of equations, common assumptions for all four MJO theories are:

- Linear damping in place of eddy dissipation of momentum (Eqs. 1a and b)
- Omission of horizontal momentum advection (Eqs. 1a and b)
- Hydrostatic balance (Eq. 1c)

- Boussinesq approximation (Eq. 1d)
- No air-sea interaction

The total, instead of local, time derivative is used only in the moisture equation because of the different treatments of moisture convergence in the four theories. Based on the first concept of the MJO [*Madden & Julian*, 1972], a first baroclinic vertical structure of the MJO is assumed, which is applied differently to the four theories. Under an assumption of separation of variables in a resting atmosphere, the hydrostatic equation (Eq. 1c), Boussinesq approximation (Eq. 1d), and thermodynamic equation (Eq. 1e) can be combined into one equation for the geopotential. This reduces the system (Eq. 1) to:

$$\frac{\partial u}{\partial t} - \beta y v = -\frac{\partial \phi}{\partial x} - \epsilon u \tag{2a}$$

$$\frac{\partial v}{\partial t} + \beta y u = -\frac{\partial \phi}{\partial y} - \epsilon v \tag{2b}$$

$$\frac{\partial \phi}{\partial t} + H\left(\frac{\partial u}{\partial x} + \frac{\partial v}{\partial y}\right) = Q_1 - \mu\phi \tag{2c}$$

$$\frac{Dq}{Dt} = -Q_2 \tag{2d}$$

where H is the equivalent depth, and μ a coefficient for thermal damping, commonly known as Newtonian cooling. This is the commonly known dry shallow-water system (Eqs. 2a – c) with a moisture equation (Eq. 2d). This system is the base for the four theories. However, (Eq. 2d) is not included in the gravity-wave theory (section 6).

In addition, a separate set of momentum equations describing motions in the planetary boundary layer:

$$\frac{\partial u_b}{\partial t} - \beta y v_b = -\frac{\partial \phi}{\partial x} - \varepsilon_b u_b \tag{3a}$$

$$\frac{\partial v_b}{\partial t} + \beta y u_b = -\frac{\partial \phi}{\partial y} - \varepsilon_b v_b \tag{3b}$$

are used only in the trio-interaction theory (section 7).

The four MJO theories differ mainly in their distinct assumptions that lead to different simplifications of Eqs. 1 and 2 and parameterization of their various terms. Specifically, they treat differently the time tendency of momentum (Eqs. 1a and b), temperature (Eq. 1e), and humidity (Eq. 1f); moisture convergence (Eq. 1f), diabatic heating (Eq. 1e), and moisture sources/sinks (Eq. 1f). For example, the three theories in sections 5-7 use diagnostic convection parameterizations, while the theory in section 4 uses

a prognostic equation for precipitation. These different treatments, their underlying assumptions, and their resulting parameterization and simplifications will be specified in the following four sections that describe the four MJO theories.

4. SKELETON AND MULTISCALE THEORY

The skeleton theory for the MJO was first introduced by *Majda and Stechmann* [2009]. It is based on the general idea that the MJO is essentially a planetary-scale envelope of synoptic- and meso-scale convective systems. This theory aims to explain the MJO using a minimal set of equations and variables, hence its name "skeleton". Discussions in this section include the original version of the skeleton theory (section 4.4) and its expansion with nonlinearity and stochastic processes (sections 4.5).

4.1 Essence

The essence produced by the skeleton theory includes:

(a) The MJO is neutrally stable. It initiates and sustains from the influence of conditional instability and instabilities of synoptic- and meso-scale convective systems;

(b) The slow eastward propagation of the MJO comes from positive lower-tropospheric moisture anomalies east of its convection center;

(c) The group velocity of the MJO is nearly zero;

(d) The dominant structure of the MJO consist of quadrupole vortices;

(e) Only the eastward propagating planetary-scale solution matches the observed structure;

(f) The stochastic version is able to self-select and excite the MJO mode, and

(g) Both nonlinearity and stochastic noise can give rise to MJO irregularity.

4.2 Assumptions

Assumptions made in the skeleton theory are:

(a) The MJO energy supply is from planetary-scale organization of synoptic- and meso-scale convective systems through a new concept of wave activity function;

(b) The wave activity function grows exponentially with lower-tropospheric moisture;

(c) The linear damping terms in the momentum equations are negligible;

(d) Horizontal advection in the moisture equation is negligible;

(e) Vertical advection in the moisture equation is retained only with a background moisture gradient;
(f) The tropical background state is in a radiative-convective equilibrium;
(g) Meridional profiles of convective heating and the wave activity are symmetric about the equator, and
(h) The equatorial long-wave approximation is applied.

4.3 Uniqueness

The wave activity is the unique aspect of the skeleton theory. It represents the average of synoptic- and meso-scale convective energy that projects into the low-frequency planetary scales. Implied by this wave activity is interaction between the MJO and its embedded synoptic- and meso-scale systems. The wave activity is introduced in this theory as a parameterization scheme. Another unique feature of the skeleton theory is that the MJO is neutrally stable.

In the original skeleton theory, there is no specific selecting mechanism for the MJO. Its neutral solutions propagate both eastward and westward at all spatial scales. But, as illustrated in Fig. 1, the wave activity envelope can force a circulation of rising and sinking air at the planetary and intraseasonal scales. It is on these scales the eastward propagating solution matches the observed MJO structure. Specific selecting mechanisms for the MJO (e.g., damping on small scales) emerge when other factors are included (e.g., stochasticity, section 4.5.2).

4.4 Mathematical Framework and Solutions

The MJO skeleton equations are derived from the simplified primitive Eq. 1. In addition to the simplified Eqs. 1a – d under assumptions (a - d) , a new concept of wave activity is introduced to represent (parameterize) the heat source in Eq. 2c $Q_1 = \bar{H}(\bar{a} + a) - S_\theta$ and the moisture sink in Eq. 2d as $Q_2 = \bar{H}(\bar{a} + a) - S_q$, where a is the anomalous amplitude of the wave activity, $\bar{a}$ its mean, $\bar{H}$ the unit of diabatic heating, and S_θ and S_q external sources of temperature and moisture, such as radiative heating and surface evaporation, respectively.

In the moisture equation (Eq. 1f), horizontal advection is ignored, and the vertical advection is retained with a background moisture gradient. When the evaporation and radiation forcing terms balance each other, i.e., $S_\theta = S_q$, moist static energy is approximately conserved.

The wave activity is constructed to be tied directly to lower-tropospheric moisture and it obeys the law of mass action in the sense that its tendency is proportional to itself compounded by lower-tropospheric moisture:

$$\frac{\partial a}{\partial t} = \Gamma q(\bar{a} + a) \tag{4}$$

where Γ is a dimensional parameter that sets the strength of the moisture and wave activity interaction. The wave activity amplitude *a* continues to grow as long as lower-atmospheric moisture anomalies are positive and decays accordingly when they are negative. This equation was constructed based on physical reasoning motivated by observed lower-tropospheric moistening proceeding MJO heating anomalies [*Myers & Waliser*, 2003; *Kikuchi & Takayabu*, 2004; *Kiladis et al.*, 2005]. It can be viewed as a parameterization scheme.

With assumption (e), the moisture and wave activity equations form a harmonic oscillating system where q and a are in quadrature. Γ, $\bar{H}$, and the background moisture gradient are the sole parameters of the systems. The last two are more or less set by the observed climatology while Γ remains ad hoc. A theoretical justification for the value of Γ used is provided in *Stechmann et al*. [2013].

All simplified primitive equations (Eq. 1) plus Eq. 4 are used in the skeleton theory. Solutions to this set of equations are obtained through projections in the vertical onto the first baroclinic mode and in the meridional direction onto the equatorially trapped Kelvin and first Rossby wave modes. The restriction to these two low-order equatorial wave modes is based on assumption (g). A simple four-equation system can then be derived to yield a wave solution with the key features outlined above [*Majda & Stechmann*, 2009, 2011]:

$$K_t + K_x = -\frac{1}{\sqrt{2}}\bar{H}A \tag{5a}$$

$$R_t - \frac{1}{3}R_x = -\frac{2\sqrt{2}}{3}\bar{H}A \tag{5b}$$

$$Q_t + \frac{1}{\sqrt{2}}\bar{Q}R_x = (-1 + \frac{1}{6}\bar{Q})(\bar{H}A) \tag{5c}$$

$$A_t = \Gamma Q(\bar{a} + A) \tag{5d}$$

where *K, R, Q, A* are amplitudes of the Kelvin mode, and first Rossby mode, moisture, and wave activity, respectively. By setting $\bar{H}\bar{a} = \bar{R}$ = 1 K day^{-1} as a radiative convective equilibrium climatology (assumption f), Eq. 5 becomes a two-parameter system, in terms of Γ and $\bar{Q}$. The linear version of this system (without the term ΓQA in the tendency equation of A_t) has four wave mode solutions, two low-frequency modes and two high-frequency modes with each pair having one eastward and one westward propagating wave. The dispersion relation for the two low-frequency modes is shown in Figs. 2a and e where both frequency and phase speed are plotted against the wavenumber for the typical parameter values $\bar{Q}$ = 0.9; Γ = 1.66, in nondimensional units, corresponding to 1.19 g kg^{-1} km^{-1} and 0.3 K day^{-1}, respectively. As it can be seen from Fig. 2, the dispersion relation of the eastward mode runs almost parallel to the wavenumber axis, suggesting a nearly zero group velocity as anticipated above. The small group velocity changes sign from positive values at small wavenumbers (1 and 2) to negative values at high wavenumbers ($\geq$ 3). More importantly, the corresponding phase speed crosses 5 m s^{-1} near wavenumber 2.

The westward branch corresponds to frequencies that are smaller than intraseasonal ones for zonal wavenumbers 1 and 2 and monotonically decreasing with increasing wavenumbers. The structure of the eastward low-frequency mode is shown in Figs. 2b and c while that of the westward mode is reported in Figs. 2f and g. The eastward mode has an interesting structure in winds and pressure presenting a quadrupole vortex straddling the equator. They are the first baroclinic mode components and as such they represent the lower-tropospheric circulation which clearly present two anti-cyclones followed by two cyclones with the wave activity peaking at the equator in phase with zonal convergence. Positive lower-tropospheric moisture anomalies on the other hand are shown to lead the convective activity. Together with the particular characteristic of its dispersion relation, the eastward low-frequency mode as presented in Figs. 2b and c, replicates the two features

listed above as a skeleton for the MJO, i.e, most fundamental physical features of the MJO that can be captured by a simplest theory. As we will see below, by adding other dynamical processes to this theory [*Majda and Stechmann*, 2011], such as nonlinear dynamics, stochasticity, and refined vertical structure, additional features among those listed in section 2, such as intermittency, meridional asymmetry, vertical tilt, etc., can be captured by this multi-scale MJO theory [*Majda & Stechamann*, 2011; *Thual et al*., 2014; *Thual et al*., 2015;*Thual & Majda*, 2015; *Thual & Majda*, 2016]. *Majda and Stechmann* [2009] pointed out that while the theory presented here is called the MJO skeleton, the muscle for the MJO body comes from upscale (thermal and momentum) eddy fluxes due to synoptic-scale waves [*Majda & Biello*, 2004; *Biello & Majda*, 2005].

The structure of the westward mode resembles that of the usual symmetric equatorial Rossby waves somewhat mimicking the features of the MJO mode but the major exception is that the equatorial flow is weaker than the off-equatorial gyres. Consistently, the bar diagrams in Fig. 2 show that while the MJO mode projects significantly onto the Rossby-Kelvin wave structures, the westward wave has a relatively small Kelvin contribution. Importantly, while the MJO mode has contributions from both Rossby and Kelvin waves, it is not the same as the classical Matsuno-Gill model that demonstrates the Kelvin wave flow east of the convection center and Rossby gyres only to the west. Here, the Rossby and Kelvin contributions are equally mixed throughout the wave cycle. Both waves have the same significant moisture and wave activity contribution justifying the terminology of moisture modes or rather moisture-coupled modes as suggested in section 2. As reported in *Majda and Stechmann* [2009, 2011], contributions from Q and A to the faster modes (not shown in Fig. 2) are negligible. More importantly as can be seen on the bar diagrams of Fig. 2, the contribution from the Kelvin wave to the MJO mode decreases significantly with the wavenumber. This is an indication that only the long waves (k=1, 2, 3) have the desired Kelvin-Rossby waves mixture (desired feature (a) in Section 2) for an MJO solution.

We now return to the dispersion relation in Fig. 2 and insist on the fact that the corresponding eigenvalues are real values and as such the associated modes, and the MJO skeleton in particular, are neutrally stable. This is analogous to the equatorially trapped wave solutions of the dry equatorial shallow-water equations first described in *Matsuno*

[1966] and believed to be the bases of convectively coupled equatorial waves [*Wheeler & Kiladis*, 1999]. In fact, *Majda and Stechmann* [2011] and *Thual et al*. [2014] show that the system of the skeleton theory remains hyperbolic and conserves a form of total energy, as long as $\bar{Q} < 1$. However, for $\bar{Q} > 1$, the low-frequency "MJO mode" becomes unstable because of too much mean state moisture. But it presents many unphysical features such as no apparent scale selection as the growth rate does not seem to decrease with increasing wavenumbers; It has a too slow propagation speed not exceeding 2 ms^{-1}, and it has a horizontal structure with lower-tropospheric moisture and wave activity in phase along the equator [Samuel Stechmann, personal communication]. These problems resemble some of the pathologies often seen in so many GCMs that are unable to reproduce MJO statistics. In fact, this can be easily corroborated from an approximate formulation of the low-frequency mode dispersion relation, $\omega \approx \sqrt{\Gamma \bar{R}\,(1-\bar{Q}\,)}$ [*Majda & Stechmann*, 2009, 2011]. For $\bar{Q} > 1$, this expression becomes complex and its real part becomes approximately zero, yielding a slow phase speed. Thus, to fully satisfy the criteria outlined in section 2, this theory predicts a moisture coupled MJO mode, which is neutral and is initiated and sustained by the natural instabilities and fluctuations of sub-planetary scale convective systems [*Majda & Stechmann*, 2009, 2011]. To mimic such sub-scale instability or rather variability, a stochastic version of this theory is introduced and studied, which is discussed in section 4.5.2.

4.5 Other Features

4.5.1 Nonlinear effects

In *Majda and Stechmann* [2011], Eq. 2 are solved numerically as an initial value problem for both cases when the forcing terms S_θ and S_q are uniform (in time and in the zonal direction) and when they are set to mimic the Indian Ocean/western Pacific warm pool. Here we summarize briefly the results and provide some of the most salient features relevant to the dynamics of the MJO.

First, in the case of a uniform forcing, when the initial condition is taken to be simply the wavenumber 2 MJO mode obtained from linear analysis, the nonlinear simulation consists of two MJO waves perpetually propagating eastward and circling the globe. Their amplitudes undulate and go through an oscillatory cycle of amplification

followed by decaying phases, all of which describe a wave envelope very slowly moving westward, i.e, displaying a negative but weak group velocity, consistent with the peculiar dispersion relation predicted by linear theory (Fig. 3a). Interestingly, when the initial condition consists of a combination of wavenumber 1 and wavenumber 2 MJO linear modes, the result is somewhat similar but the group velocity switches drastically and becomes positive (Fig. 3b).

Beside the changing group velocity, more interesting behavior is seen when the skeleton theory simulations are made under a nonuniform forcing, S_θ and S_q, mimicking the Indian Ocean warm pool, consisting of a sinusoidal profile peaking at the center of the 40000 km-wide model domain. A long time series obtained in this case with a wavenumber 2 MJO mode initial condition is presented in a time-longitude diagram (Fig. 4a). After 240 days or so the core of the variability shifts smoothly towards the center of the warm pool and consists of various periods of active and inactive MJO periods dominating the warm pool region, between 10000 km and 30000 km. A mixture of positive and negative slow group velocity episodes is apparent. Also, on the left of the domain near 11000 km, and between 2400 and 3600 days, a sequence of standing oscillations is evident and precedes the propagating MJO events. These MJO events sometimes reach the eastern edge of the warm pool, other times they disappear near the center and reappear again, consistent with the aquaplanet simulations of *Ajayamohan et al*. [2013]. In a sense, this mimics the complex behavior of MJO events in nature as it interacts with the Indo-Pacific Maritime Continent, although here, no land or diurnal cycle effects are present. However, one can think of the Maritime Continent as a region of increased forcing from a warmer ocean. The standing oscillations near 11000 km are perhaps not easily visible but *Majda and Stechmann* [2011] did a systematic projection of the nonlinear solution in Fig. 4 onto the eastward and westward low-frequency linear modes, i.e, the MJO and moist Rossby wave, and found that they coexist the most in this region and appear to have the same strength so that the net effect is a standing signal.

In Fig. 4b and c, the Kelvin and Rossby mode components in Eq. 5 are plotted separately in order to assess how much the MJO wave (which dominates the nonlinear solution) projects onto each wave mode. This needs to be viewed in the context of the Matsuno-Gill response to a moving heat source which usually shows a Kelvin wave

response east of the heating and a Rossby wave response to the west. Here, instead, the (moist) Kelvin and Rossby wave components are equally dominant everywhere inside the warm pool region. High-frequency dry Kelvin and Rossby waves, although weak, dominate the cold pool region of the domain, where they are dry because Q and A are confined to the warm pool region [*Majda and Stechmann*, 2011]. Typically, dry Kelvin waves are ejected at the end of each MJO event and their termination coincides with the initiation of the succeeding MJO event, as they circle the periodic domain. This is consistent with some hypothesized role of circumnavigating Kelvin waves in the initiation of successive MJO events [*Matthews et al*., 1999; *Ajayamohan et al*., 2013; *Powell & Houze*, 2015].

4.5.2 Stochastic skeleton theory

The MJO skeleton theory presented here is neutrally stable and its instability is assumed to come from sub-planetary scale convective signals which collectively project onto the planetary scale envelope represented by the convective wave activity a. In order to mimic such sub-planetary scale variability and its upscale effect on the MJO dynamics, *Thual et al*. [2014] introduced a stochastic theory for the wave activity dynamics into the MJO skeleton theory. Stochastic models have been long advocated as effective tools to represent variability at small, unresolved scales in climate and weather forecasting models [*Majda et al.*, 2008; *Palmer*, 2012; *Khouider et al*., 2010]. Specifically, they replaced the dynamical equation for a in Eq. 1 by a stochastic birth and death process allowing the wave activity a to either increase by a fixed increment ΔA or decrease by the same amount, within a random time period τ, according to some intuitive probability laws compatible with the original equation.

While the details of constructing the birth-death process for the Skeleton MJO theory can be found in *Thual et al*. [2014], we note that the birth and death rates of the stochastic wave activity follow the same laws of mass action used in the deterministic model of increasing and decreasing proportionally to the product of a and q, according to whether q is positive or negative, respectively. Moreover, the birth rate involves a Kronecker delta function, δ_a, which can be regarded as a convection or instability trigger at sub-planetary scales and is nonzero only when there is convective activity. This is

different from the deterministic version which is neutrally stable. Except for the "stochastizing" of the wave activity dynamics, the rest of the model equations remain the same as in Eq. 5 together with the energy conservation properties.

As in *Majda and Stechmann* [2011], *Thual et al*. [2014] conducted numerical simulations for the stochastic skeleton theory using both a uniform background and a warm-pool forcing but with arbitrary initial conditions. Examples of the results are shown in Figs. 5 and 6. The time-longitude diagrams of the MJO mode (Fig. 5) are obtained by projecting the simulated solution onto the eastward low-frequency mode from linear theory with and without the warm pool. They are almost identical except for the fact that in the warm pool case MJO signals are somewhat confined to the center of the domain. They both display a highly intermittent behavior with active periods characterized by a few successive MJO events followed by relatively quiet periods where the MJO variability is very weak or rather inexistent. During the active periods, MJO events form one after another in the form of packets somewhat similar to the trains of successive MJOs seen during the field campaign of TOGA COARE [*Kikuchi & Takayabu*, 2004] and CINDY/DYNAMO [*Yoneyama et al.*, 2013]. During the active periods, the MJO wave train has sometimes a positive group velocity and sometimes a negative group velocity, as in the nonlinear simulations (section 4.5.1). Sometimes the successive events amplify at the same location with no apparent energy propagation. This behavior is consistent with the peculiar dispersion relation which has a small group velocity that changes its sign.

The spectrum power for the simulation with a warm pool forcing (Fig. 6) exhibits peaks at four locations corresponding to the four linear modes discussed above, each of which showing a stronger peak for one or more variables. The most striking feature comes from the fact that except for θ, the low-frequency power is dominated by the MJO peak. While the main reason for this behavior is yet to be elucidated, this is in contrast to many GCMs that suffer from producing too strong power corresponding to westward low-frequency Rossby waves. Despite that the moist Rossby branch in this skeleton theory has much slower phase speeds, this behavior is qualitatively consistent with observations. The reason for the overall dominating eastward power might be related to the fact that the MJO mode has a significant Kelvin wave contribution (variable K in Eq. 5) while the moist Rossby mode is dominated by the R variable as illustrated by the bar diagrams in Fig. 2.

Along the same line, the realism of the active and inactive MJO periods lasting up to a few years suggests stochastic MJO initiation. Once in an inactive phase, the wave activity gets randomly amplified, as a rare event, and in turn it triggers moisture convergence which then further amplifies the wave activity by increasing the birth rate λ and results in MJO initiation.

4.5.3 Other physical properties

Since its conception, the skeleton MJO theory has been extensively studied and refined to include other observed features of the MJO. Here we summarize a few of these features and refer interested readers to the original papers listed here for details. *Thual et al.* [2015] added seasonal cycle variations to the background warm pool forcing allowing the warm pool to migrate north-south, mimicking the four seasons, and generate both equatorial and off-equatorial forcing for the MJO skeleton theory. This results in a response including a menagerie of equatorially symmetric MJOs with a full quadruple vortex structure, asymmetric MJOs with half the quadruple structure, and some MJO-like structure even tilted north-westward, somewhat reminiscent to boreal summer MJOs and northward monsoon intraseasonal oscillations.

Stachnik et al. [2015a] used an MJO index similar to the RMM index [*Wheeler & Hendon,* 2004] to analyze the stochastic skeleton theory output and provided a statistical assessment of this theory in comparison to observations. Using both univariate and multivariate EOFs, they quantified the number of primary, successive, circumnavigating, and terminating MJOs [*Matthews*, 2008; *Stachnik et al*., 2015b]. They found that the skeleton theory statistics compare reasonably well to observations. When the skeleton theory is forced by observed sea surface temperature (SST), *Ogrosky and Stechmann* [2015] found that over the observation period (1979-2012) the skeleton theory produced between 90 and 100 primary MJOs, between 300 and 350 successive MJOs, about 20 circumnavigating events, and 90-100 terminating events, while in the observations these numbers are 154, 330, 15, and 154, respectively. The skeleton theory seems to underestimate the number of primary and terminal events and somewhat overestimate the number of circumnavigating events. However, this remains impressive given the simplicity of the theory and the fact that these MJO categories may be sensitive to, for example,

extratropical processes, the diurnal cycle, and topography which are all neglected in the skeleton theory.

A refined vertical structure for the MJO skeleton is provided in *Thual and Majda* [2015, 2016]. Following the multicloud paradigm [*Khouider & Mjada*, 2006], they introduced three convective/wave activity functions instead of one, namely, for congestus, deep, and stratiform clouds. These functions solve a set of three differential equations allowing a progressive transition from congestus to deep to stratiform clouds. In return, congestus clouds warm the lower troposphere, deep clouds warm the entire troposphere, and stratiform clouds warm the upper troposphere. The governing equations are projected into the first and second baroclinic modes; the first being excited by deep convection while the second mode is excited by both the congestus and stratiform heating profiles, of opposite signs. Moreover, the theory is extended by a midlevel moisture anomaly, which is slaved to the congestus and stratiform wave activities by responding positively to the former and negatively to the latter.

Linear theory shows that while the extended model preserves the main modes of low frequency variability, namely the MJO and moist Rossby waves and the two (dry) high frequency modes, it also produces two extra low-frequency modes. They are much slower than the former ones, one moving westward and one moving eastward. However, the main gain here is that the MJO mode exhibits a vertical structure with a westward vertical tilt in zonal wind, moisture, temperature, and diabatic heating, as observed in nature [*Kiladis et al*., 2005]. Similarly to the coarser skeleton theory, a stochastic version for the multi-cloud skeleton theory is proposed and analyzed in *Thual and Majda* [2016]. Nonlinear simulations with the refined skeleton theory produce similar time-space spectra with a dominating MJO-like signal on intraseasonal and planetary scales with the same level of intermittency and realism.

4.6 Summary

The key motivating idea for the skeleton theory is that, in an appropriate parameter regime, lower-tropospheric moisture and convective activity are set to oscillate on the intraseasonal scale, against each other as in a predator-and-prey model. This is in contrast to the moisture-mode theory (section 5) where precipitation and moisture are in phase. The

skeleton theory yields a solution that includes most observed salient physical and morphological features of the MJO, such as its quadruple vortices and slow eastward phase speed. It also predicts a neutrally stable MJO mode. In a zonally uniform background state, the nearly zero group velocity of the MJO is consistent with the trio-interaction theory (section 7) but contrasts to the moisture-mode theory (section 5).

The idea of the skeleton theory has been extended to include nonlinearity and stochasticity. The skeleton theory has been validated against observation with a varying degree of realism, including its capability to reproduce the observed physical structure of the MJO as well as its irregularity, lifetime, and amplitude [*Stachnik et al*., 2015a; *Ogrosky & Stechmann*, 2015; *Thual & Majda*, 2015]. The skeleton theory has been applied to study interactions between the MJO and El Nino (Thual et al., 2018).

4.7 Limitations

The unique introduction of the concept of wave activity to the skeleton theory leads to its main limitation. While the equation for the wave activity (Eq. 4) is based on both principle (the law of mass action) and physical intuition motivated by the observed lower-tropospheric moisture build-up prior to MJO convective anomalies, it is not immediately clear what observed variables can be used to quantitatively validate the formulations of its tendency and its equal contributions to both Q1 and Q2. Another limitation of the original skeleton theory is the lack of a specific scale selection mechanism beside matching the horizontal structure of the eastward propagating, planetary-scale neutral solution to the observed MJO structure. This limitation is eliminated when factors that help damp small scales (e.g., stochasticity) are included.

4.8 Recommendations for Further Evaluation

Parameterization of convective amplitude in the form of the wave activity function, which is an important aspect of the theory, needs further exploration and evaluation against observations. While it is equally hard to justify an MJO theory based solely on large-scale dynamics as in the moisture-mode theory in section 5 and trio-interaction theory in section 7, it will be interesting to test and evaluate whether the energetics of the MJO is mainly an upscale build-up or whether it is a combination of both large- and small-scale dynamics

(e.g., in the gravity-wave theory in section 6). Also, observations are needed to quantify the timescale of upscale energy build-up as assumed in the skeleton model parameters. A closer connection of these model components to observations will allow in part a more proper justification for the choice of parameters such as the heating proportionality factor Γ. The spectral peak in wavenumber one produced by this theory is more evident in the wind than the heating field. It is desirable to examine what physical processes could enhance the planetary scale spectral power of precipitation in this theory.

5. MOISTURE-MODE THEORY

In this section we summarize the fundamental principles behind the "moisture-mode" theory of the MJO [*Raymond*, 2001]. Our primary focus will be on the theoretical treatment given by *Sobel and Maloney* [2012, 2013] and *Adames and Kim* [2016]. This moisture-mode treatment makes several assumptions and approximations, but has the advantage of understanding the processes that lead to the evolution of moisture within a simplified theory. Two other MJO theories by *Fuchs and Raymond* [2005, 2017] and *Khairoutdinov and Emanuel* [2018] are related to the moisture-mode concept and will be discussed in section 5.5.

5.1 Essence

The essence of this theory includes:

(a) The intraseasonal precipitation anomalies arise mainly as a result of feedbacks between water vapor above the boundary layer (hereafter referred to as free troposphere) and convection;

(b) The eastward propagation of the MJO is mainly maintained by large-scale horizontal and vertical moisture advection, which moistens the free troposphere to the east of the MJO convection center and dries to the west.

(c) The longwave cloud-radiation feedback plays a key role in generating instability for the growth and sustenance of the intraseasonal precipitation anomalies, and

(d) The spatial-scale selection is through the wide-spread nature of the cloud-radiative feedback.

5.2 Assumptions

Major assumptions and approximations in this theory are:

(a) The only prognostic equation is for moisture;

(b) Precipitation is linearly proportional to the column moisture anomalies;

(c) The anomalous wind field is in steady-state balance with the apparent heating as predicted by the Matsuno-Gill model [*Matsuno*, 1966; *Gill*, 1980] and the vertical wind is in balance with the apparent heating according to the weak temperature gradient (WTG) approximation [*Sobel et al.*, 2001];

(d) The dissipation term for the meridional wind is zero while dissipation coefficients for zonal wind and geopotential are the same;

(e) WISHE is due to the modulation of the surface wind field by the MJO winds;

(f) The mean state includes moisture that is peaked at the equator, hence with a meridional gradient on both hemispheres, and climatological-mean easterlies;

(g) Drying and moistening due to meridional moisture advection by synoptic-scale eddies are modulated by the MJO zonal wind anomalies, and

(h) Large-scale shallow circulations caused by boundary-layer frictional moisture convergence are, to first order, related to the free tropospheric zonal wind anomalies.

These assumptions and simplifications, along with other approximations to be explained below, lead to a set of linear equations that form the mathematical base of the moisture-mode theory.

5.3 Uniqueness

This moisture-mode theory is the only one of the four discussed in this article in which the only prognostic equation is for moisture and the cloud-radiative feedback is scale-dependent. It also is the only theory discussed here that suggests that cloud-radiative interactions are essential to the MJO. It is the only theory that produces a non-negligible westward group velocity of the MJO.

In this theory, longwave radiative heating of upper-level clouds induces upward motions that enhance moisture import to support convection. This leads to instability of the MJO, as illustrated in Fig. 7. This instability occurs at large-scale because of the wide-spread nature of stratiform clouds, as illustrated in Fig. 8. The MJO moves eastward

because horizonal advection of moisture results in an increase in column moisture (positive moisture tendency) east of the enhanced convection but a decrease in column moisture west of it (Fig. 9). A combination of dry static stability, the strength of moisture advection, and convective moisture adjustment timescale determines the propagation speed.

5.4 Mathematical Framework and Solutions

This theory is derived from moist wave solutions to a set of linear equations simplified from the common framework in Eq. 2, where all variables are treated as intraseasonal anomalies.

5.4.1 Moisture, precipitation and the MJO

Assumption (b) is based on observations that precipitation is highly sensitive to free-tropospheric relative humidity [*Brown & Zhang* 1997; *Raymond*, 2000; *Bretherton et al*., 2004; *Holloway & Neelin*, 2009; *Muller et al*., 2009]. When the atmosphere is moist, parcels become less diluted with dry air, which leads to stronger and more organized convection [*Raymond*, 2000; *Masunaga*, 2012; *Ahmed & Schumacher*, 2015; *Ahmed & Neelin*, 2018]. Figure 10 shows precipitation P_r as a function of column integrated relative humidity, the ratio between column water vapor and column saturation water vapor ($RH = \langle q \rangle / \langle q_s \rangle$, where angle brackets correspond to mass-weighted integration from 1000 to 100 hPa) for a region centered in the eastern Indian Ocean (95°E, 0°N). While there is a substantial amount of scattering, P_r increases exponentially with increasing RH. There is no formulation that describes this relation based on physical principles, but an empirical relation captures this exponential curve [*Bretherton et al.*, 2004]:

$$P_r = P_0 \exp(aRH) \tag{6}$$

where P_0 and a are best fit coefficients. There is a clear separation between active MJO periods (blue dots) that are characterized by high *RH* and increased rainfall, and suppressed periods (red dots) that are characterized by low *RH* and little to no rainfall. This suggests that the feedback between moisture and precipitation is central to the MJO. This is the backbone of the "moisture-mode" framework. It is noteworthy that substantial scatter exists in Fig 10. This scatter is due to other processes, such as convective available potential

788 energy (CAPE) and convective inhibition (CIN), that modulate rainfall. While a more
789 complete treatment of precipitation should include these fluctuations, some studies have
790 indicated that CAPE and CIN predominantly affect convective coupling at higher
791 frequencies than those of the MJO [*Raymond and Fuchs 2007*].

792 Linearizing Eq. 6 with respect to a slowly-varying mean state yields

$$P_r' = \frac{\langle q' \rangle}{\tau_c}, \qquad \tau_c = \frac{\langle q_s \rangle}{a\overline{P_r}} \tag{7}$$

793 where P' represents intraseasonal anomalies in precipitation, $\langle q' \rangle$ intraseasonal anomalies
794 in column moisture, and τ_c is the convective moisture adjustment timescale, the rate at
795 which the precipitation anomalies relax the column moisture anomalies back to its
796 climatological value [*Betts*, 1986; *Betts & Miller*, 1986]. Equation 7 describes a direct and
797 proportional connection between intraseasonal anomalies in precipitation and column
798 moisture. When P' is estimated via Eq. 7, it adequately captures the spatial structure and
799 amplitude of the precipitation anomalies over the ocean observed by TRMM-3B42
800 [*Adames*, 2017].

801 The equatorial tropics are characterized by a weak planetary vorticity, which leads
802 to a large Rossby radius of deformation. Because of this large radius, gravity waves
803 disperse the temperature anomalies generated by deep convection over long distances,
804 largely homogenizing the horizontal distribution of temperature in the process. This
805 adjustment process causes virtual temperature tendencies over the tropics to be small,
806 which is the justification of the WTG approximation [*Charney*, 1963; *Sobel & Bretherton*,
807 2000; *Sobel et al*., 2001; Yang & Seidel, 2020]. *Wolding et al.* [2016] found that this
808 approximation is a reasonable one over the MJO spatial and temporal scales. Thus, Eq. 1e
809 becomes a diagnostic equation for vertical velocity $(\omega \partial_p s)' = Q_1'$, where s is the dry static
810 energy. In the shallow water equations (section 3) this is expressed as $HD' = Q_1'$, where
811 $D'$is the horizontal divergence. Based on the WTG approximation, we can diagnose the
812 contributions of radiative and convective heating to the moisture tendency [*Chikira*, 2014].
813 Vertically integrating and using Eq. 6 yields a prognostic equation for the intraseasonal
814 precipitation anomalies

$$\frac{\partial P_r{}'}{\partial t} = \frac{1}{\tau_c}\left(-\langle \mathbf{V} \cdot \nabla q \rangle' + \langle \alpha \frac{Q_R'}{L_v} \rangle - \langle (1-\alpha) \frac{Q_c'}{L_v} \rangle + E' \right) \quad (8)$$

where the terms in the right hand-side correspond to horizontal moisture advection, vertical advection of moisture driven by radiation and from convective processes, respectively, and surface latent heat fluxes. α is the ratio between the vertical moisture (scaled by L_v) and dry static energy gradients [*Chikira*, 2014]. In the moisture-mode framework, these processes are responsible for the maintenance and evolution of the MJO (Fig. 11). Many studies also invoke moist static energy or moist entropy, under WTG balance, to explain the propagation of precipitation anomalies related to the MJO [*Maloney*, 2009; *Kiranmayi & Maloney*, 2011; *Andersen & Kuang*, 2012; *Sobel et al*., 2014; *Kim et al*., 2014, 2015; *Jiang*, 2017].

5.4.2 Linear wave solutions

Equation 8 can be simplified using several approximations to obtain a linear wave solution that is qualitatively consistent with the observed MJO. The approximations are based on assumptions (d) – (h) and the following points:

(i) Under the assumption (h), eddy moisture diffusion is enhanced when the anomalous zonal flow is of the same sign as the mean flow. This diffusion dries up the troposphere to the east of the enhanced convection when the mean flow is easterly. In contrast WISHE is enhanced when the anomalous zonal flow is of the same sign as the mean flow. This assumption is consistent with observations and modeling studies that show that WISHE and high-frequency horizontal moisture advection have opposite signs [*Andersen and Kuang*, 2012; *Adames*, 2017]. We neglect the contribution of high-frequency horizontal moisture advection to MJO maintenance as it is considered non-essential.

(ii) Frictional moisture convergence causes shallow circulations where ascent moistens the atmosphere to the east and dries to the west [*Adames & Wallace*, 2014, 2015], and

(iii) The MJO propagates eastward because of, to first order, the sum of horizonal and vertical moisture advection and surface fluxes.

These processes and those described in assumptions (e) – (h) have been considered important by many previous studies [*Maloney*, 2009; *Andersen & Kuang*, 2012; *Hsu & Li*, 2012; *DeMott et al.*, 2014; *Pritchard & Bretherton*, 2014; *Kim et al.*, 2014; *Adames &*

Wallace, 2015, among others]. With these approximations, Eq. 8 becomes

$$\frac{\partial P_r'}{\partial t} = \frac{1}{\tau_c}(-u'\delta\overline{q}_u - nv'\frac{\partial \overline{q}}{\partial y} - \widetilde{M}_{eff}P_r') \quad (9a)$$

$$\widetilde{M}_{eff} = \widetilde{M}(1+r) - r \quad (9b)$$

where $\delta\overline{q}_u$ is the total moistening from the anomalous zonal flow (see assumptions e – g and points i - iii above) , *n* a constant that describes the projection of the vertical structure of the horizontal wind field onto the vertical structure of moisture, and $\widetilde{M}_{eff}$ the effective gross moist stability [*Neelin & Held*, 1987; *Raymond et al*., 2009; *Benedict et al*., 2014; *Inoue & Back*, 2015]. $\widetilde{M}_{eff}$ is the effective static stability ($\widetilde{M}$) of a moist column when including the effect of the cloud-radiative feedback. $\widetilde{M}$ is related to $1-\alpha$ in Eq. 8. The impact of radiation on the effective static stability is determined by cloud-radiative feedback parameter [*Fuchs & Raymond*, 2005; *Peters & Bretherton*, 2005], also known as the greenhouse enhancement factor [*Kim et al*., 2015] $r = R'/P_r'$ which describes the anomalous cloud longwave radiative heating R' per unit of latent heat release [*Lin & Mapes*, 2004]. By applying the WTG approximation, we can describe the effective GMS as $\widetilde{M}_{eff} \simeq (P_r' - \overline{M}_q D')/P_r'$. Thus, the effective GMS can be thought as the difference between the supply of moisture by vertical moisture advection ($\overline{M}_q D'$) and the demand of moisture required to maintain precipitation, per unit of precipitation. When $\widetilde{M}_{eff}$ is negative, supply exceeds demand, causing the moisture anomalies to grow. This is the so-called moisture-mode instability described by *Raymond and Fuchs* [2009] and *Raymond et al*. [2009]. Note that we can separate D' into contributions from deep convection and radiation. Thus, radiation can cause a column to become unstable even when the net effect of deep convection is to remove moisture from the column (Fig. 7). A more comprehensive review on the GMS is offered by *Raymond et al*. [2009].

In combination with Eq. 2, Eq. 9 describes the evolution of a slowly-propagating, steady-state heat source (Fig. 9). In this framework, the only time derivative in this system of equations is in the precipitation equation through the inclusion of the moisture tendency. While this may not be accurate throughout the observed MJO cycle, it allows us to isolate and interpret the propagation of moisture within a simplified framework.

By approximating the advective processes (assumptions d and g) and surface fluxes *E'*

as driven by the MJO flow (assumption e), we can group them into what we will refer to as the "moisture advection parameter" A_{KR}. A_{KR} can be thought of as the rate in which the winds in the Matsuno-Gill response advect moisture such that there is moistening to the east of the heat source and drying to the west. It follows that the real component (which induces propagation) of a dispersion relation is

$$\mathrm{Re}(\omega) = \frac{A_{KR}}{\tau_c k} \tag{10}$$

where τ_c is held constant for simplicity (assumption b). For the sake of illustration, we now consider the case of no frictional dissipation ($\epsilon = 0$). A discussion of the importance of ϵ on the moist wave solution is offered by *Adames and Kim* [2016]. The dispersion relation in Eq. 10, along with the cases when dissipation is not neglected, is shown in Fig. 12. The above dispersion relation defines the MJO as a dispersive wave with an eastward phase speed and a westward group velocity (bottom panels in Fig. 12). This dispersion arises because the wind anomalies in the Matsuno-Gill response to an equatorial heat source are proportional to the scale of the precipitation anomalies ($u' \propto P'/k$, see Appendix C in *Adames & Kim* [2016]). Qualitatively, the dispersion curves resemble those of an equatorial Rossby wave, but exhibiting a smaller frequency and eastward propagation.

The component of the dispersion relation that corresponds to the growth and decay of the moist wave has the following form

$$\mathrm{Im}(\omega) = -\frac{\widetilde{M}^*_{tot}}{\tau_c} \tag{11a}$$

$$\widetilde{M}^*_{tot} = m(\widetilde{M}_{eff} + \widetilde{M}_h) \tag{11b}$$

where $\widetilde{M}^*_{tot}$ is the total GMS, the effective GMS $\widetilde{M}_{eff}$ augmented by meridional advection of mean moisture by the Sverdrup component of the flow $\widetilde{M}_h$ (Eq. 22 in *Adames & Kim* [2016]), and *m* is a constant. $\widetilde{M}^*_{tot}$ contains an asterisk, which denotes meridional averaging. $\widetilde{M}^*_{tot}$ can be positive or negative and is augmented by the cloud-radiative feedback parameter, *r* (Eq. 9b). Spectral analysis of satellite-derived rainfall and OLR [*Adames & Kim, 2016*] suggests that *r* decays exponentially with wavenumber via the following relation

$$r = r_0 e^{-L_r k} \tag{12}$$

where r_0 and L_r are constants; r thus favors growth at the largest scales. This scale selection mechanism arises from the wide-spread nature of the cloud radiative feedback. Upper-level clouds spread horizontally away from a region of precipitation, and the resulting area of upper-level cloudiness suppresses outgoing longwave radiation over a larger area than the precipitation anomalies do (Fig. 8, also Fig. 9 of *Adames & Kim* [2016]).

5.5 Other Features

5.5.1 WISHE-moisture mode theories

Another relevant moisture-mode theory is the one developed by *Fuchs and Raymond* [2002, 2005, 2007, 2017] and *Raymond and Fuchs* [2007]. This theory is based on similar physical principles as the theory of *Adames and Kim* [2016] discussed earlier in this section: column moisture is prognostic and is coupled to precipitation with a relaxation time based on the concept of the GMS. However, there are some notable differences. In the WISHE-moisture-mode theory:

i. The time derivatives in the momentum and thermodynamic equations are retained;
ii. Mean easterlies are essential for WISHE to operate;
iii. WISHE is the only moistening process that can induce propagation;
iv. WISHE also destabilizes the MJO, and can induce growth even if the effective GMS is positive;
v. Planetary scale selection is induced by WISHE, not by the cloud-radiative feedback, due to the retainment of zonal acceleration and the temperature tendency in their theory, and
vi. The wind field only contains a zonal component (v=0) and horizontal structure of the solution is not prescribed as a Kelvin-Rossby wave couplet.

Of these differences, the most important one is the role of WISHE in planetary-scale selection. This scale selection mechanism arises naturally from the linearized basic equations and is not based on empirical evidence such as the planetary-scale selection mechanism based on the cloud-radiation feedback discussed above. In spite of these differences, many similarities can be found between their theory and that of *Adames and Kim* [2016]. Both yield dispersive wave solutions with a group velocity near-zero for zonal wavenumber 1 and westward for larger wavenumbers. Both theories are destabilized by a

negative effective GMS.

Another variant of the WISHE-moisture mode theory was recently developed by *Khairoutdinov and Emanuel* [2018]. This theory is based on the concept of boundary-layer quasi-equilibrium. However, with the application of WTG, it can be shown that precipitation is highly correlated with free tropospheric moisture as in the moisture-mode theory. This theory shares many similarities with that of Fuchs and Raymond [2017]. For example, their solution does not include any meridional winds, the cloud-radiation feedback does not play an important role in MJO maintenance, and the dominant destabilization and eastward propagation mechanism is WISHE. There are some notable differences, however. *Khairoutdinov and Emanuel* [2018] use a convective parameterization based on the concept of boundary-layer quasi equilibrium [*Raymond* 1995; *Emanuel* 1995] instead of a parameterization that is solely based on the column moisture anomalies. Because of this parameterization, WISHE still induces a planetary-scale instability even if the WTG approximation is applied, unlike the theory of *Fuchs and Raymond* [2017] which requires the temperature tendency to be retained in order to obtain a planetary-scale instability.

While the theories of *Fuchs and Raymond* [2017] and *Khairoutdinov and Emanuel* [2018] receive support from simulations of zonally-symmetric aquaplanets [*Shi et al.*, 2018; *Khairoutdinov & Emanuel*, 2018], mechanism-denial experiments using Earth-like conditions challenges the notion that WISHE is central to the eastward propagation of the MJO [*Ma & Kuang*, 2016]. While zonal-mean winds in the equatorial belt are easterly, MJO-related convection is strongest in regions of mean lower-tropospheric westerlies [Wang, 1988]. Since these theories depend on the existence of mean easterlies for the WISHE mechanism to induce eastward propagation, their relevance to observations is frequently questioned. More research is needed to further understand the role of WISHE in the MJO.

5.5.2 Beyond the linear framework

The moisture-mode framework can be generalized beyond the linear solutions presented here. Its essence (a) to (c) have been the subject of a large number of observational, reanalysis and modeling studies [*Randall*, 2013; *Sobel et al.*, 2014;

Andersen & Kuang, 2012*; Kim et al*., 2014; *Janiga & Zhang*, 2016; *Wolding & Maloney*, 2015; *Wolding et al*., 2016, among others]. Here we briefly summarize the findings of some of these studies.

The seasonality of the MJO can be explained when considering seasonal variations in the low-frequency, background distribution of wind and moist static energy (MSE) [*Adames et al*., 2016; *Jiang et al*., 2018]. Furthermore, it can explain why the MJO propagates south of the Indo-Pacific Maritime Continent during boreal winter [*Kim et al.*, 2017]. Other studies have used the framework to interpret the MJO response to climate change [*Wolding et al*, 2017; *Adames et al.,* 2017a, b; *Rushley et al*., 2019; *Maloney et al.*, 2019]. Several studies have found that increasing a model sensitivity to convection through increasing entrainment leads to improved MJO simulation [*Tokioka et al.*, 1988; *Wang & Schlesinger*, 1999; *Woolnough et al.*, 2001; *Del Genio et al*., 2012; *Zhu & Hendon*, 2015; *Arnold & Randall*, 2015; *Kim & Maloney*, 2017], though it often results in a degraded mean state [*Kim et al.,* 2011]. Other studies have found clear links between MJO simulation skill and the climatological-mean distribution of moisture over the warm pool. Models that exhibit a more humid mean state exhibit a more robust MJO and enhanced eastward propagation due to stronger horizontal moisture advection [*Kim et al.,* 2016; *Kim*, 2017]. Numerous diagnostic tools have been developed based on the premise that MJO-related precipitation anomalies are tightly coupled to moisture [*Del Genio et al*., 2015; *Kim et al.*, 2014, 2015; *Jiang et al.*, 2016; *Gonzalez & Jiang*, 2017; *Ahn et al*., 2017]. Furthermore, multiple studies have shown the MJO amplitude in GCMs is inversely correlated with the GMS, indicating that a small GMS value may indeed be important for adequate MJO simulation [*Benedict et al*., 2014; *Jiang et al*., 2016; *Ahn et al*., 2017].

5.6 Summary

The moisture-mode framework can describe many observed features of the MJO, including its slow eastward propagation and planetary-scale selection, lower-tropospheric structure, and dependence on the low-frequency background state (through the relationship between precipitation and moisture as mediated by the convective timescale). The variant of this theory proposed by *Sobel and Maloney* [2012, 2013] and *Adames and Kim* [2016] suggests that the MJO propagation and maintenance can be explained by the evolution of moisture

alone. The cloud-radiative feedback at the MJO timescale is the main driver of instability and moisture advection is the primary propagation mechanism. There have been many studies that support the view that the MJO is a moisture mode [*Andersen & Kuang*, 2012; *Pritchard & Bretherton*, 2014; *Sobel et al*., 2014; *Janiga & Zhang*, 2016; *Jiang et al.,* 2018; *Rushley et al.,* 2019].

5.7 Limitations

This theory relies on several assumptions and parameterizations. While assumptions (a) and (c) considerably simplify the basic equations, it is unclear whether the main conclusions of this theory depend exclusively on these assumptions. The scale-dependence of the cloud-radiative feedback (Eq. 12) needs to be supported by observations and comprehensive modeling evidence. The parameterization of precipitation solely in terms of water vapor (Eq. 6) can be improved to better fit the observations (Fig. 10). It is still a challenge to provide unambiguous observational evidence of a westward group velocity. The justification of using the current value of the Rayleigh friction coefficient for planetary scale selection remains to be made. The theory assumes global-mean easterlies, similar to the WISHE-moisture mode theories (section 5.5.1). It is unclear whether this assumption is appropriate since the MJO tends to occur in regions of mean westerly flow, even though this assumption is not critical to the moisture-mode theory.

5.8 Recommendations for Further Evaluation

The theoretical framework presented by *Adames and Kim* [2016] makes several predictions that can be tested. For example:

(a) Test whether the intraseasonal precipitation anomalies are the result of changes free-tropospheric moisture only;

(b) Seek observational and modeling evidence to support that the cloud-radiative feedback is scale-dependent;

(c) Confirm the main findings of the theory using a more comprehensive theoretical model with prognostic equations for wind and temperature;

(d) More mechanism-denial experiments [*Kim et al.,* 2011; *Pritchard & Bretherton*, 2014; *Pritchard & Yang*, 2016; *Ma & Kuang*, 2016; *Shi et al*., 2018] need to be performed

in order to isolate the most important mechanisms for MJO eastward propagation.

There have been studies that challenge the moisture-mode view of the MJO [*Arnold & Randall*, 2015; *Pritchard & Yang*, 2016; *Kacimi & Khouider*, 2018; *Chen & Wang*, 2018]. Future work should expand the theoretical framework to reconcile the studies that support and challenge this theory and explain some of the additional desired features discussed in section 3.

6. GRAVITY-WAVE THEORY

The gravity-wave theory of the MJO was proposed by *Yang and Ingersol*l [2013] using a two-dimensional (2D) shallow-water model. The eastward propagation was explained by the east-west asymmetry of gravity waves. The selection mechanism for the zonal scale of the MJO was discussed in *Yang and Ingersoll* [2014] using a one-dimensional (1D) model without latitudinal dependence. In the 1D model, the physics (convection/radiation parameterization) is almost identical to that in the 2D model. This model has five dimensional parameters: β, gravity wave speed, temporal scale, spatial scale, and number density of convective events. The first four parameters are well-constrained by observations. Because there are two dimensions (length and time), only three of the five parameters are independent. The model outcome is robust over a wide range of values of the last independent parameters.

6.1 Essence

The essence of this theory includes:

(a) The MJO is a large-scale envelope of short-lived, synoptic-scale (order of 1,000 km) westward inertia-gravity waves (WIG) and eastward inertia-gravity waves (EIG);

(b) The MJO propagates eastward because EIG travel faster than WIG due to the beta effect, and

(c) The horizontal scale of the MJO is determined by the mean free path of gravity waves—the average distance travelled by gravity waves without intercepting a convective storm.

6.2 Assumptions

This theory is derived from shallow-water equations (Eqs. 2a - c) under the

following main assumptions:

(a) High-frequency WIG and EIG are essential to the MJO;

(b) There is no scale separation between convective storms and inertia-gravity waves. As a consequence, convection is treated as a triggered process, and CAPE can be accumulated at a short (gravity-wave) timescale;

(c) Precipitation is triggered only when a certain threshold (layer thickness or geopotential) is reached in the environment;

(d) Radiation-convection equilibrium exists not only at the global scale, but also at the MJO scale (30-60 days, zonal scale ~ 10,000 km);

(e) The radiative cooling rate is constant in time and space, neglecting radiative feedbacks (both clear-sky and cloud feedbacks), and

(f) The temporal and spatial scales of convective storms are set to constant for simplicity.

Assumptions (b) and (c) are based on observations. In the recent DYNAMO field campaign [*Yoneyama et al*., 2013], intermittent and energetic rainstorms were frequently observed in association with gravity waves, and there were significant fluctuations in CAPE during the life cycle of such rainstorm episodes [*Zuluaga & Houze,* 2013]. In the DYNAMO observations, precipitation occurred when CAPE exceeded a threshold value, which is consistent with the triggering mechanism in the gravity-wave theory. Assumption (d) is valid when averaged over the entire life cycle (30-60 days) and spatial scale (10,000 km) of the MJO, in which there are a large number of convective storms. Convection is, therefore, in statistical equilibrium with radiation.

6.3 Uniqueness

The gravity-wave theory is a multi-scale model that explicitly represents gravity-wave dynamics and the MJO. This is the only one among the four discussed in this article that does not explicitly include moisture. The role of moisture in the MJO is implicit in allowing precipitation to occur and convective instability to accumulate (*i.e.*, the threshold of convection), and in the use of a moist gravity wave speed. This is also the only one of the four theories discussed in this article that uses CAPE as a closure of cumulus parameterization and represents convection as a triggered process. Triggered convection is

fundamentally different from quasi-equilibrium convection, which has been widely used to parameterize convection in GCMs. The success of the gravity-wave model points to ways to improve convection parameterization in GCMs.

The gravity-wave theory proposes that the large-scale, long-lasting MJO is a wave envelope of small-scale, short-lived WIG and EIG waves. Because of Earth's differential rotation—the β effect, EIG propagates faster than WIG (Fig. 13, left). This small asymmetry leads to the eastward propagation of the wave envelope (Fig. 13 right). If there is no such zonal asymmetry between EIG and WIG, this theory predicts that the MJO would be stationary (Fig. 13 middle).

The gravity-wave theory suggests that the horizontal scale of the MJO is determined by the mean free path of gravity waves—the average distance travelled by gravity waves without intercepting a convective storm (Fig. 14, left). Faster gravity waves or fewer (stronger) convective storms favor larger MJOs (Fig. 14, middle), and slower gravity waves or more (weaker) convective storms favor smaller MJOs (Fig. 14, right). The spatial scale of the MJO can be derived using the Buckingham Pi Theorem, also known as the dimensional analysis [*Kundu* 2015; *Barenblatt* 2003]. According to this theorem, there are only three independent free parameters. The gravity-wave theory includes the smallest number of parameters (five) among the four theories discussed in this article.

6.4 Mathematical Framework and Solutions

The MJO is commonly considered a large-scale, slowly varying mode. This allows treatment of convection as a quasi-equilibrium (QE) process because of the scale separation between the MJO and individual convective storms. The QE convection emphasizes the collective impact of a number of convective storms on large-scale, slowly varying circulations, suggesting that convective storms consume CAPE almost instantaneously. In contrast, in the gravity-wave theory, short-lived, small-scale gravity waves are essential to the MJO dynamics, so there is no scale separation between convective storms and gravity waves. Convective storms are energetic and intermittent in observations [*Zuluaga & Houze,* 2013] and are represented in this theory as a triggered process: CAPE can be accumulated and is released only when a certain threshold is exceeded (assumption c). In this theory, Q_1 in Eq. 2c is expressed as:

$$Q = \begin{cases} \frac{Q_0}{\tau_c A_c}\left[1 - \left(\frac{\Delta t - \tau_c/2}{\tau_c/2}\right)^2\right]\left(1 - \frac{L^2}{R_c^2}\right) & where\ \phi < \phi_c, 0 < \Delta t < \tau_c, L^2 < R_c^2 \\ 0 & otherwise \end{cases} \quad (13)$$

where

ϕ_c is the threshold for geopotential to trigger convection,

$c \equiv \sqrt{\phi_c}$ is the gravity-wave phase speed,

Q_0 is the convective heating amplitude per event,

τ_c is the duration of individual convective storms (different from that in section 5),

Δt is the period of time since convection is triggered,

A_c is the area of convective storms,

R_c is the radius of individual convective storms,

$L = \left(\Delta x^2 + \Delta y^2\right)^{1/2}$ is the distance from the convective center, where Δx and Δy are zonal and meridional distances from the convective center, respectively.

There are five relevant parameters in this theory: c, β, τ_c, R_c, and S_c (the number density of convective storms). The first two parameters are standard for all equatorial beta-plane shallow-water systems. The latter three arise from the convection scheme (Eq. 13). The scales in time and space are explicit in Eq. (13), and the number density is derived from the mass or energy balance of this theory. At a steady state, assumption (d) suggests $n \times Q_0 \sim r \times A \times T$, where n is the number of convective storms over the area of A and the period of T, and r is the radiation cooling rate. The number density is then given by

$$S_c \equiv \frac{n}{A \times T} \sim \frac{r}{Q_0} \quad (14)$$

which measures the relative strength between convective heating and radiative cooling. The five parameters have two units: length and time.

The MJO is successfully simulated using a 2D shallow-water model [*Yang & Ingersoll,* 2013]. There are planetary-scale envelopes propagating eastward at about 3 ms^{-1} (Fig. 15 left panel). The simulated MJO is further confirmed by a 2D spectral analysis (Fig. 15 right), which shows strong spectral peak at the low-frequency and positive low-wavenumber region.

Figure 16 shows the convection-gravity wave resonance, the basis for the MJO. Triggered by a local minimum of geopotential (*e.g.*, at day 163.75), convection increases the geopotential for a finite time period τ_c. The geopotential reaches a local maximum and then starts to decay when convection is switched off. This cycle repeats itself a few times at the same location, which resembles basic features of a standing wave.

Within the large-scale envelope of the MJO, the EIG and WIG have the same meridional structures and similar phase speeds toward the opposite directions, so they could form quasi-standing waves. Because EIG propagates slightly faster than WIG, the large-scale envelop slowly drifts to the east (Fig. 15 left panel), with a speed of

$$c = 0.5 \times (c_{EIG} - c_{WIG}). \quad (15)$$

This scaling was then tested against 60 shallow-water simulations with a wide range of parameter values (Fig. 17 Left panel). The simulation results in general fall along and fit the overall trend of the theoretical curves. This success suggests that the eastward propagation of the MJO can arise from the zonal asymmetry between EIG and WIG, which is fundamentally due to the beta effect.

The MJO was also successfully simulated by the 1D beta-plane model (Fig. 3 in *Yang & Ingersoll* [2014]). This 1D model was used to understand the zonal scale of the MJO. There are two different methods to derive a scaling for the MJO zonal wavenumber *k*. One is by combining physical intuition, Buckingham Pi theorem and numerical simulation results. In theory, the MJO wavenumber is given by, $\hat{k} = F(\hat{\tau}, \hat{R}_c, \hat{S}_c)$, where variables with carets are non-dimensional. Because the temporal and spatial scales of the MJO envelope are much larger than those of individual storms, we may further assume that the MJO envelope does not *feel* the individual storms, leading to $\hat{k} = F(\hat{S}_c)$. Identifying the function form, however, requires numerical simulations. In a log-log plot of $\hat{k}$ and $\hat{S}_c$, all simulation results fall along a straight line with a slope of 0.5 (Fig. 17 Right panel). This suggests

$$\hat{k} = \hat{S}_c^{1/2}. \quad (16)$$

The other method is to consider the energy balance of individual MJO events. When multiple MJO events coexist, they are statistically identical. For a time period of $\frac{\lambda}{c} \sim \frac{k^{-1}}{c}$ and the zonal scale of $\lambda \sim k^{-1}$, the total convective heating balances radiative cooling:

$$q_0 \sim r\frac{k^{-1}}{c}k^{-1} \implies k \sim \left(\frac{S_c}{c}\right)^{1/2} \quad (17)$$

where the number of convective events was assumed to be constant and of unity. This is indeed the same equation as Eq. 16.

Equation 17 is a scaling theory, which was derived by combining physics laws and empirical evidence (simulation results or constant scaling factors). It explains the dependence of k on S_c and c, but cannot explain why the scaling factor is of unity as in many other scaling theories.

Observational support of the gravity-wave theory comes from the seasonality of the MJO and gravity waves (Fig. 16 in *Kikuchi* [2014]). Significant gravity wave signals have been observed in the high-frequency branch of the tropical wave spectrum, and its strength co-varies with the MJO spectral power (Fig. 18). In strong MJO seasons (winter and spring), the amplitudes of EIG and WIG are comparable, suggesting that they could pair and form the quasi-stationary IG wave envelope—the MJO. In weak MJO seasons (summer and fall), the amplitudes of WIG are much stronger than the amplitudes of EIG, and this asymmetry may limit the pairing of EIG and WIG and thereby the strength of the MJO. The gravity-wave theory can, therefore, explain the seasonality of the MJO.

In this theory, the basic features of the MJO arise only from convection-wave interaction and do not depend on the mean state, such as background wind, temperature, and moisture distributions. The only asymmetry in this theory is beta, which leads to the eastward propagation of the MJO but is not responsible for its emergence. The MJO is, therefore, a form of *convective self-aggregation* in the gravity-wave theory, as its existence and development do not rely on any asymmetries of the background fields and boundary conditions [*Held et al.*, 1993; *Bretherton et al.*, 2005; *Yang*, 2018a, 2018b, 2019].

What leads to aggregation? The aggregation mechanism is via resonance between convection and gravity waves. One would think that small-scale, short-lived convective events are difficult to generate a large-scale, long-lasting response (MJO). This would be true if the model is forced at short time scales by convection, especially since the advection terms are negligible (linear dynamics). This model is, however, self-excited as opposed to externally forced. Convection excites quasi-standing IG waves, which triggers the next-cycle convection in the vicinity of recent convection events. At the statistically steady state, there is a large-scale, slowly varying envelope of convection events. Because convection

is positive only, this large-scale aggregate appears as a new signal in the spectral domain. We refer to this effect as rectification of the direct-current convection. A similar rectification effect was introduced in *Yang and Ingersoll* [2011] to explore if the MJO is a wave packet of mixed Rossby-gravity (MRG) waves.

6.5 Other Features

This theory also offers predictions that can be validated in the future: The MJO becomes faster, bigger, and stronger with warming. This prediction relies on increasing water vapor in the atmosphere in warmer climates according to the Clausius-Clapeyron relation. The increasing water vapor has two effects: 1) stronger stratification, and 2) stronger rainstorms that release more latent heat. The first effect leads to faster gravity waves [e.g., *Kuang*, 2008], which then leads to faster MJOs (Eq. 15). The second effect leads to smaller number density of convective events as radiation varies slower than convection. Faster waves and smaller number density together lead to large zonal scale of the MJO in warmer climates (Eq. 10). Because the MJO is the large-scale envelope of individual storms, it becomes stronger if individual ones become stronger. These predictions were explicitly tested against a suite of global simulations with uniform SSTs ranging from 1°C to 35°C [*Pritchard & Yang*, 2016].

As shown in Fig. 13, the shallow-water model can reproduce quasi-stationary convective self-aggregation when rotation is switched off [*Yang* 2020]. This result agrees well with recent simulations by global climate models [*Arnold & Randall* 2016; *Pritchard & Yang* 2016] and cloud-resolving models [*Khairoutdinov & Emanuel* 2019]. This agreement across such a wide range of model hierarchy suggests that the Yang-Ingersoll convection parameterization might have captured some essential aspects of interactions between convection and atmospheric flows.

6.6 Summary

Yang and Ingersoll [2013, 2014] suggested that the MJO is a large-scale envelope of convective events that are linked by small-scale gravity waves. In the gravity-wave theory, convective storms are triggered when the layer thickness is lower than a threshold. Once it is triggered, convection increases the mass of this layer and excites gravity waves,

which transport mass anomalies away from the convective center and effectively reduces the layer thickness locally. This process, in turn, can excite the next cycle of convective events. The convection-wave interaction is responsible for aggregation of rainstorms, and the aggregated rainfall envelope has a "direct current" (DC) component due to the rectification of positive-only convective heating. This is the fundamental reason why short-lived, small-scale gravity waves can produce long-lasting, large-scale MJO events.

This theory reproduces main observed features of the MJO over a wide range of parameter values (over one order of magnitude for key parameters). It challenges the traditional view that considers the MJO as a large-scale mode and it suggests that successful MJO simulations require accurate representations of short-lived, small-scale gravity waves and thereby individual rainstorms. This provides a potential explanation as to why quasi-equilibrium convection schemes cannot simulate a realistic MJO, because gravity waves are heavily damped under the quasi-equilibrium adjustment [*Emanuel et al*. 1994]. This might be a reason why GCMs tend to underrepresent the MJO variability. The gravity-wave theory points to ways to improve convection parameterization—moving away from QE convection.

6.7 Limitations

The threshold behavior of convective parameterization makes it challenging to perform linear analysis and obtain analytical solutions. The dependence of the MJO zonal scale on the number density of precipitation is derived using dimensional analysis, where the constant scaling factor has to be determined using numerical experiments. It is desirable to quantify the number density of the convective events and to identify the co-variance between the MJO and IG waves in the physical space using observations. The propagation speed of the MJO is near the slow end (around 3 ms^{-1}) when gravity wave speed is set to 20 ms^{-1}.

6.8 Recommendations for Further Evaluation

Here are a few suggestions to further test the gravity-wave theory:

(a) Search for gravity waves in the physical domain using observation and reanalysis data. The observation of *Kikuchi* [2014] that the amplitudes and characteristics of gravity

waves and the MJO co-vary at seasonal timescales in the Fourier domain is consistent with this theory. Such a relation, however, has not been established in the physical domain (time and space) [e.g., *Yang & Ingersoll*, 2011; *Dias et al.,* 2013]. The reason for this could be (1) previous studies focused on either EIG or WIG, not the EIG-WIG envelope, and (2) previous studies used the data with low time sampling rate and focused on low-frequency variability (e.g., up to 0.5 cycle per day or CPD). Future studies may focus on the EIG-WIG envelope at higher frequencies (e.g., beyond 0.5 CPD) and its relationship with the MJO in the physical domain.

(b) Test the triggered convection using observation and cloud-resolving models. This includes testing whether CAPE is accumulated at the gravity wave timescale, and whether convection triggering is related to the geopotential and static stability anomalies.

(c) Test the proposed scaling. This requires varying parameters over a wide range, for example, in a GCM. The scaling predictions are qualitatively consistent with the MJO behavior in a suite of extreme-climate-change experiments [*Pritchard & Yang*, 2016].

7. CONVECTIVE-DYNAMIC-MOISTURE TRIO-INTERACTION THEORY

This section is devoted to describe the trio-interaction theory of the MJO proposed by *Wang et al*. [2016] and further elaborated by *Wang and Chen* [2017], *Liu and Wang* [2017], and *Chen and Wang* [2018]. The trio-interaction theory of the MJO was developed from the frictionally coupled Kelvin-Rossby wave theory [*Wang* 1988a; *Wang & Rui* 1990b] by including prognostic moisture variation (the moisture mode, section 5). This theory extends the Matsuno-Gill model [*Matsuno*, 1966; *Gill*, 1980] by including interactive convective heating, moisture conservation, and boundary-layer (BL) dynamics.

7.1 Essence

The most critical component of this theory is the convectively coupled Kelvin-Rossby wave structure and the phase lead of BL convergence to convective heating. In consequence:

(a) The fundamental MJO physics is rooted in the feedbacks between the dynamics (frictionally-driven BL convergence and equatorial wave dynamics), moisture, and diabatic heating from convection and radiation;

(b) The BL feedback is responsible for the selection of the zonal scale and eastward propagation of the MJO;

(c) The eastward propagation speed of the MJO is determined by the basic state moist static energy, the moisture feedback, and the coupling of Kelvin and Rossby waves, and

(d) The BL feedback and the cloud-radiative feedback produce the instability for the growth of the MJO.

7.2 Assumptions

(a) The BL dynamics can be represented by a barotropic prognostic equation;

(b) The BL depth is constant in time and space;

(c) The long-wave (semi-geostrophic) approximation is applied to the free troposphere but not the BL;

(d) Total moisture convergence is due to the sum of BL and lower free tropospheric convergence of mean moisture by the anomalous winds, and

(e) BL convergence is determined by the lower-tropospheric geopotential anomaly.

7.3 Uniqueness

This trio-interaction theory integrates four major possesses proposed in the existing theoretical MJO frameworks developed over the past three decades. It can accommodate a variety of simplified convective schemes. Among the MJO theories discussed in this article, this is the only one in which the BL convergence feedback plays an essential role in generating eastward propagation, planetary-scale instability, and the coupled Kelvin-Rossby wave structure of the MJO.

In this theory, the equatorial Kelvin-Rossby wave couplet constitutes the most fundamental structure of the MJO and its interaction with convective heating and moisture provides the essential mechanism for the MJO, as illustrated in Fig. 19. The BL moisture convergence, induced by the wave structure, generates positive moisture and heating anomalies to the east of an MJO convection center, leading to its eastward propagation and preferred growth on the planetary scale. The slow propagating speed is determined by a combination of the basic state MSE, the enhanced Rossby wave response by moisture feedback, and the coupling between the Rossby and Kelvin waves.

7.4 Mathematical Framework and Solutions

The trio-interaction theory consists of the linear system representing the lowest baroclinic mode in the free troposphere and a barotropic, steady-state boundary layer, which provides a lower boundary condition for the free tropospheric motion. This forms a simple 1 and ½ layer model on the equatorial beta-plane [*Wang & Rui*, 1990b]. Using the horizontal velocity scale C_0, length scale $(C_0/\beta)^{1/2}$, time scale $(\beta/C_0)^{-1/2}$, geopotential scale C_0^2, moisture scale $d_0\Delta p/g$, where $d_0=2p_2C_pC_0^2/\Delta pRL_c$, the non-dimensional governing equations for perturbation motions may be written as follows:

$$(\partial/\partial t+\varepsilon)u-yv=-\partial\emptyset/\partial x \quad (18a)$$

$$(\partial/\partial t+\varepsilon)v+yu=-\partial\emptyset/\partial y \quad (18b)$$

$$(\partial/\partial t+\mu)\emptyset+D+dD_b=-(P_r-R) \quad (18c)$$

$$\partial q/\partial t+\overline{q_L}D+\overline{q_b}D_b=-P_r+E_v \quad (18d)$$

$$D_b=d_1\nabla^2\emptyset+d_2\partial\emptyset/\partial x+d_3\partial\emptyset/\partial y \quad (18e)$$

In Eq. 18, u, v and ϕ represent the lower tropospheric zonal wind, meridional wind and geopotential, respectively; μ and ε are longwave Newtonian cooling and Rayleigh friction coefficients, respectively; P_r and R denote precipitation and cloud-radiative heating rate, respectively; D and D_b are the lower-tropospheric and BL divergence, respectively; d is non-dimensional BL depth; q denotes the column-integrated moisture anomaly in the free troposphere; q_L and q_b are, respectively, normalized basic-state specific humidity at the lower tropospheric layer and BL, both are controlled by the mean state moisture or underlying SST; E_v is the evaporation rate. Equations 18a - c are based on Eqs. 2a - c. Eq. (18d) is the vertically integrated moisture conservation equation in which D_b is derived from the steady barotropic BL equations (3). Detailed derivation is referred to *Wang and Li* [1994], *Wang & Chen* [2017], and *Liu and Wang* [2017]. Equation 18 is a closed system only when precipitation P_r and cloud-radiative heating R are parameterized using large-scale variables.

The trio-interaction theory produces a planetary scale unstable mode that propagates eastward slowly with a period of 30–80 days in a form of a coupled Kelvin-Rossby wave structure with its major convection led by BL low pressure. For the purpose of demonstrating this, the simplified Betts-Miller (B-M) scheme is used and cloud-

radiation heating and surface evaporation are neglected, although their inclusion is straightforward and leads to qualitatively the same conclusion.

Wave-like normal mode solutions were obtained for a linear heating case by *Liu and Wang* [2017] using truncated meridional modes following *Majda and Stechmann* [2009]. Figure 20 shows the results of the linear analysis. The red curves represent the trio-interaction mode with two major feedback mechanisms combined: the BL frictional coupled Kelvin-Rossby feedback (FC) and moisture feedback (MF). For a given uniform background SST of 29.5ºC, the growth rate decreases with increasing wavenumber, indicating a preferred planetary scale (Fig. 20, left panel). When basic state SST is 30.5ºC, both zonal wavenumbers 1 and 2 are unstable. The periodicity falls in 30-80 day range, implying a slow eastward propagation speed (Fig. 20 right panel). The frequency is weakly dependent of the wavenumber, indicating that it has a near-zero group velocity (Fig. 20 right).

The mechanisms that are responsible for the behavior of trio-interaction mode can be understood this way: The frictional feedback (shown by the black curves) alone produces the most unstable longest wave that possesses a reasonable periodicity between 30-90 days, but the periods of the wavenumber 2 to 4 fall in a range of 15 to 30 days, implying they move eastward too fast. On the other hand, the moisture feedback alone (blue curves) yields a damping mode that propagates too slow so that the corresponding period is longer than 120 days. Based on Fig. 20, instability of the trio-interaction mode is rooted in the frictional feedback; meanwhile, the moisture feedback acts to reduce the growth rate as precipitation consumes moisture, slows down the fast propagation of the frictional-feedback mode, and also makes the dispersion relation of the trio-interaction mode nearly wavelength independent.

When heating takes a positive-only form, nonlinear solutions were obtained by solving an initial value problem [*Wang & Chen*, 2017]. Figure 21 shows results for a specified SST distribution (Fig. 21a), which resembles an SST field in the Indo-Pacific warm pool. The initial perturbation is a low pressure at the equator around 40°E. The simulated precipitation anomaly moves eastward from 60°E to 170°E with a speed about 5 ms^{-1}, comparable to observations (Fig. 21b). The simulated precipitation anomaly amplifies over the Indian and western Pacific warm pool and slightly weakens over the

Maritime Continent and quickly decays near the dateline, indicating a life cycle modulated by basic state SST (or MSE). The simulated lower-tropospheric geopotential and wind fields display a coupled Kelvin-Rossby wave package (Fig. 21c), which is comparable to observations (Fig. 21d). The simulated BL frictional convergence is located underneath and to the east of the major convection center (Fig. 21e), a feature resembling the observed (Fig. 21f).

The theory reveals a critical linkage between MJO propagation and MJO structural asymmetry (Fig. 22). The MJO eastward propagation speed decreases when a westerly intensity index (i.e., the Rossby-Kelvin ratio) increases or when the Rossby wave component is enhanced. This theoretical finding is supported by observations and the climate models' simulation results (Wang and Lee 2017).

The BL convergence feedback provides a robust mechanism for the eastward propagation because the MJO convective heating-induced BL convergence is located to the east of convection. *Wang and Rui* [1990] have shown that the Kelvin wave-induced BL convergence displays an equatorial maximum that coincides with the easterly flow of the Kelvin wave; while the Rossby wave-induced BL convergence has not only an off-equatorial maximum coinciding with the Rossby wave lows but also an equatorial maximum convergence to the east of the Rossby wave lows. Therefore, when convective heating excites the Rossby wave lows to its west and Kelvin wave low to its east, the Kelvin and Rossby waves would produce a unified BL moisture convergence field (Figs. 21e and 7.3f). As a result, the BL moisture convergence can accumulate moist static energy in front of the convection, increase convective instability and congestus cloud heating, leading to eastward propagation of the convective center. Thus, the trio-interaction theory explains why the BL convergence and associated pre-moistening, pre-destabilization, and shallow and congestus clouds all lead the MJO major convection.

The BL convergence feedback provides a strong instability mechanism and a planetary wave selection mechanism by interacting with the associated convective heating. The growth rate increases with increasing basic state SST or moist static energy. First, the BL feedback provides wave selection and propagation mechanisms for moisture mode. As shown in Fig. 20, moisture feedback alone produces a damping mode with a period longer than 120 days for all wavenumbers. Thus without cloud-radiative heating the moisture

mode is a nearly stationary, damping mode, which agrees with the moisture mode obtained by *Sobel and Maloney* [2012]. Although the cloud-radiative feedback can generate instability by increasing moisture convergence, it cannot produce a preferred planetary-scale unstable mode unless the coefficient r is assumed to be dependent of the zonal wavenumber. Including BL convergence feedback can make the moisture mode unstable and select the most unstable planetary scale (Fig. 20). Second, the BL feedback can provide a wave selection mechanism for the skeleton mode. The skeleton theory with wave activity ensemble heating produces two sets of neutral modes, one propagates eastward with a 30-80 day period and the other propagates westward with 50-120 day period [*Majda & Stechmann*, 2009]. By adding BL effects, as shown by *Liu and Wang* [2012], the eastward propagation mode becomes unstable and the longest wave has the largest growth rate, meanwhile the westward propagating planetary scale skeleton modes become damped (Fig. 23). Thus, the BL feedback can destabilize the neutral skeleton mode and select eastward propagating planetary-scale mode.

The reason for the unstable mode to have a preferred planetary scale is that the BL convergence is out of phase with main convection and wave-induced moisture convergence. This phase shift effectively reduces the strength of the interaction between wave-induced heating and the overturning circulation, prohibiting unstable wave-CISK. The BL convergence to the east of main convection induces condensational heating, which overlaps the positive temperature (or lower-tropospheric low pressure) anomaly, thereby generating eddy available potential energy and kinetic energy for unstable growth. The efficiency of energy generation by the BL convergence depends on the covariance between the BL convergence and low pressure [*Wang* 1988a]. The BL convergence is better collocated with the Kelvin wave low-pressure for longer waves [*Chen & Wang*, 2018]. Thus, the energy generation by the BL convergence is more efficient at longer wavelengths, thereby leading to the preferred planetary scale growth.

The BL convergence feedback also provides a mechanism to couple the Kelvin and Rossby waves together with convective heating led by the BL convergence. This is demonstrated by a comparison of the results derived from the same model but with and without BL dynamics [*Wang et al.*, 2016]. Results in Fig. 24 demonstrate that under the positive-only heating, an initial dry Kelvin-wave low-pressure induces precipitation, which

1449 further excites a coupled Kelvin–Rossby system at day 2. The trio-interaction mode
1450 exhibits a coupled Kelvin-Rossby structure in the presence of BL (Fig. 24a); however,
1451 without the BL dynamics, the Kelvin and Rossby waves are decoupled with convection:
1452 the Rossby wave moves westward and the Kelvin wave moves eastward (Fig. 24b).
1453 Therefore, the moisture feedback cannot generate the MJO. Similarly, without BL
1454 dynamics, the Kuo scheme and wave activity ensemble (skeleton model) scheme also
1455 cannot hold the Kelvin and Rossby wave together (Fig. 24c and d). Using all four schemes
1456 consistently demonstrates that it is the BL frictional moisture convergence that is
1457 responsible for the coupling among convection, Kelvin and Rossby waves, and the BL
1458 feedback provides an instability source and selects preferred planetary scales.
1459
1460 *7.5 Other Features*
1461 The trio-interaction theory can accommodate a variety of simplified convective and
1462 cloud-radiative heating parameterizations:
1463 (a) Betts-Miller (B-M) scheme [*Frierson et al*., 2004; *Wang & Chen*, 2017] in which the
1464 moisture is relaxed back to a significant fraction of the saturation value when there is
1465 enough moisture for convection, namely $P_r = (q+\alpha\Phi)/\tau$, where τ is a convective
1466 adjustment time.
1467 (b) Bretherton scheme [*Bretherton et al*., 2004] in which precipitation is proportional to
1468 the column integrated moisture, i.e., $P_r = q/\tau$, a special case of the Betts-Miller scheme
1469 (section 5).
1470 (c) Wave activity ensemble scheme in which the precipitation tendency is assumed to be
1471 proportional to perturbation moisture [*Majda & Stechmann*, 2009]: $\partial P_r/\partial t = \Gamma\, q_{low}$, where
1472 q_{low} is the lower-tropospheric moisture which can be approximated by q, Γ is a parameter
1473 representing the strength of the moisture and wave activity interaction (section 4).
1474 (d) Kuo scheme [*Kuo* 1974; *Wang & Rui*, 1990b] in which precipitation is balanced by
1475 column integrated moisture convergence and surface evaporation:
1476 $P_r = Ev - bH(\bar{q}_L D + \bar{q}_b D_b)$ with a precipitation efficiency parameter b, normally taken as
1477 0.9.
1478 (e) Triggered convective heating [*Yang & Ingersoll*, 2013] in which convection is assumed
1479 to occur in a small area, and is triggered when a pressure anomaly is lower than a threshold

(section 6).

(f) Cloud-radiation feedback scheme [*Fuchs & Raymond*, 2005; Peters & Bretherton, 2005] in which the reduction of radiative cooling is proportional to convective heating associated with precipitation: $R = - rP_r$ (section 5).

The trio-interaction theory demonstrates that different parameterization schemes can produce different MJO circulation structures, thus different propagation speeds. Figure 25 compares structures of lower-tropospheric zonal winds obtained from the trio-interaction models with the Betts-Miller and Kuo schemes, respectively**.** With the Kuo scheme, the Kelvin wave (KW) easterly is stronger than Rossby wave westerly. But with the Betts-Miller scheme (with moisture feedback) Rossby wave westerly is stronger than the Kelvin wave easterly. Thus, different schemes result in differing MJO horizontal circulation patterns, especially, the relative strength of the Rossby vs Kelvin wave components, which can be measured by the ratio of the maximum Rossby wave westerly vs. maximum Kelvin wave easterly, i.e., the Rossby-Kelvin ratio (Fig. 22).

The trio-interaction theory elaborates important roles of the four feedback processes, i.e., BL convergence feedback, moisture feedback, wave feedback, and cloud-radiation feedback. As shown in section 7.4, the BL feedback couples the equatorial Kelvin and Rossby waves with convective heating and selects preferred eastward propagation and a planetary-scale unstable mode. The moisture feedback mainly acts to reduce the propagation speed and the growth rate of the short waves, and to produce a more realistic circulation structure [*Wang and Chen* 2016]. The wave feedback plays an important role in slowing down eastward propagation and increasing growth rate for planetary waves [*Liu and Wang* 2017]. The cloud-radiative feedback can generate instability by increasing moisture convergence, but it cannot produce a preferred planetary-scale unstable mode unless the coefficient *r* is assumed to be dependent of the zonal wavenumber [*Chen and Wang*, 2018a].

In the trio-interaction theory, basic state SST controls the energy source of MJO convective heating by modulating basic state moist static energy. When SST increases, the lower troposphere moisture increases accordingly, which enhances the heating rate, thus reducing the effective static stability and the corresponding moist Kelvin wave speed. As shown in Fig. 26, the dry Kelvin (gravity) wave speed is 50 ms^{-1}, whereas the convectively

coupled Kelvin wave speed decreases with increasing SST, having a value of 19 $ms^{-1}$for SST=29 °C. The SST-dependence of the propagation speed is consistent with the observed slow propagation over the warm pool and fast propagation over the cold ocean *[Knutson et al.,* 1986]. Furthermore, due to the coupling of Kelvin and Rossby waves under Kuo-scheme heating (without the moisture feedback) the propagation speed is further reduced from 19 to 14 ms^{-1} because the Rossby wave component induced by β-effect tends to move westward. Lastly, the moisture feedback under the simplified B-M scheme can significantly slow down the eastward propagation speed from 14 to about 5 ms^{-1}. This is because the moisture feedback under the Betts-Miller scheme is shown to reinforce the coupling between precipitation heating and Rossby waves [*Wang & Chen*, 2017]; thus the Rossby wave component is enhanced, which substantially slows down the eastward propagation.

The result from the trio-interaction model suggests that the coupled Rossby-Kelvin structure of the MJO should not be taken as a Gill pattern. The Gill pattern has a Rossby-Kelvin intensity ratio of 2.2, while observed MJO shows a Rossby-Kelvin ratio about 1.0 [*Wang & Lee*, 2017]. This difference arises primarily from the nature of atmospheric heating: In the Gill solution, the heating is given (the dynamic feedback is not allowed), whereas in the MJO, heating is interactive with equatorial waves, thereby the structure varies depending on how convective heating is parameterized.

Based on the trio-interaction theory, the BL convergence feedback and congestus/ shallow cloud heating can have a positive feedback, which implies that this interactive process should be represented correctly in numerical modeling of MJO, including the lower-tropospheric convective mixing and low-cloud feedback, shallow and congestus cumulus and BL turbulence parameterization. MJO simulations may be improved if shallow and congestus cloud heating and their interaction with BL moisture convergence can be enhanced in models. This has been demonstrated by global model experiments [*Yang and Wang* 2018].

The theory suggests that diagnosis of structural asymmetry may help reveal the model deficiency in representing complex trio-interaction processes. The zonal structural asymmetry generated by BL convergence feedback includes the phase leading of BL moisture convergence to major convection, lower tropospheric moistening and

destabilization (increase of the convective instability) because of the BL convergence, the 700hPa diabatic heating, and generation of MJO available potential energy. These implications have led to a new dynamics-oriented diagnostic metric for MJO simulation [*Wang et al.,* 2018]. Additionally, in this theory the energy released from convective heating comes from the basic state moist static energy that is largely controlled by the surface air specific humidity or the basic state SST.

7.6 Summary

The convection-dynamics-moisture trio-interaction theory suggests that the MJO originates from the interaction among the diabatic heating from convection and radiation, moisture, and dynamics (frictionally-driven BL convergence and equatorial waves). The general model with a simplified Betts-Miller cumulus parameterization scheme produces a trio-interaction mode that is unstable at the planetary-scales, propagates eastward and exhibits a coupled Kelvin-Rossby wave structure. The trio-interaction theory predicts BL low-pressure and convergence leads MJO major convection, which is consistent with observations [*Madden & Julian*, 1972; *Hendon & Salby*, 1994; *Salby et al.,* 1994*; Jones & Weare*, 1996; *Maloney & Hartmann*, 1998, *Matthews*, 2000; *Sperber*, 2003; *Lin et al.*, 2004; *Tian et al*., 2006]. In both observation [*Benedict & Randall*, 2007; *Hsu & Li*, 2012] and model simulation [*Jiang et al*., 2015] BL convergence has been found to be closely associated with eastward propagation, shallow/congestus cloud heating east of an MJO convection center, and vertically rearward titled structure of the MJO. Models simulating realistic MJO propagation exhibit a structure with leading BL convergence that is consistent with this theory [*Wang & Lee,* 2017]. According to this theory, the BL frictional convergence stimulates MJO eastward propagation in GCMs by moistening the lower troposphere to the east of a precipitation center.

The theory demonstrates the dependence of the MJO structure on cumulus parameterization schemes and reveals the dependence of MJO propagation on its zonal structural asymmetry (relative intensity of the "Rossby wave" westerly versus "Kelvin wave" easterly). Such asymmetry has been commonly documented by observations and global model simulations. The observed and realistically simulated MJO eastward propagations are characterized by stronger Kelvin easterlies than Rossby westerlies in the

lower troposphere, while models that simulate strong Rossby westerlies tend to show a stationary MJO [*Wang & Lee*, 2017; *Wang et al.*, 2018].

7.7 Limitations

The results of the theory depend on a constant BL depth and a Rayleigh frictional coefficient of O($10^{-5}S^{-1}$) that was considered to be too large [*Moskowitz & Bretherton*, 2000]. However, diagnosis of the surface momentum balance over the tropical Pacific Ocean indicates that an adequate value for the Rayleigh frictional coefficient is O ($10^{-5}S^{-1}$) [*Murphree & van den Dool*, 1988; *Murakami et al.*, 1992; *Deser* 1993]. So, it remains an issue regarding the value of boundary-layer damping coefficient. Embracing all known major processes makes this theory capable of comparison of four feedback processes, but also makes it less distinct except for the boundary-layer dynamics. Although it has been demonstrated with a coupled climate model that enhanced boundary-layer convergence feedback to the lower tropospheric heating in both the Tidtke and relaxed Arakawa–Schubert convective schemes have significantly improved the quality of MJO simulation [*Yang & Wang*, 2018], it remains to be seen whether this test result applies to other models. The propagation speed of the MJO is sensitive to SST is another issue [*Wang & Chen*, 2017].

7.8 Recommendations for Further Evaluation

The key to test this theory independently lies in its assumption of the key role of the BL interaction with lower tropospheric heating in MJO physics. While multiple studies indicate that boundary-layer motions are important to the MJO [*Maloney & Hartmann*, 1998; *Lee et al*., 2003; *Hsu & Li*, 2012], other studies argue that they are of little relevance [*Chao & Chen*, 2001; *Kim et al*., 2011; *Shi et al*., 2018]. BL convergence can be driven by friction and interact with shallow cloud diabatic heating and cloud-scale eddies [*Stevens et al*., 2002; *Back & Bretherton*, 2009]. It is desirable to quantify the relative contributions of these processes to total BL convergence. Constraining BL in GCMs in ways to test the theory should be considered very carefully. Sensitivity and mechanism-denial experiments of the BL interaction with shallow cloud heating can help evaluate this theory.

8. COMPARISON

In this section we compare the four MJO theories summarized in sections 4 – 7. We first list the assumptions that apply to all four theories (section 8.1). Then we distinguish assumptions for specific theories (section 8.2). This is followed by a discussion on the different selection mechanisms proposed by the four theories (section 8.3). The degrees to which these theories meet the criteria set in section 2 are examined (section 8.5).

All notations used in the four theories are not the same, making a direct comparison difficult. To facilitate their direct comparison, the notations in the trio-interaction theory are used, because this model includes a variety of parametrization processes (section 7.5) and each of the theories can be presented to a certain degree by this general model through introducing different assumptions.

8.1 Common assumptions and limitations

The common assumptions that are made in all four theories are the same as those used to derive the general framework in Eq. 2. Briefly, they are: (a) Boussinesq approximation, (b) MJO as an atmospheric internal mode with the first baroclinic vertical structure, (c) an equatorial beta plane, and (d) linear and hydrostatically balanced large-scale motions (top five rows in Table 1).

These common assumptions simplify the mathematical framework and allow analytical solutions in most cases. They, however, make it impossible to study (i) roles of atmosphere-ocean interaction (assumption b), (ii) effects of higher vertical modes related to stratiform and lower-tropospheric heating (assumption b), and (iii) effects of nonlinear advection (assumption e). Some of these limitations have already been studied using more complicated models and some remain to be elucidated in future work.

8.2 Specific assumptions and approximations

The four theories include different processes based on various assumptions and approximations (Table 1).

(1) Resting basic state. This assumption is made in all but the moisture-mode theory, where a mean easterly is assumed. This assumption eliminates the possibility of studying the seasonality and interannual variability of the MJO.

(2) Wave activity. This assumption is unique to the skeleton theory, where it is used to parameterize convection. This assumption can be accommodated in the trio-interaction theory.

(3) Cloud-radiative heating. This is essential in the moisture-mode theory, where it is responsible for planetary wave selection. It is also included in the trio-interaction theory, although it is not essential. This process is neglected in the skeleton and gravity-wave theories.

(4) Horizontal moisture advection. It is essential in the moisture-mode theory but of secondary importance in the trio-interaction theory. This process is not included in the skeleton and gravity-wave theories.

(5) Long wave approximation. This assumption is made explicitly in the skeleton and trio-interaction theories. It is implicit in the moisture-mode theory through steady-state assumption for the motion. The gravity-wave theory is the only one of the four that does not make this assumption.

(6) Boundary-layer dynamics. This is essential only in the trio-interaction theory. It is of secondary importance in the moisture-mode theory. It is not included in the skeleton and gravity-wave theories.

(7) No zonal momentum tendency. This assumption is made only in the moisture-mode theory.

(8) Weak temperature gradient approximation. This assumption is made only in the moisture-mode theory, where temperature tendency is ignored.

(9) Moisture tendency. This is neglected only in the gravity-wave theory. It is essential to the other three theories.

(10) Rossby-Kelvin structure. It is represented dynamically in the skeleton theory, assumed steady-state in the moisture-mode theory, and a product of the long-wave approximation in trio-interaction theory. It is not assumed or produced in the gravity-wave theory.

(11) Positive-only precipitation. This assumption is made in the gravity-wave theory and in a nonlinear version of the trio-interaction theory.

(12) Linear damping of momentum and Newtonian cooling. They are included in the moisture-mode and trio-interaction theories, but not the skeleton and gravity-wave theories.

(13) Radiative-convective equilibrium. This assumption is made in the skeleton and

moisture-mode theories, not in the gravity-wave and trio-interaction theories.

(13) Large-scale envelope of convection. This assumption is made in the skeleton theory in association with the wave activity concept. It is implied in the gravity-wave theory. The moisture-mode and trio-interaction theories do not include this assumption.

(14) Convective trigger. This assumption is made only in the gravity-wave theory.

Several processes are parameterized in different ways in the four MJO theories (Table 2)

(1) Convection. In the skeleton theory, precipitation and convective heating are parameterized in terms of wave activity and lower-tropospheric moisture. Precipitation is parameterized as a linear function of column integrated moisture in the moisture-mode theory. In the gravity-wave theory, convection is parameterized as intermittent storms that are triggered when geopotential is below a given threshold. Different parameterization schemes yield different results in the trio-interaction theory. One of them is a simplified Betts-Miller parameterization scheme.

(2) Cloud-radiation feedback. In the moisture-mode theory, this is parameterized to be proportional to precipitation and decaying exponentially with zonal wavenumber. In the trio-interaction theory, it is assumed constant but can be parameterized as in the moisture-mode theory. Cloud-radiation feedback is not included in the skeleton and gravity-wave theories.

(3) Wave activity. This is included only in the skeleton theory as part of its parameterization of convective heating. It is formulated to oscillate against lower-tropospheric moisture.

(4) Moisture advection parameter. This is parameterized only in the moisture-mode theory as a sum of moistening processes by meridional and zonal winds.

The four MJO theories also differ from each other in terms of the value of main parameters and constants they use (Table 3). Because of the different assumed processes, approximations, parameterizations, and constants applied to the four MJO theories, further research is needed to confirm what processes are necessary and sufficient for the MJO and what parameter ranges are realistic for the MJO.

8.3 Interpretation of the basic features of the MJO

The four theories provide different interpretations for the most fundamental

features of the MJO, namely, its spatial scale and eastward propagation speed (Table 4).

Selection of planetary scale: In the skeleton theory without stochastic damping, the zonal scale of the MJO is selected when the predicted horizontal structure of the MJO matches the observed. In its stochastic version, the selection is through stochastic damping of small scales. In the moisture-mode theory, the zonal scale is selected by the vertical motion imparted by anomalous radiative heating that is stronger for larger scales. In the gravity-wave theory the horizontal scale is determined by the travel distance of gravity waves and intensity of precipitation. The trio-interaction theory selects the zonal scale through instability generated by BL convergence and damping of small scales by tropospheric moisture feedback. When BL convergence feedback is added to the skeleton theory, it generates an unstable planetary-scale mode.

Selection of eastward propagation: The skeleton theory produces neutral solutions that propagate both eastward and westward. At planetary scales, the eastward propagating solutions match the observed features of the MJO (horizontal structure, propagation speed) whereas the westward propagating solutions do not. In the moisture-mode theory, the eastward propagation is caused by advection of moisture by the wind anomalies. In the gravity-wave theory, the MJO propagates eastward because EIG travels faster than WIG due to the β effect. In the trio-interaction theory, the BL moisture convergence generates positive moisture and heating anomalies to the east of an MJO convection center, leading to its eastward propagation.

The slow propagation speed: In the skeleton theory, the key factor for the speed is the wave activity parameter (Γ). In the moisture-mode theory, the dry static stability, the strength of moisture advection, and convective moisture adjustment timescale determine the propagation speed. The small difference between the speeds of EIG and WIG gives rise to the MJO speed in the gravity-wave theory. In the trio-interaction theory, the MJO propagation speed is determined by three factors: (a) the basic state MSE, which affects the heating intensity and effective static stability, (b) moisture feedback which enhances the Rossby wave component and slows down the eastward propagation, and (c) the coupling of Kelvin and Rossby waves.

8.4 Feedback processes

The different assumptions made in the four theories (section 8.2) lead to different explanations for MJO dynamics (section 8.3). Properties of the MJO solutions also depend on the convection parameterization [Wang et al. 2016]. It is fundamental to understand the critical processes described in these theories. To this end, we further compare how various feedback processes are responsible for the major features of the MJO in the four theories.

There are six most relevant feedback processes in the four MJO theories. They are the BL feedback, moisture feedback, Kelvin-Rossby wave feedback, cloud-radiation feedback, gravity-wave feedback, and wave-activity feedback. There is also wind-evaporation feedback [*Emanuel*, 1987; *Neelin et al*., 1987]. It is not essential in any of the four theories reviewed here but is the base for other versions of the moisture-mode theory [*Fuchs & Raymond*, 2017; *Khairoutdinov & Emmanuel*, 2018; section 5.5.1].

Table 5 summarizes the roles of these feedbacks in the four theories. The top row of Table 5 lists the six feedback processes and left column the key observed features of the MJO. Their connections to the individual MJO theories described in sections 4 – 7 are marked in the table. Several other studies using the trio-interaction theory also include these feedback processes [*Wang et al*., 2016; *Wang & Chen*, 2017; *Liu & Wang*, 2017; *Chen & Wang*, 2018].

The BL feedback represents the effect of BL frictional moisture convergence on convection. It is present in both moisture-mode and trio-interaction theories. In the trio-interaction theory it plays an essential role in the feedback of the equatorial Kelvin and Rossby waves to convective heating, selecting preferred eastward propagation, and generating a planetary-scale unstable mode. In the moisture-mode theory, this feedback plays a secondary role of enhancing MJO propagation but it is not allowed to produce MJO instability. The skeleton and gravity-wave theories do not include this feedback. This is a fundamental discrepancy among the four MJO theories. BL moisture convergence leading the MJO convection has been repeatedly observed [*Maloney & Hartmann* 1998, *Lee et al*., 2003; *Hsu & Li*, 2011]. As recommended in section 7.8, the degree to which the observed BL moisture convergence is caused by BL friction and other processes (i.e., cloud heating and large-scale eddies) need to be quantified.

The moisture feedback refers to the effect of evolving tropospheric moisture on convection. It is included in three MJO theories. In the skeleton theory, lower-tropospheric

moisture is coupled with the wave activity function to determine the strength of convective heating. The column moisture dynamics are crucial to the eastward propagation of the MJO and help produce instability in the moisture-mode theory. In the trio-interaction theory, it mainly acts to reduce the propagation speed, suppresses the growth of short waves, and improves the horizontal structure. This feedback is not included in the gravity-wave theory. This fundamental discrepancy can be pushed to an extreme as to whether the MJO is a dry mode (section 9).

The Kelvin-Rossby wave feedback represents the role of the Kelvin-Rossby dynamics in the MJO. In the skeleton theory it generates horizontal moisture convergence. In the moisture-mode theory, it provides the main mechanism for the horizonal moisture advection. This feedback plays an essential role in the trio-interaction theory by slowing down eastward propagation and increasing the growth rate for planetary waves. This feedback is not included in the gravity-wave theory.

The cloud-radiative feedback is the enhancement of total diabatic heating by large-scale cloud radiative heating. In the moisture-mode theory, it provides the main mechanism for instability and the spatial-scale selection of the MJO. In the trio-interaction theory, this feedback is secondary but can generate instability and produce a preferred planetary-scale unstable mode only if the feedback coefficient depends on the wavenumber as in the moisture-mode theory. The skeleton and gravity-wave theories do not include this feedback. This is another fundamental discrepancy among the four MJO theories. As recommended in section 5.8, whether the cloud-radiative feedback is scale-dependent needs further evidence.

The gravity-wave feedback represents the role of synoptic-scale gravity waves in the MJO. It is essential to determine the scale selection and eastward propagation of the MJO only in the gravity-wave theory. This feedback can also be parameterized in the trio-interaction theory, but it does not play any significant role [*Wang & Chen*, 2017]. Whether gravity waves are essential to the MJO needs to be supported by evidence of their coherence in space and time.

The wave-activity feedback is viewed as a planetary-scale envelope of synoptic- and meso-scale convective heating that interacts with large-scale moisture only in the skeleton theory, where it is used to parameterize large-scale convective heating of the MJO.

It remains to be confirmed whether interaction between synoptic and large-scale convective activities can be represented in such a simple form.

8.5 Other discrepancies

There is another fundamental but unsettled discrepancy among the four theories: whether multi-scale interaction is explicitly required. It is for the skeleton and gravity-wave theories, but not for the other two. Multi-scale structures of the MJO have been commonly observed [*Nakazawa*, 1988; *Chen et al*., 1996; *Kikuchi et al*., 2017]. Their roles in the MJO have long been speculated but explored theoretically only during the last decade [*Majda & Biello*, 2004; *Biello & Majda*, 2005; *Majda & Stechamann*, 2009; *Wang and Liu, 2011; Khouider el al*., 2012; *Liu and Wang, 2012, 2013*]. Observational studies are not in clear agreement on whether specific waves preferentially occur during MJO events [*Kikuchi et al*., 2017; *Dias et al*., 2017].

Other properties of the MJO are also produced by the four theories to different extents. The MJO is unstable in the moisture-mode and trio-interaction theories but neutral in the skeleton and gravity-wave theories. The moisture-mode theory produces westward group velocity for the MJO, while the trio-interaction theory produces negligible group velocity. The skeleton theory may produce a westward group velocity in the presence of a warm pool. Whether the observed MJO has westward group velocity is a matter of debate [*Adames & Kim*, 2016; *Chen & Wang*, 2018].

8.6 Evaluation against criteria for MJO theories

Based on the discussions presented, we conclude that all four theories meet the MJO theory criteria proposed in section 2 to varying degrees with the limitations discussed in subsection 7 for each theory. As pointed out earlier, further work is needed to justify some of the assumptions made and approximation/parameterization adopted in these theories.

9. Additional remarks

9.1 Recent developments

There have been new theories published during the preparation of this article. The MJO has been interpreted in terms of vortex dynamics. *Yano and Tribbia* [2017] describe

the vortex pair west of an MJO heating center as the main MJO structural element. The slow eastward propagation arises from a nonlinear solitary Rossby-wave solution to a shallow-water system. In *Hayashi and Itoh* [2018], the vortex pair slowly moves eastward because of strong stretching of planetary vorticity in the lower troposphere due to deep convection. In this study, convection does not result from a prognostic moisture equation. Rather, it is prescribed from vertical velocities at the top of the boundary-layer in a manner similar to wave-CISK [*Lindzen,* 1974]. These two studies do not deny the importance of moisture, diabatic heating and the Kelvin-wave structure east of an MJO convection center. But they suggest that to a leading–order approximation, the slow eastward propagation of the MJO might be explained in terms of dry dynamics of cyclonic vortex pair ("Rossby vortices") typically observed west of an MJO heating center.

In a sharp contrast, *Fuchs and Raymond* [2017] obtained a v=0 solution from a set of linear equations on the equatorial β-plane including moisture and buoyancy (section 5.5.1). This solution, with its spatial structure of zonal wind commonly observed east of an MJO convection center, has the greatest growth rate at the lowest zonal wavenumber (k=1). The Rossby-vortex dynamics plays no role in the dynamics of their wave solution. The weak temperature gradient approximation is not strictly made in this theory to allow global-scale instability, which is distinct from the moisture-mode theory discussion in section 5. *Khairoutdinov and Emanuel* [2018] further advances the original WISHE theory of the MJO [*Emanuel* 1987] by including cloud-radiative feedback (section 5.5.1). Even though their solution includes structure of vortices, they do not play an essential role in determining the growth rate and phase speed of the MJO, as in *Fuchs and Raymond* [2017].

These four recent studies contrast the theories that place the Rossby-Kelvin couplet structure at the center of the MJO dynamics (sections 4, 6 and 7). Differences among the four MJO theories reviewed in this article and perhaps other newly developed MJO theories illustrate the progress made during the past decade or so in regard to the understanding of MJO dynamics. They also demonstrate the need of further advances in the understanding: Either the MJO can be driven by any of the proposed mechanisms, or our current diverse thinking on MJO dynamics needs to converge.

9.2 Future directions

As stated in section 2, explaining the spatial and temporal scale selection is most fundamental to an MJO theory. It is desirable, however, that an MJO theory also explains other observed features of the MJO. Among all, the life cycle of the MJO is perhaps the most basic next to the scale selection. The complete life cycle of the MJO consists of three major stages: initiation, propagation over the Indo-Pacific warm pool, and termination of its convection over the central and eastern Pacific. All MJO theories include explanations for the eastward propagation. Some of them can explain the termination of the MJO over the cold sea surface of the central and eastern Pacific cold tongue: the required background state (e.g., diabatic heating, moisture gradient, density of storms) no longer exists. A complete theory of the MJO should also explain its initiation.

MJO initiation takes place in the tropics over a wide range of longitudes [*Matthews*, 2008], but mainly over the Indian Ocean [*Zhang & Ling*, 2017]. A main mystery of MJO initiation is its irregularity. There appears to be random occurrence of MJO initiation in a group of more than one, which is known as successive MJO events, and isolated MJO initiation without any immediately preceding or following event, known as the primary MJO [*Matthews*, 2008]. These two types of MJO initiation should be explained by an MJO theory. The irregularity of the MJO may be related to stochastic processes in the atmosphere (section 4.3).

Most MJO events initiated over the Indian Ocean become weakened when they propagate over the Indo-Pacific Maritime Continent (MC). A large fraction (up to 40-50%) of them terminate prematurely over the MC [*Zhang & Ling*, 2017; *Kerns & Chen,* 2020] and fail to propagate into the Pacific. This is known as the barrier effect of the MC on the MJO. If the MJO is driven by moisture variability (sections 4, 5, and 7), then it is natural to consider the barrier effect in term of moisture supply [*Kim et al*., 2014, 2017; *Feng et al*., 2015]. A significant difference in moisture transport over the MC between MJO events that propagate through the MC and those that do not has yet to be established [*Zhang & Ling*, 2017]. MJO events that cross the MC exhibit an MSE signature that propagates to the south of the islands of the MC instead of propagating across them [*Kim et al.,* 2017]. Using detailed diagnostics of MJO propagation over the MC based on the dynamical processes established by the MJO theories [*Wang et al.,* 2018] may determine if the current MJO theories can explain the barrier effect of the MC.

It has been shown that MJO properties are related to the stratospheric quasi-biennial oscillation (QBO), particularly in boreal winter [*Liu et al*., 2014; *Yoo & Son*, 2016; *Nishimoto & Yoden*, 2017; *Son et al.,* 2017]. Stronger MJO activity tends to occur more frequently during QBO easterly phases than westerly phase. This is manifested as a greater number of MJO events initiated over the Indian Ocean and longer zonal propagation due to a weaker barrier effect of the MC [*Son et al*., 2017; *Zhang & Zhang*, 2018]. Several mechanisms have been proposed to explain this QBO-MJO connection in terms of the tropopause height and temperature, vertical wind shear across the tropopause, upper-tropospheric static stability, and solar activity [*Yoo & Son*, 2016; *Hood*, 2017; *Nishimoto & Yoden*, 2017, *Martin et al.*, 2019]. None of these are based on the existing MJO theories. None of the existing MJO theories consider the variability of the tropopause essential to the MJO. Explaining the observed QBO-MJO connection provides another opportunity to test MJO theories.

It is desirable to diagnose MJO simulations by numerical models using metrics based on the dynamical processes established by the MJO theories [*Wang et al*., 2018]. Improved MJO simulations must, however, be a natural consequence of overall model advancement in all aspects, instead of tuning to benefit only MJO simulations. Diagnoses of MJO simulations using metrics based on dynamical processes should be part of the general model evaluation. It is desirable to have metrics based on a dynamic framework that include equatorial waves as well as the MJO [*Stechmann and Hottovy*, 2017].

In summary, the reviewed four MJO theories have demonstrated a diversity in the explanations for the propagation and scale selection mechanisms of the MJO. The four distinct theories presented here and others represent a major advancement of our understanding of the MJO. It is still a challenge to determine which mechanisms are most fundamental to the observed MJO. The disagreements of the four theories point to future opportunities: understanding and reconciling the disagreements by combining observations and novel modeling strategies could be the path toward the next breakthroughs.

Acknowledgements: The authors would like to thank Brandon Wolding and two anonymous reviewers for their candid and constructive comments on an earlier version of this manuscript. We also thank co-authors of the original papers on the theories, Daehyun

Kim and Sam Stechmann, for their comments on the manuscript. Discussions with and comments from Eric Maloney, Adam Sobel, and Sulian Thual on various parts of this article are appreciated. This study was supported by the National Oceanic and Atmospheric Administration (NOAA) grant NA15OAR4310099 and the National Science Foundation (NSF) Climate Dynamics Division grants AGS-1540783 to BW; by the NSF Climate Dynamics Division grant AGS-1841559 to ÁFA; by the U.S. Department of Energy, Office of Science, Office of Biological and Environmental Research, Climate and Environmental Sciences Division, Regional & Global Climate Modeling Program, under Award DE-AC02-05CH11231, the Laboratory Directed Research and Development (LDRD) funding from Berkeley Lab, provided by the Director, Office of Science, of the U.S. Department of Energy under Contract DE-AC02-05CH11231, and a Packard Fellowship for Science and Engineering to DY, and by NOAA grant NA13OAR310161 and Office of Naval Research PISTON grant via Colorado State University to CZ. This is PMEL contribution 4789 (CZ). No data were used in this study except those from the cited references.

Glossary

anticyclonic: Clockwise in the Northern Hemisphere, counterclockwise in the Southern Hemisphere

convective available potential energy (CAPE): The maximum buoyancy of an undiluted air parcel, related to the potential updraft strength of thunderstorms

convective inhibition (CIN): The amount of energy required to overcome the negatively buoyant energy the environment exerts on an air parcel to prevent it from becoming free convective

baroclinic: Variation with depth of motions associated with variation of density with depth. In this review this term describes vertical structures in which winds or currents reverse directions.

β-effect: Effect of Earth's rotation and curvature on its fluid

β-plane: An approximation of the spherical earth as a plane with a rate of rotation (corresponding to the Coriolis parameter) that varies linearly with the north–south distance

Betts-Miller scheme: A numerical representation of atmospheric convection based on the relaxation of temperature and moisture towards a quasi-equilibrium thermodynamic structure; designed by *Betts and Miller* [1986]

Boussinesq approximation: Density variations are ignored except where they appear in terms multiplied by the gravity, introduced by Joseph Valentin Boussinesq (1842–1929).

Buckingham Pi theorem: An equation involving n number of physical variables which are expressible in terms of k independent fundamental physical quantities can be expressed in terms of p = n - k dimensionless parameters

convective instability of the second kind (CISK): A process whereby lower-tropospheric convergence in the wind field produces convection and cumulus formation, thereby releasing latent heat

congestus: A form of cumulus cloud with their tops normally below 6,000 m

cyclonic: Counterclockwise in the Northern Hemisphere, clockwise in the Southern Hemisphere

diabatic heating: A thermodynamic process in which the system (e.g. an air parcel) exchanges energy with its surroundings by virtue of a temperature difference between them

dispersive waves: Waves of different wavelengths travel at different phase speeds

effective gross moist stability: A measure of the *NGMS* that incorporates the energetic input of radiative heating

empirical orthogonal function (EOF): A method of decomposing a signal in terms of orthogonal basis functions in time and/or space determined from data

equatorial β-plane: An approximation where the Coriolis parameter is set to vary linearly in latitude from its value of zero at the equator

Gill model: Steady-state linear shallow-water equations with a prescribed, isolated heating source centered at or near the equator, derived by *Gill* (1980)

geopotential: The potential energy of a unit mass relative to sea level, numerically equal to the work that would be done in lifting the unit mass from sea level to the height at which the mass is located. Also known as geopotential height or dynamic height (in oceanography).

gross moist stability (GMS): The net column divergence of vertically-integrated vertical moist static energy advection, measuring the efficiency of the advective export of moist static energy by large-scale circulations. Positive (negative) GMS corresponds to net export (input) of energy

group velocity: The velocity of the envelope of a group of waves of nearly equal frequencies

gross moist stability: Ratio of vertically integrated horizontal divergence of a conserved quantity in adiabatic processes to a measure of the strength of moist convection per unit of area

inertio-gravity waves: Gravity waves (waves with restoring force by gravity and buoyancy) in a rotating system with kinetic energy being its only energy form

Indian Ocean Dipole (IOD): An irregular oscillation of sea-surface temperatures in which the western Indian Ocean becomes alternately warmer and then colder than the eastern part of the ocean

Kelvin wave: A type of low-frequency gravity wave trapped to a vertical boundary, or the equator, which propagates anticlockwise (in the Northern Hemisphere) along the boundary (or equator)

Kuo scheme: A parameterization scheme in which precipitation is proportional to the amount of lower-tropospheric moisture convergence, designed by *Kuo* [1974]

law of mass action: The rate of an elementary reaction is proportional to the product of the concentration of the reactants

long-wave approximation: The ratio between meridional and zonal length scales is sufficiently small that meridional wind is negligibly small, geostrophic balance holds in the meridional direction, and *inertio-gravity waves* can be ignored.

meso-scale: Horizontal scales ranging from a few to several hundred kilometers

moist static energy: A thermodynamic variable calculated by hypothetically lifting air adiabatically to the top of the atmosphere and allowing all water vapor present in the air to condense and release latent heat

Navier–Stokes equations: A set of equations describing the velocity, pressure, temperature, and density of a viscous fluid

normal mode: A pattern of motion in which all parts of the system move sinusoidally with the same frequency and with a fixed phase relation

normalized gross moist stability (NGMS): The ratio of *gross moisture stability* to intensity of convection per unit area (e.g., vertically integrated dry static energy advection)

mixed layer: A layer in which active turbulence homogenizes over a range of depths

planetary boundary layer: The lowest part of the atmosphere that is directly influenced by its contact with a planetary surface

planetary scale: A length of the same general order as the planetary radius

quasi-equilibrium: A state in which the system deviates from equilibrium only by an infinitesimal amount

real-time multivariate MJO (RMM) index: An index measuring the phase and amplitude of the MJO derived from an *EOF* analysis of upper- and lower-level zonal winds and outgoing long-wave radiation designed by *Wheeler and Hendon* [2004]

Rossby wave: A wave in the atmosphere or ocean that owes its existence to the Earth's rotation

shallow-water equations (model): A set of equations simplified from the *Navier–Stokes equations* by vertical integration in the case where the horizontal length scale is much greater than the vertical length scale

static stability: The ability of a fluid at rest to resist the effects of buoyancy to become turbulent or laminar

stratiform clouds: Clouds of extensive horizontal development, as contrasted to the vertically developed cumuliform types

stratospheric quasi-biennial oscillation (QBO): An oscillation in the zonal winds of the equatorial stratosphere with a period between 24 and 30 months

synoptic scale: Length from several hundred kilometers to several thousand kilometers

wave-CISK: A form of *CISK* where lower-tropospheric convergence is provided by waves

weak temperature gradient (WTG) approximation: The dominant energy balance in the tropical free troposphere is between diabatic heating **(**cooling**)** and adiabatic cooling **(**warming**)** when the relatively weak horizontal temperature gradient is ignored.

Wheeler-Kiladis spectra: Two-dimensional (in zonal wavenumber and frequency) spectra normalized by background noise to highlight signals of equatorial waves, designed by *Wheeler and Kiladis* [1999]

wind-evaporation feedback (WEF): Enhanced surface evaporation due to wind anomalies as a main energy source for atmospheric perturbations

wind-induced surface heat exchange (WISHE): Same as *WEF*

References

Adames, Á. F. (2017). Precipitation budget of the Madden-Julian Oscillation, *Journal of the Atmospheric Sciences*, *74*(6), pp.1799-1817.

Adames, Á. F., & Kim, D. (2016). The MJO as a Dispersive, Convectively Coupled Moisture Wave: Theory and Observations. J. Atmos. Sci., 73 (3), 913-941.

Adames, Á. F., Kim, D., Sobel, A. H., Del Genio, A. & Wu, J. (2017a). Changes in the structure and propagation of the MJO with increasing CO2, J. Adv. Model. Earth Syst., 9, doi:10.1002/2017MS000913.

Adames, Á.F., Kim, D., Sobel, A.H., Del Genio, A. and Wu, J., (2017b). Characterization of moist processes associated with changes in the propagation of the MJO with increasing CO2. *Journal of advances in modeling earth systems*, *9*(8), pp.2946-2967.

Adames, Á. F., & Wallace, J. M. (2014). Three-dimensional structure and evolution of the vertical velocity and divergence fields in the MJO. J. Atmos. Sci., 71, 4661–4681.

Adames, Á. F., & Wallace, J. M. (2015). Three-Dimensional Structure and Evolution of the Moisture Field in the MJO. J. Atmos. Sci., 72 (10), 3733-3754.

Adames, Á.F., Wallace, J.M., & Monteiro, J.M. (2016). Seasonality of the structure and propa- gation characteristics of the MJO, J. Atmos. Sci., 73, 3511-3526.

Ahmed, F. & Neelin, J.D. (2018). Reverse engineering the tropical precipitation-buoyancy relationship. *Journal of the Atmospheric Sciences*, (2018).

Ahmed, F., & Schumacher, C. (2015). Convective and stratiform components of the precipitation-moisture relationship. Geophysical Research Letters, 42 (23), 10,45310,462,

Ahn, M.-S., Kim, D., Sperber, K.R., Kang, I.-S., Maloney, E., Waliser, D., Hendon, H. on behalf of WGNE MJO Task Force. (2017). MJO Simulation in CMIP5 Climate Models: MJO Skill Metrics and Process-Oriented Diagnosis. *Climate Dynamics* 49, no. 11: 4023–45.

Ajayamohan, R.S., Khouider, B., & Majda, A.J. (2013). Realistic initiation and dynamics of the Madden-Julian oscillation in a coarse resolution aquaplanet GCM. Geophys Res Lett 40:62526257

Andersen, J. A., & Kuang, Z. (2012). Moist Static Energy Budget of MJO-like Disturbances in the Atmosphere of a Zonally Symmetric Aquaplanet. J. Climate, 25

(8), 2782-2804.

Anderson, J. R., & Stevens, D. E. (1987). The response of the tropical atmosphere to low frequency thermal forcing, J. Atmos. Sci., 44, 676–686.

Arnold, N. P., & Randall, D. A. (2015). Global-scale convective aggregation: Implications for the Madden-Julian Oscillation, J. Adv. Model. Earth Syst., 7, 1499–1518, doi:10.1002/2015MS000498.

Barenblatt, G.I., 2003. *Scaling* (Vol. 34). Cambridge University Press.

Benedict, J. J., & Randall, D. A. (2007). Observed Characteristics of the MJO Relative to Maximum Rainfall. J. Atmos. Sci., 64 (7), 2332-2354.

Benedict, J. J., E. D. Maloney, A. H. , D. M. W. Frierson, 2014: Gross Moist Stability and MJO Simulation Skill in Three Full-Physics GCMs. J. Atmos. Sci., 71, 3327–3349, doi: 10.1175/JAS-D-13-0240.1.

Bretherton, C. S., Peters, M. E. & Back, L. E. (2004). Relationships between water vapor path and precipitation over the tropical oceans. J. Climate., 17, 1517-1528.

Betts, A. K. (1986). A new convective adjustment scheme. Part I: Observational and theoretical basis. Quarterly Journal of the Royal Meteorological Society, 112 (473), 677-691.

Betts, A., & Miller, M. (1986). A new convective adjustment scheme. Part II: Single column tests using GATE wave, BOMEX, ATEX and arctic air-mass data sets. Quarterly Journal of the Royal Meteorological Society, 112 (473), 693-709.

Biello J.A., & Majda, A.J. (2005). A new multiscale model for the Madden–Julian oscillation. J Atmos Sci 62:1694–1721

Blade, I., & Hartmann, D. L. (1993). Tropical intraseasonal oscillation in a simple nonlinear model, J. Atmos. Sci., 50, 2922– 2939.

Bretherton, C. S., Peters, M. E. & Back, L. E. (2004). Relationships between Water Vapor Path and Precipitation over the Tropical Oceans. J. Climate, 17 (7), 1517-1528.

Brown, R. G., & Zhang, C. (1997). Variability of midtropospheric moisture and its effect on cloud-top height distribution during TOGA COARE. *J. Atmos. Sci.*, **54**, 2760–2774.

Chang, C. P. (1977). Viscous internal gravity waves and low- frequency oscillations in the tropics, J. Atmos. Sci., 34, 901 – 910.

Chang, C. P., & Lim, H. (1988). Kelvin wave-CISK: A possible mechanism for the 30-50

2153 day oscillations, J. Atmos. Sci., 45, 1709 – 1720.
2154 Chao, W. C. (1987). On the origin of the tropical intraseasonal oscillation, J. Atmos. Sci.,
2155 44, 1940–1949.
2156 Chao, W. C. and B. Chen, 2001: The role of surface friction in tropical intraseasonal
2157 oscillation. Mon. Wea. Rev., 129, 896–904.
2158 Charney, J. G. (1963). A Note on Large-Scale Motions in the Tropics. J. Atmos. Sci., 20
2159 (6), 607-609.
2160 Chen, G., and B. Wang (2017): Reexamination of the wave activity envelope convective
2161 scheme in theoretical modeling of MJO. *J. Climate*, 30(3), 1127-1138.
2162 Chen, G.-S. and B. Wang (2018a): Dynamic moisture mode versus moisture mode in MJO
2163 dynamics: importance of the wave feedback and boundary layer convergence
2164 feedback. *Climate Dyn.*, doi.org/10.1007/s00382-018-4433-7.
2165 Chen. G. & Wang, B. (2018b). Does MJO have a westward group velocity? J. Climate, 31,
2166 2435-2443.
2167 Chen, S.S., Kerns, B.W., Guy, N., Jorgensen, D.P., Delanoë, J., Viltard, N., Zappa, C.J.,
2168 Judt, F., Lee, C.Y. & Savarin, A. (2016). Aircraft observations of dry air, the ITCZ,
2169 convective cloud systems, and cold pools in MJO during DYNAMO. *Bulletin of the*
2170 *American Meteorological Society*, *97*(3), pp.405-423.
2171 Chen, S. S., Mapes, B. E. & Houze Jr. R. A. (1996). Multiscale variability of deep
2172 convection in relation to large-scale circulation in TOGA COARE, J. Atmos. Sci., 53,
2173 1380–1409.
2174 Chikira, M. (2014). Eastward-propagating intraseasonal oscillation represented by Chikira-
2175 Sugiyama cumulus parameterization. Part II: Understanding moisture variation under
2176 weak temperature gradient balance. J. Atmos. Sci., 71 (2), 615-639.
2177 Chao, W. C. (1987), On the origin of the tropical intraseasonal oscillation, J. Atmos. Sci.,
2178 44, 1940–1949.
2179 Crueger, T., & Stevens, B. (2015). The effect of atmospheric radiative heating by clouds
2180 on the Madden-Julian Oscillation, J. Adv. Model. Earth Syst., 07,
2181 doi:10.1002/2015MS000434.
2182 Crum, F. X., & Dunkerton, T. J. (1992). Analytic and numerical models of wave-CISK
2183 with conditional heating, J. Atmos. Sci., 49, 1693–1708.

2184 Del Genio, A.D., Chen, Y.-H., Kim, D. and Yao, M.-S. (2012). The MJO transition from
2185 shallow to deep convection in CloudSat/CALIPSO data and GISS GCM simulations. *J.*
2186 *Climate*, **25**, 3755-3770, doi:10.1175/JCLI-D-11-00384.1.
2187 Del Genio, A.D., Wu, J., Wolf, A.B., Chen, Y.H., Yao, M.-S. & Kim, D.
2188 (2015). Constraints on cumulus parameterization from simulations of observed MJO
2189 events. *J. Climate*, **28**, no. 16, 6419-6442, doi:10.1175/JCLI-D-14-00832.1.
2190 DeMott, C. A., Klingaman, N. P. & Woolnough, S. J. (2015). Atmosphere-ocean coupled
2191 processes in the Madden-Julian oscillation, *Rev. Geophys., 53*,
2192 doi:10.1002/2014RG000478.
2193 Derbyshire, S. H., Beau, I., Bechtold, P., Grandpeix, J.Y., Piriou, J.M., Redelsperger, J.-L.
2194 & Soares, P. M. M. (2004). Sensitivity of moist convection to environmental humidity.
2195 Quart. J. Roy. Meteor. Soc, 130 (604), 3055-3079.
2196 Deser, C. (1993). Diagnosis of the surface momentum balance over the tropical Pacific
2197 Ocean. *J. Climate,* **6**, 64-74.
2198 Dias, J., Leroux, S., Tulich, S.N. and Kiladis, G.N. (2013). How systematic is organized
2199 tropical convection within the MJO?. *Geophysical Research Letters*, *40*(7), pp.1420-
2200 1425.
2201 Emanuel, K. A. (1987). An air-sea interaction model of intraseasonal oscillations in the
2202 tropics. J Atmos Sci, 44, 2324-2340.
2203 Emanuel, K., Neelin, J.D. & Bretherton, C. (1994). On large-scale circulations in
2204 convecting atmospheres, Q. J. R. Meteorol. Soc., 120, 1111–1143.
2205 Feng, J., T. Li, and W. Zhu, 2015: Propagating and nonpropagating MJO events over
2206 Maritime Continent. J. Climate, 28, 8430–8449.
2207 Flatau M, Flatau P.J., Phoebus P. & Niiler P.P. (1997). The feedback between equatorial
2208 convection and local radiative and evaporative processes: the implications for
2209 intraseasonal oscillations. J Atmos Sci 54:2373–2386.
2210 Frederiksen, J. S. (2002). Genesis of intraseasonal oscillations and equatorial waves J.
2211 Atmos. Sci. 59 2761–81
2212 Frierson, D. M., Majda, A. J. & Pauluis, O. M. (2004). Large scale dynamics of
2213 precipitation fronts in the tropical atmosphere: A novel relaxation limit.
2214 Communications in Mathematical Sciences, 2, 591-626.

Fuchs, Ž., & Raymond, D. J. (2002). Large-Scale Modes of a Nonrotating Atmosphere with Water Vapor and Cloud–Radiation Feedbacks. J. Atmos. Sci., 59, 1669-1679.

Fuchs, Ž., & Raymond, D. J. (2005). Large-Scale Modes in a Rotating Atmosphere with Radiative–Convective Instability and WISHE. J. Atmos. Sci., 62, 4084–4094, doi: 10.1175/JAS3582.1.

Fuchs, Ž., & Raymond, D. J. (2007). A simple, vertically resolved model of tropical disturbances with a humidity closure. Tellus, 59A, 344–354, https://doi.org/10.1111/j.1600-0870.2007.00230.x.

Fuchs, Ž., & Raymond, D. J. (2017). A simple model of intraseasonal oscillations, J. Adv. Model. Earth Syst., 9, 1195–1211, doi:10.1002/2017MS000963.

Kiladis, G. N., Straub, K. H. & Haertel, P.T. (2005). Zonal and vertical structure of the Madden-Julian oscillation. J Atmos Sci, 62 :27902809, 2005.

Gill, A. E. (1980). Some simple solutions for heat-induced tropical circulation. Quart. J. Roy. Meteor. Soc., 106 (449), 447-462.

Gonzalez, A. O., & Jiang, X. (2017). Winter mean lower tropospheric moisture over the Maritime Continent as a climate model diagnostic metric for the propagation of the Madden-Julian oscillation. *Geophys. Res. Lett.*, **44**, 2588–2596, doi:https://doi.org/10.1002/2016GL072430.

Gottschalck, J., and Coauthors (2010). A Framework for Assessing Operational Madden-Julian Oscillation Forecasts: A CLIVAR MJO Working Group Project. *Bull. Amer. Meteor. Soc.*, **91**, 1247-1258.

Hayashi, M. & Itoh, H. (2017). A New Mechanism of the Slow Eastward Propagation of Unstable Disturbances with Convection in the Tropics: Implications for the MJO. *Journal of the Atmospheric Sciences*, *74*(11), pp.3749-3769.

Hayashi, Y., & Golder, D. G. (1986). Tropical intraseasonal oscillation appearing in the GFDL general circulation model and FGGE data. Part I: Phase propagation, J. Atmos. Sci., 43, 3058–3067.

Hendon, H. H., & Liebmann, B. (1990). The intraseasonal (30– 50 day) oscillation of the Australian summer monsoon, J. Atmos. Sci., 47, 2909–2923.

Hendon, H.H. & Salby, M.L. (1994). The Life Cycle of the Madden-Julian Oscillation. J. Atmos. Sci., 51:22252237.

2246 Holloway, C. E., & Neelin, J. D. (2009). Moisture vertical structure, column water vapor,
2247 and tropical deep convection. J. Atmos. Sci., 66, 1665–1683,
2248 doi:10.1175/2008JAS2806.1.
2249 Hood, L. L. (2017). QBO/solar modulation of the boreal winter Madden-Julian oscillation:
2250 A prediction for the coming solar minimum, Geophysical Research Letters, 44(8),
2251 3849-3857.
2252 Hoskins, B., & Wang, B. (2006). Large-scale atmospheric dynamics. The Asian Monsoon,
2253 B. Wang, Ed., Springer, 357-415.
2254 Houze Jr, R.A., Chen, S.S., Kingsmill, D.E., Serra, Y. & Yuter, S.E. (2000). Convection
2255 over the Pacific warm pool in relation to the atmospheric Kelvin-Rossby
2256 wave. *Journal of the Atmospheric Sciences*, *57*(18), pp.3058-3089.
2257 Hsu, H.-H., Hoskins, B. J. & Jin, F.-F. (1990). The 1985/86 in- traseasonal oscillation and
2258 the role of the extratropics, J. Atmos. Sci., 47, 823–839.
2259 Hsu, P.-C., & Li, T. (2012). Role of the Boundary Layer Moisture Asymmetry in Causing
2260 the Eastward Propagation of the Madden–Julian Oscillation*. J. Climate., 25, 4914-
2261 4931.
2262 Hu, Q., & Randall, D. A. (1994). Low-frequency oscillations in radiative-convective
2263 systems, J. Atmos. Sci., 51, 1089–1099.
2264 Hu, Q., & Randall, D. A. (1995). Low-frequency oscillations in radiative-convective
2265 systems. Part II: An idealized model, J. Atmos. Sci., 52, 478–490.
2266 Hung, M. P., Lin, J. L., Wang, W. Q., Kim, D., Shinoda, T. & Weaver, S. J. (2013). MJO
2267 and convectively coupled equatorial waves simulated by CMIP5 climate models, J.
2268 Clim., 26(17), 6185–6214, doi:10.1175/Jcli-D-12-00541.1.
2269 Inoue, K. Á.F. Adames and K. Yasunaga (2020): Vertical Velocity Profiles in Convectively
2270 Coupled Equatorial Waves and MJO: NewDiagnoses of Vertical Velocity Profiles in
2271 the Wavenumber-Frequency Domain. Journal of the Atmospheric Sciences,
2272 https://doi.org/10.1175/JAS-D-19-0209.1
2273 Inoue, K. & Back, L. E. (2015). Gross Moist Stability Assessment during TOGA COARE:
2274 Various Interpretations of Gross Moist Stability. J. Atmos. Sci., 72 (11), 4148-4166.
2275 Inoue, K. & Back, L. E. (2017). Gross Moist Stability Analysis: Assessment of Satellite-
2276 based Products in the GMS Plane. J. Atmos. Sci., *J. Atmos. Sci.*, **74**, no. 6, 1819-1837,

doi:10.1175/JAS-D-16-0218.1.

Janiga, M.A. & Zhang, C. (2016). MJO Moisture Budget during DYNAMO in a Cloud-Permitting Model. *J. Atmos. Sci*., 73, 2257-2278.

Jiang X. (2017). Key processes for the eastward propagation of the Madden-Julian Oscillation based on multi-model simulations. J. Geophys. Research - Atmosphere, 122, doi:10.1002/2016JD025955

Jiang, X., & Coauthors (2015). Vertical structure and physical processes of the Madden-Julian oscillation: Exploring key model physics in climate simulations. Journal of Geophysical Research: Atmospheres.

Jiang, X., Zhao, M., Maloney, E. D. & Waliser, D. E. (2016). Convective moisture adjustment time scale as a key factor in regulating model amplitude of the Madden-Julian Oscillation, Geophys. Res. Lett., 43, doi:10.1002/2016GL070898.

Jiang, X., Adames, Á.F., Zhao, M., Waliser, D. & Maloney, E. (2018). A Unified Moisture Mode Framework for Seasonality of the Madden–Julian Oscillation. J. Climate, 31, 4215–4224, https://doi.org/10.1175/JCLI-D-17-0671.1

Jones, C., & Weare, B. C. (1996). The role of low-level moisture convergence and ocean latent heat flux in the Madden-Julian Oscillation: An observational analysis using ISCCP data and ECMWF analyses, J. Clim., 9, 3086–3104.

Johnson, R., Ciesielski, P., Ruppert, Jr., J. & Katsumata, M. (2015). Sounding-Based Thermodynamic Budgets for DYNAMO. J. Atmos. Sci. *72*(2), 598-622

Kacimi, A. & Khouider, B. (2018). The transient response to an equatorial heat source and its convergence to steady state: implications for MJO theory. *Climate dynamics*, *50*(9-10), pp.3315-3330.

Kemball-Cook, S. R., & Weare, B. C. (2001). The onset of convection in the Madden Julian Oscillation, J. Clim., 14, 780–793.

Kerns, B.W., & Chen, S.S. (2020): A 20-Year Climatology of Madden-Julian Oscillation Convection: Large-Scale Precipitation Tracking From TRMM-GPM Rainfall. Journal of Geophysical Research - Atmospheres. https://doi.org/10.1029/2019JD032142.

Khairoutdinov, M. F., & Emanuel, K. (2018). Intraseasonal variability in a cloud-permitting near-global equatorial aquaplanet model. *J. Atmos. Sci*., **75**, 4337-4355, doi:10.1175/jas-d-18-0152.1.

2308 Khouider, B., Biello, J. A. & Majda, A. J. (2010). A stochastic multicloud model for
2309 tropical convection. Comm. Math. Sci., 8, 187216.
2310 Khouider, B., Han, Y., Majda, A.J. and Stechmann, S.N. (2012). Multiscale waves in an
2311 MJO background and convective momentum transport feedback. *Journal of the*
2312 *Atmospheric Sciences*, *69*(3), 915-933.
2313 Kikuchi, K. (2014). An introduction to combined Fourier–wavelet transform and its
2314 application to convectively coupled equatorial waves. *Climate dynamics*, *43*(5-6),
2315 pp.1339-1356.
2316 Kikuchi, K., & Takayabu, Y. N. (2004). The development of organized convection
2317 associated with the MJO during TOGA COARE IOP: Trimodal characteristics.
2318 Geophys. Res. Lett., 31, L10101, doi:10.1029/2004GL019601
2319 Kikuchi, K., Kiladis, G.N., Dias, J. & Nasuno, T. (2017). Convectively coupled equatorial
2320 waves within the MJO during CINDY/DYNAMO: slow Kelvin waves as building
2321 blocks. *Climate Dynamics*, pp.1-20.
2322 Kiladis, G.N, Dias, J., Straub, K. H., Wheeler, M. C., Tulich, S. N., Kikuchi, K.,
2323 Weickmann, K. M. & Ventrice, M. J. (2014). A Comparison of OLR and Circulation-
2324 Based Indices for Tracking the MJO. Mon. Wea. Rev., 142, 1697–1715, doi:
2325 10.1175/MWR-D-13-00301.1.
2326 Kiladis, G. N., Straub, K. H. & Haertel, P. T. (2005). Zonal and vertical structure of the
2327 Madden-Julian oscillation, J. Atmos. Sci., 62, 2790–2809.
2328 Kim, D., Ahn, M.-S., Kang, I.-S. & Del Genio, A. D. (2015). Role of Longwave Cloud–
2329 Radiation Feedback in the Simulation of the Madden–Julian Oscillation. J. Climate,
2330 28 (17), 6979–6994.
2331 Kim, D., Kim, H. & Lee, M.-I. (2017). Why does the MJO detour the Maritime Continent
2332 during austral summer? Geophys. Res. Lett., 44, 2579–2587.
2333 Kim, D., Kug, J.-S. & Sobel, A. H. (2014). Propagating versus Nonpropagating Madden–
2334 Julian Oscillation Events. J. Climate, 27 (1), 111–125.
2335 Kim, D. & Maloney, E. D. (2017). Review: Simulation of the Madden-Julian oscillation
2336 using general circulation models, *The Global Monsoon System, 3rd Edition, C.-P.*
2337 *Chang et al., Eds.*, 119-130.
2338 Kim, D., Sobel, A. H., & Kang, I.-S. (2011). A mechanism denial study on the Madden-

Julian Oscillation, *J. Adv. Model. Earth Syst.*, 3, M12007, doi:10.1029/2011MS000081.

Kim, D., Sobel, A. H., Maloney, E. D., Frierson, D. M. W. & Kang, I.-S. (2011). A systematic relationship between intraseasonal variability and mean state bias in AGCM simulations. J. Climate, 24, 5506–5520, doi:10.1175/2011JCLI4177.1.

Kim, D., K. Sperber, W. Stern, D. Waliser, I.-S. Kang, E. Maloney, W. Wang, K. Weickmann, J. Benedict, M. Khairoutdinov, M.-I. Lee, R. Neale, M. Suarez, K. Thayer-Calder, and G. Zhang (2009). Application of MJO simulation diagnostics to climate models. *J. Climate*, 22, 6413-6436.

Kim, H.-M. (2017), The impact of the mean moisture bias on the key physics of MJO propagation in the ECMWF reforecast, *J. Geophys. Res. Atmos.*, 122, 7772– 7784,

Kim, H., Kim, D., Vitart, F., Toma, V.E., Kug, J. & Webster, P.J. (2016). MJO Propagation across the Maritime Continent in the ECMWF Ensemble Prediction System. J. Climate, 29, 3973–3988.

Kim, H.M., Webster, P.J., Toma, V.E. & Kim, D. (2014). Predictability and prediction skill of the MJO in two operational forecasting systems. *Journal of Climate*, *27*(14), pp.5364-5378.

Kiranmayi, L., & Maloney, E. D. (2011). Intraseasonal moist static energy budget in reanalysis data. J. Geophys. Res., 116 (D21), 1-12.

Knutson, T.R., Weickmann, K.M., & Kutzbach, J.E. (1986). Global-scale intraseasonal oscillations of outgoing longwave radiation and 250 mb zonal wind during Northern Hemisphere summer. *Monthly weather review*, *114*(3), pp.605-623.

Kuang, Z. (2008). A moisture-stratiform instability for convectively coupled waves. *Journal of the Atmospheric Sciences*, *65*(3), pp.834-854.

Kundu, P. K., Cohen, I. M., & Dowling, D.R. (2012). Fluid Mechanics. 5. ed. Elsevier.

Kuo, H. L. (1974). Further studies of the parameterization of the influence of cumulus convection on large-scale flow. *Journal of the Atmospheric Sciences*, *31*(5), 1232-1240.

Lau, K., & Peng, L. (1987). Origin of low-frequency (intraseasonal) oscillations in the tropical atmosphere. Part I: Basic theory. J Atmos Sci, 44, 950-972.

Lau, N.C. & Lau, K.M. (1986). The structure and propagation of intraseasonal oscillations

appearing in a GFDL general circulation model. *Journal of the atmospheric sciences*, *43*(19), pp.2023-2047.

Lee, M.-I., I.-S. Kang, and B. E. Mapes, 2003: Impacts of cumulus convection parameterization on aqua-planet AGCM simulations of tropical intraseasonal variability. J. Meteor. Soc. Japan, 81, 963–992.

Lee, S.-S., Wang, B., Waliser, D. E., Neena, J. M., Lee, J.-Y. (2015). Predictability and prediction skill of the boreal summer intraseasonal oscillation in the Intraseasonal Variability Hindcast Experiment, Climate Dyn., 45 (7-8), 2123-2135. DOI 10.1007/s00382-014-2461-5.

Li, X. & Cho, H. R. (1997). Development and propagation of equatorial waves. Adv. Atmos. Sci. China, 14, 323-338.

Lin, J. W.-B., Neelin, J.D. & Zeng, N. (2000). Maintenance of tropical intraseasonal variability: Impact of evaporation-wind feedback and midlatitude storms. *J. Atmos. Sci.*, **57**, 2793-2823.

Lin, X., & Johnson, R. H. (1996). Heating, moistening, and rainfall over the western Pacific warm pool during TOGA COARE, J. Atmos. Sci., 53, 3367–3383.

Lin, J. & Mapes, B.E. (2004). Radiation Budget of the Tropical Intraseasonal Oscillation. *J. Atmos. Sci.*, **61**, 2050–2062.

Lindzen, R.S. (1974). Wave-CISK in the Tropics. *J. Atmos. Sci.*, **31**, 156–179.

Ling, J., Li, C., Li, T., Jia, X., Khouider, B., Maloney, E., Vitart, F., Xiao, Z. and Zhang, C. (2017). Challenges and Opportunities in MJO Studies. *Bulletin of the American Meteorological Society*, *98*(2), 53-56.

Ling, J., Zhang, C., Wang, S., & Li, C. (2017). A new interpretation of the ability of global models to simulate the MJO, *Geophys. Res. Lett*., 44, doi:10.1002/ 2017GL073891.

Liu, C., B. Tian, K. F. Li, G. L. Manney, N. J. Livesey, Y. L. Yung, and D. E. Waliser (2014), Northern Hemisphere mid-winter vortex-displacement and vortex-split stratospheric sudden warmings: Influence of the Madden-Julian Oscillation and Quasi-Biennial Oscillation, Journal of Geophysical Research: Atmospheres, 119(22).

Liu, F., & Wang, B. (2012). A model for the interaction between 2-day waves and moist Kelvin waves. *J.Atmos. Sci.*, 69, 611-625, doi: 10.1175/JAS-D-11-0116.

Liu, F., & Wang, B. (2013). Impacts of upscale heat and momentum transfer by moist

Kelvin waves on the Madden-Julian oscillation: a theoretical model study. *Climate Dyn.*, 40(1-2), 213-224, doi: 10.1007/s00382-011-1281-0.

Liu, F., & Wang, B. (2017). Effects of moisture feedback in a frictional coupled Kelvin-Rossby wave model and implication in the Madden-Julian oscillation dynamics. Clim. Dynam., *48*(1-2), 513-522.

Ma, D., & Kuang, Z. (2016). A mechanism-denial study on the Madden-Julian Oscillation with reduced interference from mean state changes, *Geophys. Res. Lett.*, 43, 2989– 2997

Madden, R.A., & Julian, P. R. (1971). Detection of a 40–50-day oscillation in zonal wind in tropical Pacific. J. Atmos. Sci., 28, 702–708, doi:10.1175/1520-0469(1971)028,0702: DOADOI.2.0.CO;2.

Madden, R.A., & Julian, P. R. (1972). Description of global-scale circulation cells in tropics with a 40–50 day period. J. Atmos. Sci., 29, 1109–1123, doi:10.1175/1520-0469(1972)029,1109:DOGSCC.2.0.CO;2.

Majda A.J. & Biello, J.A. (2004). A multiscale model for tropical intraseasonal oscillations. Proc Natl Acad Sci USA 101:4736–4741

Majda, A. J., Franzke, C. & Khouider, B. (2008). An applied mathematics perspective on stochastic modelling for climate. Philos. Trans. Roy. Soc.,A366, 24272453.

Majda, A. J, & Stechmann, S. N. (2009). The skeleton of tropical intraseasonal oscillations. Proceedings of the National Academy of Sciences 106:8417-8422

Majda, A. J, & Stechmann, S. N. (2011). Nonlinear dynamics and regional variations in the MJO skeleton. J. Atmos. Sci., 68, 30533071.

Maloney, E. D. (2009). The moist static energy budget of a composite tropical intraseasonal oscillation in a climate model. J. Climate, 22 (3), 711-729.

Maloney, E.D, Adames, Á.F. & Bui, H.X. (2019). Madden–Julian Oscillation Changes under Anthropogenic Warming." *Nature Climate Change* 9, no. 1: 26–33.

Maloney, E.D., & Hartmann, D.L. (1998). Frictional moisture convergence in a composite life cycle of the Madden-Julian Oscillation. *J. Climate*, **11**, 2387-2403.

Martin, Z., Wang, S., Nie, J. & Sobel, A. (2019). The Impact of the QBO on MJO Convection in Cloud-Resolving Simulations. *J. Atmos. Sci.,* **76**, 669–688.

Masunaga, H. (2012). Short-term versus climatological relationship between precipitation

and tropospheric humidity. J. Climate, 25 (22), 7983-7990

Matsuno, T. (1966). Quasi-geostrophic motions in the equatorial area. J. Meteor. Soc. Japan, 44, 25-43.

Matthews, A.J. (2000). Propagation mechanisms for the Madden-Julian oscillation. *Quart. J. Roy. Meteor. Soc.*, **126**, 2637-2651.

Matthews, A.J. (2008). Primary and successive events in the Madden-Julian Oscillation. Quart. J. Roy. Meteor. Soc., 134: 439453

Matthews, A.J., Slingo, J.M., Hoskins, B.J. & Inness, P.M. (1999). Fast and slow kelvin waves in the Madden-Julian Oscillation of a GCM, Q. J. Roy. Meteor. Soc., 125, 14731498.

Moskowitz, B. M., & Bretherton, C. S. (2000). An Analysis of Frictional Feedback on a Moist Equatorial Kelvin Mode. J. Atmos. Sci., 57, 2188-2206.

Muller C.J., Back L.E., O'Gorman P.A., Emanuel K.A. (2009). A model for the relationship between tropical precipitation and column water vapor. Geophys. Res. Lett. 36: L16804, doi: 10.1029/2009GL039667

Murakami, T., B. Wang, and S. W. Lyons (1992). Summer monsoons over the Bay of Bengal and the eastern North Pacific. *J. Meteor. Soc. Japan*, **70**, 191-210.

Murphree, T. and H. van den Dool (1988). Calculating winds from time mean sea level pressure fields. *J. Atm. Sci.*, **45**, 3269-3281.

Myers, D. S., & Waliser, D. E. (2003). Three-dimensional water vapor and cloud variations associated with the Madden-Julian Oscillation during Northern Hemisphere winter, J. Clim., 16, 929 – 950.

Nakazawa, T. (1988). Tropical super clusters within intraseasonal variations over the western Pacific, J. Meteorol. Soc. Jpn., 66, 823 – 836.

National Academies of Sciences, Engineering, and Medicine. (2016). Next Generation Earth System Prediction: Strategies for Subseasonal to Seasonal Forecasts. Washington, DC: The National Academies Press. doi: 10.17226/21873.

Neena, J.M., Lee, J.-Y., Waliser, D.E., Wang, B. & Xianan, J. (2014). Predictability of the Madden-Julian Oscillation in the Intraseasonal Variability Hindcast Experiment (ISVHE). *J. Climate*, 27, 4531-4543.

Neelin, J. D., & Held, I. M. (1987). Modeling Tropical Convergence Based on the Moist

Static Energy Budget. Monthly Weather Review, 115 (1), 3-12.

Neelin, J. D., Held, I. M. & Cook, K. H. (1987). Evaporation-wind feedback and low-frequency variability in the tropical atmosphere. J Atmos Sci, 44, 2341-2348.

Neelin, J. D., & Yu, J.-Y. (1994). Modes of tropical variability under convective adjustment and the Madden–Julian oscillation. Part I: Analytical theory. J. Atmos. Sci., 51, 1876–1894.

Nishimoto, E., & Yoden, S. (2017). Influence of the Stratospheric Quasi-Biennial Oscillation on the Madden–Julian Oscillation during Austral Summer, Journal of the Atmospheric Sciences, 74(4), 1105-1125.

Ogrosky, H. R., & Stechmann, S. N. (2015). The MJO skeleton model with observation-based background state and forcing. Q. J. Roy. Met. Soc., DOI: 10.1002/qj.2552

Palmer, T. N. (2012). Towards the probabilistic Earth-system simulator: A vision for the future of climate and weather prediction. Quart. J. Roy. Meteor. Soc., 138, 841861.

Peters, M. E., & Bretherton, C. S. (2005). A Simplified Model of the Walker Circulation with an Interactive Ocean Mixed Layer and Cloud-Radiative Feedbacks. J. Climate., 18, 4216-4234.

Pritchard, M. S., & Bretherton, C. S. (2014). Causal Evidence that Rotational Moisture Advection is Critical to the Superparameterized Madden-Julian Oscillation. J. Atmos. Sci., 71 (2), 800-815.

Pritchard, M.S. & Yang, D. (2016). Response of the superparameterized Madden–Julian oscillation to extreme climate and basic-state variation challenges a moisture mode view. *Journal of Climate*, *29*(13), pp.4995-5008.

Powell, S. W. (2016). Updraft buoyancy within and moistening by cumulonimbi prior to mjo convective onset in a regional model. J. Atmos. Sci., doi:10.1175/JAS-D-15-0326.1

Powell, S. W., & Houze, Jr., R. A. (2015). Effect of dry large-scale vertical motions on initial MJO convective onset, Journal of Geophysical Research: Atmospheres, 120(10), 4783-4805.

Randall, D. A. (2013). Beyond deadlock. *Geophys. Res. Lett.*, **40**, 1-7.

Ray, P., Zhang, C., Dudhia, J., & Chen, S.S. (2009). A Numerical Case Study on the Initiation of the Madden-Julian Oscillation. *J. Atm. Sci*., 66, 310-331.

2494 Raymond, D. J. (2000). Thermodynamic control of tropical rainfall. Q.J.R. Meteorol. Soc.,
2495 126: 889–898. doi:10.1002/qj.49712656406
2496 Raymond, D. J. (2001). A new model of the Madden-Julian Oscillation. J. Atmos. Sci., 808
2497 58 (18), 2807-2819.
2498 Raymond, D. J., & Fuchs, Z. (2007). Convectively coupled gravity and moisture modes in
2499 a simple atmospheric model, Tellus, Ser. A, 59, 627–640.
2500 Raymond, D. J., & Fuchs, Z. (2009). Moisture Modes and the Madden-Julian Oscillation.
2501 J. Climate, 22 (11), 3031-3046.
2502 Raymond, D. J., Sessions, S. L., Sobel, A. H. & Fuchs, Z. (2009). The Mechanics of Gross
2503 Moist Stability. J. Adv. Model. Earth Syst., 1 (3).
2504 Roundy, P. E. (2008). Analysis of convectively coupled Kelvin waves in the Indian Ocean
2505 MJO. J. Atmos. Sci., 65, 1342–1359.
2506 Roundy, P. E., (2012). Observed structure of convectively coupled waves as a function of
2507 equivalent depth: Kelvin waves and the Madden–Julian oscillation. J. Atmos. Sci., 69,
2508 2097–2106, doi:10.1175/JAS-D-12-03.1.
2509 Rui, H. & Wang, B. (1990). Development characteristics and dynamic structure of tropical
2510 intraseasonal convection anomalies. J Atmos Sci 47:357–379
2511 Rushley, S.S., Kim, D. & Adames, Á.F. (2019). Changes in the MJO under Greenhouse
2512 Gas–Induced Warming in CMIP5 Models. *J. Climate*, **32**, 803–821.
2513 Salby, M. L., & Garcia, R. R. (1987). Transient response to localized episodic heating in
2514 the tropics. Part I: Excitation and short- time, near-field behavior, J. Atmos. Sci., 44,
2515 458–498.
2516 Salby, M.L., Garcia, R.R. & Hendon, H.H. (1994). Planetary-scale circulations in the
2517 presence of climatological and wave-induced heating. *J. Atmos. Sci*., **51**, 2344-2367.
2518 Salby, M.L. & Hendon, H.H., (1994). Intraseasonal behavior of clouds, temperature, and
2519 motion in the Tropics. *Journal of the Atmospheric Sciences*, *51*(15), pp.2207-2224.
2520 Shi, X., Kim, D., Adames, Á.F. & Sukhatme, J., 2018. WISHE-Moisture Mode in an
2521 Aquaplanet Simulation. *Journal of Advances in Modeling Earth Systems*, *10*(10),
2522 pp.2393-2407.
2523 Slingo, J. M., et al. (1996). Intraseasonal oscillations in 15 atmospheric general circulation
2524 models: Results from an AMIP diagnostic subproject, Clim. Dyn., 12, 325–357.

2525 Sobel, A.H. and Bretherton, C.S. (2000). Modeling tropical precipitation in a single
2526 column. *Journal of climate*, *13*(24), pp.4378-4392.
2527 Sobel, A., & E. Maloney, E. (2012). An idealized semi-empirical framework for modeling
2528 the Madden-Julian oscillation. J. Atmos. Sci., 69 (5), 1691{1705.
2529 Sobel, A., & E. Maloney, E. (2013). Moisture Modes and the Eastward Propagation of the
2530 MJO. J. Atmos. Sci., 70 (1), 187-192.
2531 Sobel, A., Maloney, E., Bellon, G. & Frierson, D. (2008). The role of surface fluxes in
2532 tropical intraseasonal oscillations. *Nature Geoscience*, **1**, 653-657.
2533 Sobel, A., Wang, S. & Kim, D. (2014). Moist static energy budget of the MJO during
2534 DYNAMO. J. Atmos. Sci., 71 (11), 4276-4291
2535 Sobel, A. H., Nilsson, J. & Polvani, L. M. (2001). The Weak Temperature Gradient
2536 Approximation and Balanced Tropical Moisture Waves. J. Atmos. Sci., 58 (23), 3650-
2537 3665.
2538 Son, S.-W., Lim, Y., Yoo, C., Hendon, H. H. & Kim, J. (2017). Stratospheric Control of
2539 the Madden–Julian Oscillation, Journal of Climate, 30(6), 1909-1922.
2540 Sperber, K.R. (2003). Propagation and the vertical structure of the Madden-Julian
2541 Oscillation. *Mon. Wea. Rev.*, **131**, 3018-3037.
2542 Sperber, K. R., J. M. Slingo, P. M. Inness, and K. M. Lau (1997), On the maintenance and
2543 initiation of the intraseasonal oscillation in the NCEP/NCAR reanalysis and the GLA
2544 and UKMO AMIP simulations, Clim. Dyn., 13, 769–795.
2545 Stachnik, J.P., Waliser, D.E. & Majda, A.J. (2015a). Precursor environmental conditions
2546 associated with the termination of Madden- Julian oscillation events. J. Atmos. Sci.,
2547 *72*(5), pp.1908-1931. doi: http://dx.doi.org/10.1175/JAS-D-14-0254.1
2548 Stachnik, J. P., Waliser, D. E., Majda, A. J. Stechmann, S. N. & Thual, S. (2015b).
2549 Evaluating MJO event initiation and decay in the skeleton model using an RMM-like
2550 index, J. Geophys. Res. Atmos., 120, 11,48611,508, doi:10.1002/ 2015JD023916.
2551 Stechmann, S. N., & Hottovy, S. (2017). Unified spectrum of tropical rainfall and waves
2552 in a simple stochastic model. Geophysical Research Letters, 44, 10,713–10,724.
2553 Stechmann, S. N., & Majda, A. J. (2015). Identifying the Skeleton of the Madden–Julian
2554 Oscillation in Observational Data. Mon. Wea. Rev., 143, 395-416.
2555 Stechmann, S. N., Majda, A. J. & Skjorshammer, D. (2013). Convectively coupled

waveenvironment interactions. Theor. Comput. Fluid Dyn., 27 (34), 513-532.

Stevens, B., Duan, J., McWilliams, J.C., Münnich, M. and Neelin, J.D. (2002). Entrainment, Rayleigh friction, and boundary layer winds over the tropical Pacific. *Journal of climate*, *15*(1), pp.30-44.

Sugiyama, M. (2009). The Moisture Mode in the Quasi-Equilibrium Tropical Circulation Model. Part I: Analysis Based on the Weak Temperature Gradient Approximation. J. Atmos. Sci., 66 (6), 1507-1523.

Sukhatme, J. (2014). Low-frequency modes in an equatorial shallow-water model with moisture gradients. Quart. J. Roy. Meteor. Soc., 140, 1838–1846, doi:10.1002/qj.2264.

Thual, S., & Majda, A. J. (2015). A Suite of Skeleton Models for the MJO with Refined Vertical Structure, Mathematics of Climate and Weather Forecasting, DOI: http://dx.doi.org/10.1515/mcwf-2015-0004

Thual, S., & Majda, A. J. (2016). A skeleton model for the MJO with refined vertical structure, Clim. Dyn., 46: 2773. doi:10.1007/s00382-015-2731-x.

Thual, S., Majda, A. J. & Stechmann, S. N. (2014). A stochastic skeleton model for the MJO, J. Atmos. Sci., 71, 697715.

Thual, S., Majda, A. J. & Stechmann, S. N. (2015). Asymmetric intraseasonal events in the stochastic skeleton MJO model with seasonal cycle, Clim. Dyn., 45, 603618, doi:10.1007/s00382-014-2256-8.

Tian, B., Waliser, D.E., Fetzer, E.J., Lambrigtsen, B.H., Yung, Y.L. and Wang, B. (2006). Vertical moist thermodynamic structure and spatial–temporal evolution of the MJO in AIRS observations. *Journal of the atmospheric sciences*, *63*(10), pp.2462-2485.

Tokioka, T., Yamazaki, K., Kitoh, A. & Ose, T. (1988). The equatorial 30–60-day oscillation and the Arakawa–Schubert penetrative cumulus parameterization. *J. Meteor. Soc. Japan*, **66**, 883–901.

Trenberth, K. E. (1997). The definition of el nino, Bulletin of the American Meteorological Society, 78(12), 2771-2777.

Vitart, F. & Molteni, F. (2010). Simulation of the Madden–Julian Oscillation and its teleconnections in the ECMWF forecast system. *Quart. J. Roy. Meteor. Soc.*, **136**, 842–855. DOI:10.1002/qj.623

Waliser, D. E., Lau, K. M., Stern, W., & Jones, C. (2003). Potential predictability of the

Madden–Julian oscillation. Bull. Amer. Meteor. Soc., 84, 33–50, doi:10.1175/BAMS-84-1-33.

Wang, B. (1988a). Dynamics of Tropical Low-Frequency Waves: An Analysis of the Moist Kelvin Wave. J. Atmos. Sci., 45, 2051-2065.

Wang, B. (1988b). Comments on "An air-sea interaction model of intraseasonal oscillation in the tropics". J. Atmos. Sci., 45, 3521-3525.

Wang, B., (2012). Theory. Intraseasonal Variability in the Atmosphere-Ocean Climate System, 2nd ed., W. K. M. Lau, and D. E. Waliser, Eds., Springer, 335-398.

Wang, B., & Chen, G. (2017). A general theoretical framework for understanding essential dynamics of Madden-Julian Oscillation, Climate Dynamics. *Climate Dynamics*, *49*(7-8), pp.2309-2328.

Wang B, & Chen, J. (1989). On the zonal-scale selection and vertical structure of equatorial intraseasonal waves. Q J R Meteorol Soc 115:1301–1323

Wang, B. & Lee, S.S. (2017). MJO Propagation Shaped by Zonal Asymmetric Structures: Results from 24 GCM Simulations. *Journal of Climate*, *30*(19), pp.7933-7952.

Wang, B., Lee, S.-S., Waliser, D.E., Zhang, C., Sobel, A., Maloney, E., Li, T., Jiang, X., & Ha., K.-J. (2018). Dynamics-oriented diagnostics for the Madden-Julian Oscillation. *J. Climate, 31* (8), 3117–3135.

Wang, B., & Li, T. (1994). Convective Interaction with Boundary-Layer Dynamics in the Development of a Tropical Intraseasonal System. J. Atmos. Sci., 51, 1386-1400.

Wang, B., & Liu, F. (2011). A Model for Scale Interaction in the Madden-Julian Oscillation. *J. Atmos. Sci.*, 68, 2524-2536.

Wang, B., Liu, F. & Chen, G. (2016). A trio-interaction theory for Madden–Julian oscillation. Geosci. Lett. (2016) 3:34. DOI 10.1186/s40562-016-0066-z

Wang, B., & Rui, H. (1990a). Synoptic climatology of transient tropical intraseasonal convection anomalies: 1975-1985. *Meteor. Atmos. Phys.*, 44(1-4), 43-61.

Wang, B., & Rui, H. (1990b). Dynamics of the coupled moist Kelvin-Rossby wave on an equatorial β-plane. J Atmos Sci, 47, 397-413.

Wang, B., & Xie, X. (1997). A model for the boreal summer Intraseasonal Oscillation. *J. Atmos. Sci.*, 54, 72-86.

Wang, B., & Xie, X. (1998). Coupled Modes of the Warm Pool Climate System Part I: The

Role of Air-Sea Interaction in Maintaining Madden-Julian Oscillation. *J. Climate*, 11, 2116-2135.

Wang, W., & Schlesinger, M. E. (1999). The dependence on convective parameterization of the tropical intraseasonal oscillation simulated by the UIUC 11-layer atmospheric GCM, J. Clim., 12, 1423–1457.

Wedi, N. P., & Smolarkiewicz, P. K. (2010). A nonlinear perspective on the dynamics of the MJO: Idealized large-eddy simulations. J. Atmos. Sci., 67, 1202–1217.

Wheeler, M. C., & Hendon, H. H. (2004). An All-Season Real-Time Multivariate MJO Index: Development of an Index for Monitoring and Prediction. Mon Weather Rev, 132, 1917-1932.

Wheeler. M. & Kiladis, G. N. (1999). Convectively Coupled Equatorial Waves: Analysis of Clouds and Temperature in the Wavenumber-Frequency Domain. J. Atmos. Sci., 56:37-399.

Wolding, B. O., & Maloney, E. D. (2015). Objective Diagnostics and the Madden-Julian Oscillation. Part II: Application to Moist Static Energy and Moisture Budgets. J. Climate, 28 (19), 7786-7808,

Wolding, B.O., Maloney, E.D. & Branson, M. (2016). Vertically resolved weak temperature gradient analysis of the Madden-Julian Oscillation in SP-CESM. *Journal of Advances in Modeling Earth Systems*, *8*(4), pp.1586-1619.

Wolding, B. O., E. D. Maloney, S. Henderson, & M. Branson (2017). Climate change and the Madden-Julian Oscillation: A vertically resolved weak temperature gradient analysis, J. Adv. Model. Earth Syst., 9, doi:10.1002/2016MS000843.

Woolnough, S. J, Slingo, J. M., & Hoskins, B. J. (2001). The organization of tropical convection by intraseasonal sea surface temperature anomalies. Quart. J. Roy. Meteor. Soc., 127, 887–908.

Yamagata, T., & Hayashi, Y. (1984). A simple diagnostic model for the 30–50 day oscillation in the tropics, J. Meteorol. Soc. Jpn., 62, 709–717.

Yanai, M., Esbensen, S., & Chu, J.-H. (1973). Determination of bulk properties of tropical cloud clusters from large-scale heat and moisture budgets. J. Atmos. Sci., 30, 611–627.

Yang, D. (2018a). Boundary layer diabatic processes, the virtual effect, and convective self-aggregation. *Journal of Advances in Modeling Earth*

Systems, 10, 2163 - 2176.

Yang, D. (2018b). Boundary Layer Height and Buoyancy Determine the Horizontal Scale of Convective Self-Aggregation. *Journal of Atmospheric Sciences*, 75, 469–478.

Yang, D. (2019). Convective Heating Leads to Self-Aggregation by Generating Available Potential Energy. *Geophysical Research Letters.* doi: 10.1029/2019GL083805

Yang, D. (2020). A Shallow Water Model for Convective Self-Aggregation. EarthArXiv. Submitted.

Yang, D., Adame, A., Zhang, C., Wang, B., & Khouider, B. (2020). A Review of MJO Theories. In *The Multi-Scale Global Monsoon System*, C.-P. Chang (ed.), World Scientific Publishing Company. Accepted.

Yang, D., & Ingersoll, A. P. (2011). Testing the Hypothesis that the MJO is a Mixed Rossby–Gravity Wave Packet. *Journal of Atmospheric Sciences*, 68, 226–239.

Yang, D., & Ingersoll, A. P. (2013). Triggered convection, gravity waves, and the MJO: A shallow-water model. *J. Atmos. Sci.*, **70**, 2476–2486.

Yang, D., & Ingersoll, A. P. (2014). A Theory of the MJO Horizontal Scale. Geophys. Res. Lett., 41, doi:10.1002/2013GL058542.

Yang, D. and S.D. Seidel, 2020: The Incredible Lightness of Water Vapor. J. Climate, 33, 2841–2851.

Yang, Y.-M., B. Wang (2018). Improving MJO simulation by enhancing the interaction between boundary layer convergence and lower tropospheric heating. *Climate Dyn.*, doi.org/10.1007/s00382-018-4407-9.

Yano, J.I. & Tribbia, J.J. (2017). Tropical Atmospheric Madden–Julian Oscillation: A Strongly Nonlinear Free Solitary Rossby Wave? *Journal of the Atmospheric Sciences*, *74*(10), pp.3473-3489.

Yoneyama, K., Zhang, C., & Long, C. N. (2013). Tracking pulses of the Madden-Julian oscillation. Bull. Amer. Meteor. Soc., 94, 1871-1891.

Yoo, C., & Son, S. W. (2016). Modulation of the boreal wintertime Madden-Julian oscillation by the stratospheric quasi-biennial oscillation. Geophysical Research Letters, 43, 1392–1398. https://doi.org/10.1002/2016GL067762

Yu, J.-Y., & Neelin, J. D. (1994). Modes of tropical variability under convective

adjustment and the Madden-Julian Oscillation. Part II: Numerical results, J. Atmos. Sci., 51, 1895– 1914.

Zhang, C. (1996). Atmospheric intraseasonal variability at the surface in the western Pacific Ocean, J. Atmos. Sci., 53, 739– 785.

Zhang, C. (2005). Madden-Julian Oscillation. *Rev. of Geophysics*, 43, RG2003, doi:10.1029/2004RG000158, 2005

Zhang C. (2013). Madden–Julian oscillation: bridging Weather and Climate. Bull. Am. Meteorol. Soc. 94:1849–1870.

Zhang, C. & Dong, M., (2004). Seasonality in the Madden–Julian oscillation. *Journal of climate*, *17*(16), pp.3169-3180.

Zhang, C, Dong, M., Gualdi, S., Hendon, H. H., Maloney, E. D., Marshall, A., Sperber, K. R., & Wang, W. (2006). Simulations of the Madden-Julian Oscillation in Four Pairs of Coupled and Uncoupled Global Models. *Climate Dynamics*, 27, 573-592. DOI: 10.1007/s00382-006-0148-2.

Zhang, C. & Ling, J. (2017). Barrier Effect of the Indo-Pacific Maritime Continent on the MJO: Perspectives from Tracking MJO Precipitation. *J. Climate*, 30, 3439-3459.

Zhang, C., & McPhaden, M. J. (2000), Intraseasonal surface cooling in the equatorial western Pacific, J. Clim., 13, 2261– 2276.

Zhang, C. & Zhang, B. (2018). QBO-MJO Connection. *Journal of Geophysical Research: Atmospheres*, *123*(6), pp.2957-2967.

Zhu, H., & Hendon, H. (2015). Role of large scale moisture advection for simulation of the MJO with increased entrainment. Quart. J. Roy. Meteor. Soc., doi:10.1002/qj.2510.

Zuluaga, M.D., & Houze, Jr., R.A. (2013). Evolution of the Population of Precipitating Convective Systems over the Equatorial Indian Ocean in Active Phases of the Madden–Julian Oscillation. *Journal of the Atmospheric Sciences*, 70, 2713-2725.

Figure Captions

Figure 1 Schematic representation of the concept of wave activities. The dotted line represents the wave activity amplitude or large-scale convective envelope embedding synoptic- and meso-scale convective systems (cloud symbols) with their up- and down-drafts (thin arrows). Thick arrows represent corresponding large-scale circulations. The solid (thick) line represents the lower-tropospheric moisture which is set to oscillate against the wave activity. The hollow arrow on top indicates the direction of wave propagation on a space-time plane.

Figure 2 Low-frequency linear modes of the MJO skeleton theory. Phase speed (a) and frequency (e) plots, structure of the MJO mode (b and c) and the moist Rossby wave (f and g), bar diagrams showing the relative contribution of each one of variables (K, R, Q, A, see Eq. 4.2) in the MJO (d) and the moist Rossby modes (h). Circles in (a) and (e) mark the k=4 Rossby wave shown in (f) and (g) and k=1 MJO shown in (b) and (c). Shading in panels (b), (c), (f), (g) is the wave activity. Contours are for pressure in (b) and (f) and lower-tropospheric moisture in c and g. Notice the different zonal scales in (b), (c), (f) and (g). Adopted from *Majda and Stechmann* [2011].

Figure 3 Time-longitude diagrams from nonlinear simulations of the MJO skeleton theory in a uniform background. (a) Wavenumber 2 MJO initial condition resulting in a negative group velocity and (b) combination of wavenumber 1 and 2 MJO modes initial condition resulting in a positive group velocity. Adopted from *Majda and Stechmann* [2011].

Figure 4 Time-longitude diagrams from nonlinear simulations of the MJO skeleton theory with a warm pool forcing. (a) Total heating field for the total 3600 days duration of the simulation showing regions of active and suppressed MJO within the warm pool in the center of the domain. (b) and (c) contributions from the Kelvin and Rossby wave components to the heating field after 2400 days. Adopted from *Majda and Stechmann* [2011].

Figure 5 Time-longitude diagrams of the MJO mode for cases of (a) the uniform forcing

and (b) the warm pool forcing from numerical simulations using the stochastic skeleton theory. Adopted from *Thual et al.* [2014]

Figure 6 Time-space power spectra for u, θ, q, and a in the warm pool case. The dispersion relations are highlighted with circles. Adopted from *Thual et al*. [2014]

Figure 7 Schematic describing how longwave radiative heating can destabilize an otherwise stable moist column, causing growth of the convective anomalies. In the absence of cloud-radiative interactions (top panel), vertical motions from deep convection (ω_c, blue arrows) would not import enough moisture to compensate for the loss of moisture through condensation. Thus, deep convection would act to dry the column, weakening the intraseasonal precipitation anomalies. When cloud-radiative interactions are present (lower panel), upper level clouds reduce the amount of outgoing longwave radiation, thus heating the column. This heating is balance by anomalous upward motions (ω_r, orange arrows), which imports moisture into the column. These upward motions can cause the net import of moisture to exceed the loss of moisture through condensation, and moisture mode instability ensues.

Figure 8 Schematic describing the mechanism in which the interactions between convection and radiation lead to planetary-scale selection. In a moist atmosphere, upper-tropospheric clouds expand far away from a region of precipitation (clouds with blue arrows). This region reduces the outgoing longwave radiation, effectively warming the troposphere. Upward motions (orange arrows) result in order to maintain the WTG balance. These upward motions advect moisture upward and reduce GMS, moistening the troposphere.

Figure 9 Schematic showing the structure and propagation mechanism of the MJO as interpreted by the moisture-mode theory. Regions of enhanced and suppressed column moisture (dark and light gray-shaded ovals in the plate, respectively) are co-located with enhanced and suppressed convection (green arrows), respectively. Suppression of outgoing longwave radiation (curved arrows) acts to warm the troposphere. This warming

is balanced by enhanced vertical motion, which advects moisture upward, maintaining the region of enhanced precipitation (orange arrows). The inverse occurs in the region of suppressed convection. The anomalous heating and associated patterns of divergence lead to planetary wave responses (blue arrows). These modulate the distribution of moisture through horizontal and vertical moisture advection, as well as by modulating the surface latent heat fluxes. This modulation results in a positive moisture tendency (dash-dot line) and as such the precipitation anomalies propagate eastward.

Figure 10 Scatterplot of TRMM 3B42 Precipitation P as a function of ERA-Interim column relative humidity RH averaged over a 5 degree box centered over the equator at 95°E. The black line depicts the nonlinear least squares fit of the points in the scatterplot. The dashed yellow line shows the Taylor series linearization of the exponential fit for a reference relative humidity profile of RH = 0.74, centered on the gray circle. Blue dots correspond to active MJO conditions over the Indian Ocean (Phase 2 of the OLR MJO index, or OMI index of *Kiladis et al.* 2014), red dots correspond to suppressed MJO conditions over the Indian Ocean (Phase 6 of OMI). The large red and blue circles correspond to the centroids of the red and blue cluster of points, respectively.

Figure 11 TRMM 3B42 precipitation (colors, mm day^{-1}) and precipitation tendency (contours, interval 0.075 mm day^{-2}) for Phase 3 of OMI. The anomalies have been smoothed using a 5-point running mean to improve its presentation.

Figure 12 Frequency (top left panel), growth rate (top right), phase speed (bottom left) and group velocity (bottom right) of the moist wave solution obtained by *Adames and Kim* [2016]. The dash-dot line corresponds to the case of no dissipation, while the dashed and solid lines are the cases where the dissipation length scales are 3.6×10^7 m and 1.3×10^7 m, respectively. For these plots, $\tau = 12$ hours, AKR = 2.5×10^{-8} m^{-1}, the NGMS ($\widetilde{M}$) is 0.1, and $r_0 = 0.2$. The dotted lines correspond to a timescale of 50 days in the top-left panel, a phase speed of 5 m s^{-1} in the bottom-left panel, and a group velocity of -2 m s^{-1} in the bottom-right panel.

Figure 13 Propagation mechanism of the MJO in the gravity-wave theory. Left: Dispersion relation of inertia-gravity waves. The dashed line represents the dispersion relation symmetric about east and west: $\omega(-k) = \omega(k)$. The solid line represents the dispersion relation with an eastward tilt, as in Earth's tropical atmosphere. Middle: Standing waves when $c_W = c_E$. Right: Eastward propagating wave envelopes when $c_W < c_E$.

Figure 14 Spatial scale of the MJO in the gravity-wave theory. Left: The time-space area occupied by one convection event. The zonal scale in this plot is analogous to the mean free path of convective storms. Middle: Wavenumber one case: strong storm and fast waves. Right: Wavenumber two case: weak storm and slow waves.

Figure 15 Simulation results of the Yang-Ingersoll model (2D). Left: Time-longitude plot of zonal wind (ms^{-1}) averaged over latitudes of -15º to 15º. Black is positive, and white is negative. Right: 2D power spectrum of the symmetric component of zonal wind over latitudes of -15º to 15º. Red represents high spectral density, and blue represents low spectral density. Solid lines are dispersion curves for equatorial waves. The absolute amplitude is not relevant in this model because dynamics is linear. This figure is adopted from *Yang and Ingersoll* [2013].

Figure 16 Left: Zoomed-in time-longitude plot of geopotential (m^2s^{-2}). Black is positive, and gray is negative. Right: Zoomed-in time-longitude plot of convective heating (m^2s^{-3}). This figure is adopted from *Yang and Ingersoll* [2013).

Figure 17 Left: Propagation scaling. All markers are simulation results, and the solid lines are based on Eq. (6.3). Right: Wavenumber scaling. All markers are simulation results with different parameter values. The solid line shows the slope of 0.5 as predicted by Eq. (6.4). This figure is adopted from *Yang and Ingersoll* (2013, 2014).

Figure 18 Zonal wavenumber-frequency power spectrum estimates using CLAUS brightness temperature (Tb) for July 1983–June 2006 for the equatorially symmetric

components based on the combined Fourier wavelet transform method. (a) The strong MJO season—December, January, and February. (b) The weak MJO season—June, July, and August. This figure is reproduced from *Kikuchi* [2014].

Figure 19 Schematic diagram illustrating the most fundamental three-dimensional structure and essential physics of the MJO in the trio-interaction theory. BLMC represents boundary-layer (BL) moisture convergence, K-Low the low-pressure center of the Kelvin wave, R-Low the low-pressure centers of the Rossby wave, IO the Indian Ocean, MC the Maritime Continent, and WP the western Pacific. Thick lines with arrows represent zonal-vertical circulation of the MJO, thin lines with arrows the circulation associated with the Rossby wave, and thin straight arrows the circulation associated with the Kelvin wave. Thick hatched arrows represent vertical motions, thin hatched arrows meridional flows in the boundary layer induced by friction acting upon the easterly anomalies of the Kelvin wave. Adopted from *Wang et al.* [2016].

Figure 20 Comparison of (left panel) the growth rate (day^{-1}), and (right) frequency (cycle per day) as functions of wavenumber obtained from three theoretical models, namely, the frictional coupled K-R model (FC; black), the moisture-mode model (MF; blue), and the combined FC-MF or trio-interaction model (red). The basic state SST of 29.5^{o}C is uniform. The results from the trio-interaction theoryl with a warmer SST of 30.5^{o}C and a cooler SST of 28.5^{o}C are also shown for comparison. Adopted from *Liu and Wang* [2017].

Figure 21 MJO mode simulated using the trio-interaction theory with nonlinear B-M scheme in a varying background SST (^{o}C). (a) Idealized Indo-Pacific warm pool SST configuration. (b) Time-longitude diagram of simulated precipitation rate (mm day^{-1}) along the equator. (c) Simulated normalized low-level (700-hPa) wind (vectors), geopotential height (contours) and precipitation (shading) at day 7. (d) Observed horizontal structures of MJO during November - March, namely, regressions of 700-hPa wind (ms^{-1}, vectors), geopotential height (m, contours), as well as precipitation (mm day^{-1}, shading) with respect to the precipitation index over the eastern Indian Ocean (averaged over 5°S - 5°N; and

70°E - 90°E). (e) Simulated equatorial (averaged between 5°S and 5°N) precipitation (red), column-integrated moisture (green) and BL convergence (blue). (f) Same as (e) except for observations. The observational datasets are ERA-interim and TRMM precipitation from 1998 to 2015. Adopted from *Wang et al.* [2016]

Figure 22 Propagation speed as a function of a westerly intensity index in the trio-interaction theory with the B–M scheme (red dots) and Kuo scheme (blue dots), respectively. The westerly intensity index is defined as the ratio of the maximum MJO westerly versus the maximum MJO easterly speed averaged between 5°S and 5°N (the R-K ratio). The sizes of the dots are proportional to SST, which varies from 27.0 to 29.5 °C, with a 0.5 °C interval. Adopted from *Wang and Chen* [2017]

Figure 23 Comparison of results from the skeleton theory (section 4.4) and a frictional skeleton model [*Liu & Wang* 2012] in terms of frequency (period) as a function of wavenumber. Gray dots denote neutral skeleton mode from the skeleton theory without the BL effect. Colored circles denote unstable frictional skeleton mode derived from the frictional skeleton model. Red (Blue) colored circles denote growing (damping) modes. The diameters of the circles represent the magnitude of growth rates with maximum growth rate being 0.11 day^{-1}. Adopted from *Liu and Wang* [2012].

Figure 24 Comparison of the evolution/propagation of the simulated MJO modes using (from left to right): (a) the B-M scheme with BL dynamics, (b) B-M scheme without BL dynamics, (c) Kuo scheme without BL dynamics, and (d) Wave Activity Ensemble scheme without BL dynamics. Sequential maps of precipitation rate (color shading) and lower troposphere geopotential height (contours) are shown. All fields are normalized by their respective maxima (absolute values) at each panel. The contours start from −0.9 with an interval 0.2. The basic state SST is uniform at 29.0 °C. Adopted from *Wang et al.* [2016]

Figure 25 Comparison of horizontal structures of the MJO modes simulated by (a) the Kuo and (b) B–M scheme at day 20. All fields are normalized by their respective maxima (absolute values) at each panel. The green lines outline the region where the normalized

precipitation rate is larger than 0.1. The thin solid (dashed) contours indicate positive (negative) lower-tropospheric zonal wind speed with a contour interval of 0.2. The thick black solid line denotes zero contours. The green dot in each panel represents the location of maximum precipitation. Adopted from *Wang and Chen* [2017].

Figure 26 Eastward propagation speed as a function of SST for dry Kelvin wave (dry-K), moist Kelvin wave (moist-K), coupled Kelvin–Rossby waves in simulations using the Kuo scheme and the Betts-Miller (B-M) scheme. Adopted from *Wang and Chen* [2017]

2902

2903

2904 Table 1 Main Assumed Processes and Approximations

	Skeleton	Moisture Mode	Gravity Wave	Trio Interaction
Boussinesq approximation	√	√	√	√
Internal and first baroclinic mode	√	√	√	√
Equatorial β-plane	√	√	√	√
Linear dynamics	√	√	√	√
Hydrostatic balance	√	√	√	√
Resting basic state	√		√	√
Wave activity tendency	√			
Cloud-radiative heating		√		√
Horizontal moisture advection		√		√
Longwave approximation	√	√		√
Boundary-layer dynamics		√		√
No zonal momentum tendency		√		
Weak temperature gradient approximation		√		
Moisture tendency	√	√		√
Prescribed Rossby-Kelvin structure	√	√		
Positive only precipitation anomalies			√	√
Linear damping of momentum		√		√
Newtonian cooling		√		√
Radiative-convective equilibrium	√	√		
Large-scale envelope of convection	√			
Convective trigger			√	

2905
2906

2907
2908 Table 2 Main Parameterization and Closure Assumptions

	Skeleton	Moisture Mode	Gravity Wave	Trio Interaction
Precipitation (convective heating)	Proportional to lower-tropospheric humidity and wave activity	Proportional to column moisture	Triggered by geopotential minimum	Betts-Miller Bretherton Kuo
Cloud radiation feedback		Proportional to precipitation, decaying exponentially with zonal wavenumber		Constant or as in the moisture-mode theory
Wave Activity	Oscillating against lower-tropospheric moisture			
Moisture advection parameter A_{KR}		Sum of meridional and zonal wind moistening processes		

2909
2910

2911 Table 3 Main Parameters and Constants

	Skeleton	Moisture Mode	Gravity Wave	Trio Interaction
Convective timescale	relaxation (through Γ) (5 hrs)	Relaxation (13 hrs)	Duration of storm events (6 hrs)	Relaxation (12 hrs)
Momentum damping		0.3 day^{-1}		0.06 day^{-1}
Newtonian cooling		0.3 day^{-1}		0.12 day^{-1}
Background diabatic heating	1 K day^{-1}	2 K day^{-1}		
Background moisture vertical gradient	1.19g kg^{-1} km^{-1}	1.26g kg^{-1} km^{-1}		Exponentially decrease with a scale height of 2.2 km
number density of storms			1 per 1000 km^2 day^{-1}	

2912
2913
2914 Table 4 Explanations of the Most Fundamental Features of the MJO

	Skeleton	Moisture Mode	Gravity Wave	Trio Interaction
Selection of spatial scale	Matching observed horizontal structure; Stochastic damping of small scales in the stochastic version	Nonlocal long-wave cloud-radiative effect	Gravity-wave speed and the number density of storms	Instability generated by boundary-layer frictional convergence and damping of moisture feedback
Selection of eastward propagation	Neutral eastward propagating mode with moistening east of convection matching the observed MJO structure	Moistening to the east and drying to the west of convection	Faster EIG speed than WIG	BL moisture convergence to the east of convection, and zonal asymmetry in the Kelvin-Rossby circulation
Selection of timescale or propagation speed	Wave activity parameter Γ, background moisture gradient, and gravity-wave speed	Moisture gradients, dry static stability, convective moisture adjustment timescale	Difference between EIG and WIG speeds	Basic state moist static energy, moisture feedback, and coupling of Kelvin and Rossby waves

2915
2916

2917
2918 Table 5 Roles of different feedbacks

MJO mechanisms	BL Feedback	Moisture Feedback	K-R Wave Feedback	Cloud-Radiation Feedback	Gravity Wave Feedback	Wave-activity feedback
Planetary Scale Selection	Trio-Interaction		Skeleton	Moisture-mode	Gravity-wave	Skeleton
Eastward Propagation	Moisture-mode Trio-Interaction	Skeleton Moisture-mode	Skeleton		Gravity-wave	Skeleton
Propagation Speed	Trio-Interaction	Trio-Interaction	Trio-Interaction		Gravity-wave	
Instability	Trio-Interaction	Moisture-mode Trio-Interaction	Trio-Interaction	Moisture-mode Trio-Interaction		Stochastic skeleton

2919
2920

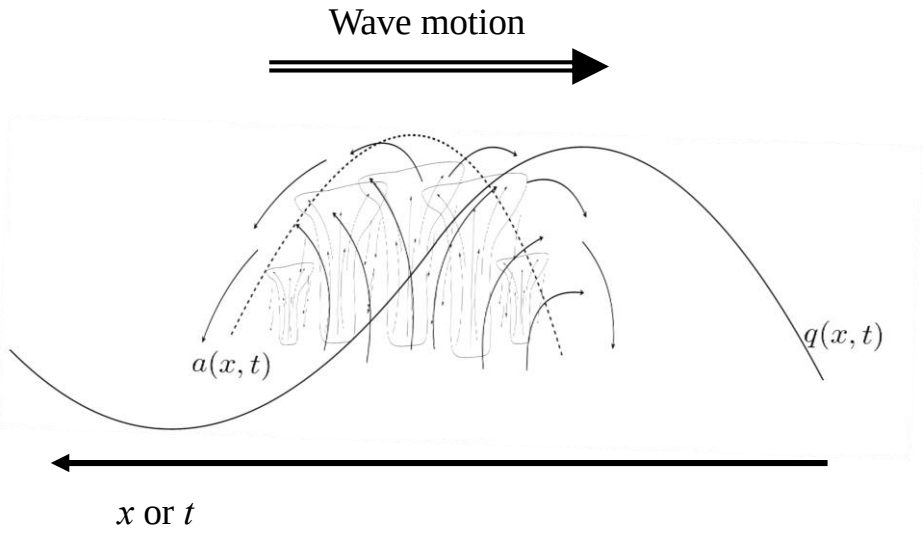

Figure 1 Schematic representation of the concept of wave activities. The dotted line represents the wave activity amplitude or large-scale convective envelope embedding synoptic- and meso-scale convective systems (cloud symbols) with their up- and down-drafts (thin arrows). Thick arrows represent corresponding large-scale circulations. The solid (thick) line represents the lower-tropospheric moisture which is set to oscillate against the wave activity. The hollow arrow on top indicates the direction of wave propagation on a space-time plane.

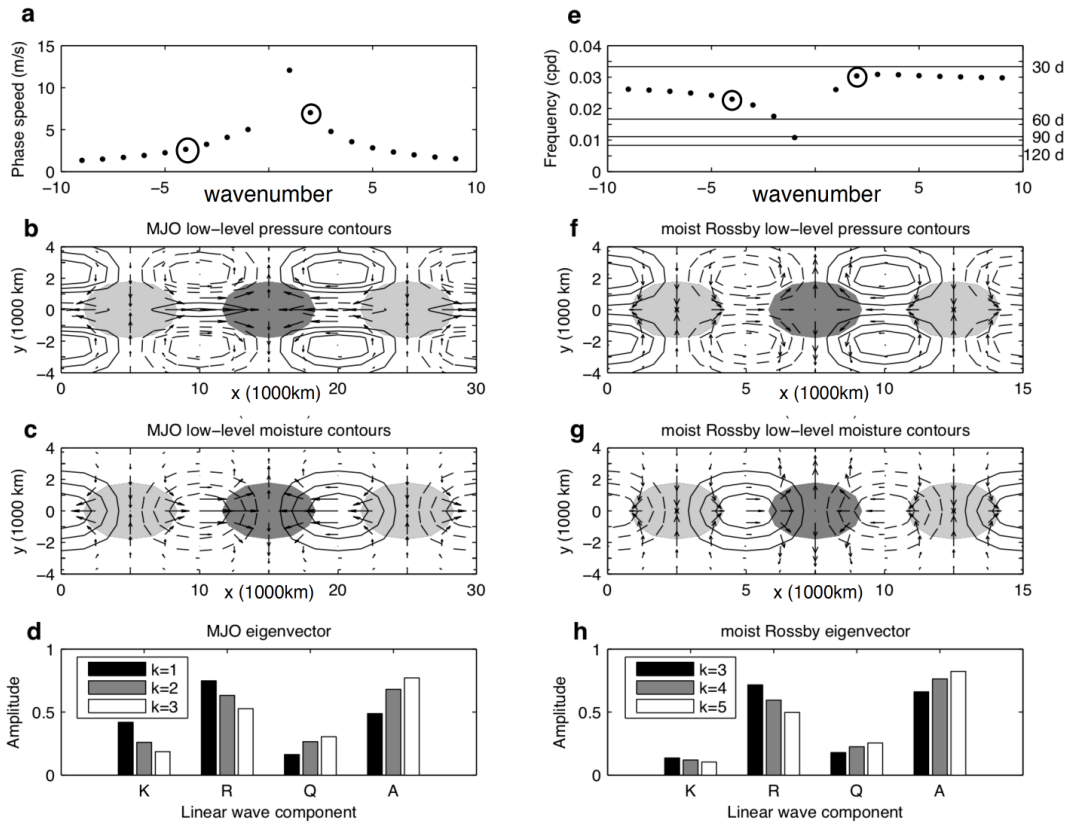

Figure 2 Low-frequency linear modes of the MJO skeleton theory. Phase speed (a) and frequency (e) plots, structure of the MJO mode (b and c) and the moist Rossby wave (f and g), bar diagrams showing the relative contribution of each one of variables (K, R, Q, A, see Eq. 4.2) in the MJO (d) and the moist Rossby modes (h). Circles in (a) and (e) mark the k=4 Rossby wave shown in (f) and (g) and k=1 MJO shown in (b) and (c). Shading in panels (b), (c), (f), (g) is the wave activity. Contours are for pressure in (b) and (f) and lower-tropospheric moisture in c and g. Notice the different zonal scales in (b), (c), (f) and (g). Adopted from *Majda and Stechmann* [2011].

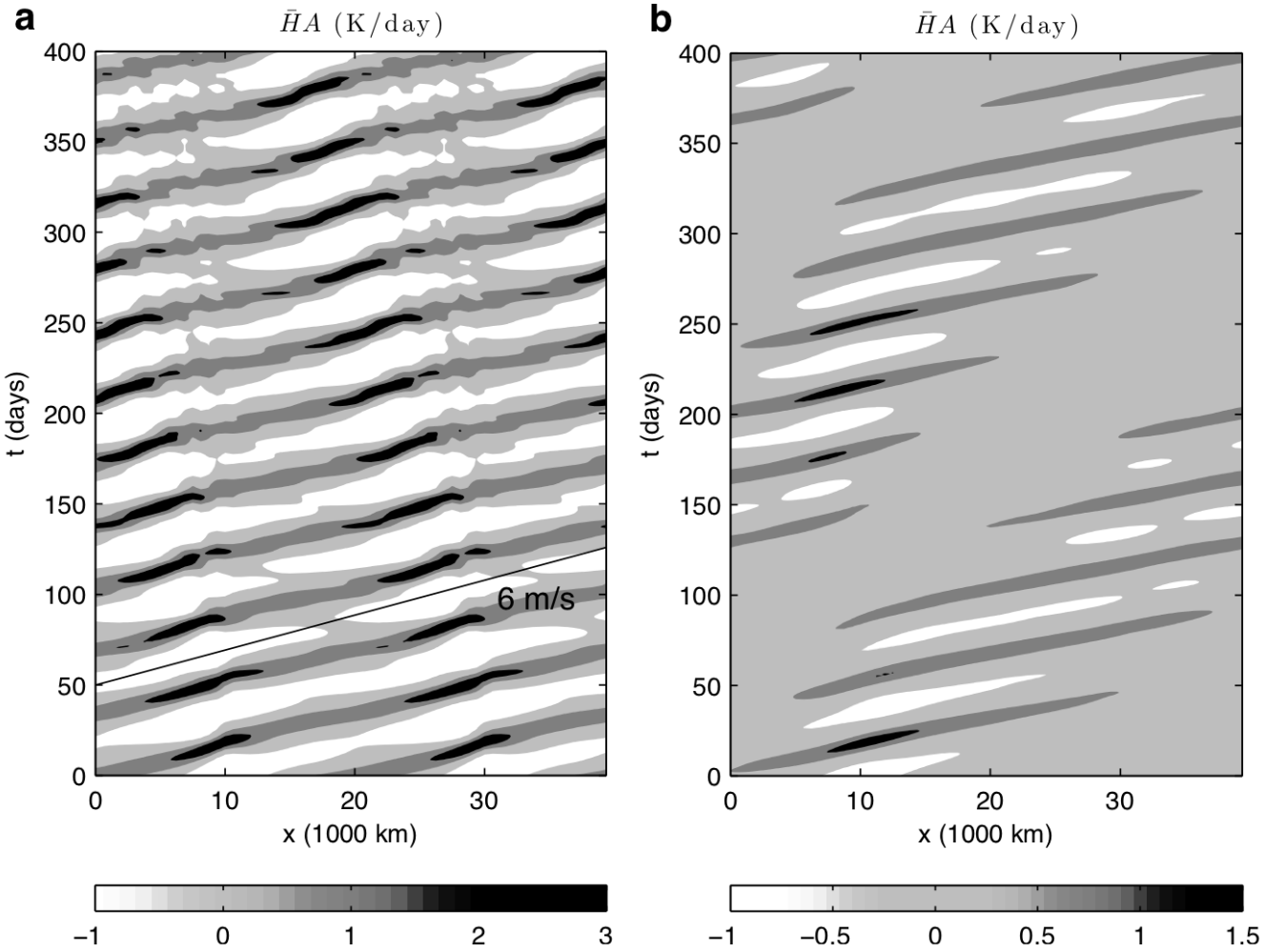

Figure 3 Time-longitude diagrams from nonlinear simulations of the MJO skeleton theory in a uniform background. (a) Wavenumber 2 MJO initial condition resulting in a negative group velocity and (b) combination of wavenumber 1 and 2 MJO modes initial condition resulting in a positive group velocity. Adopted from *Majda and Stechmann* [2011].

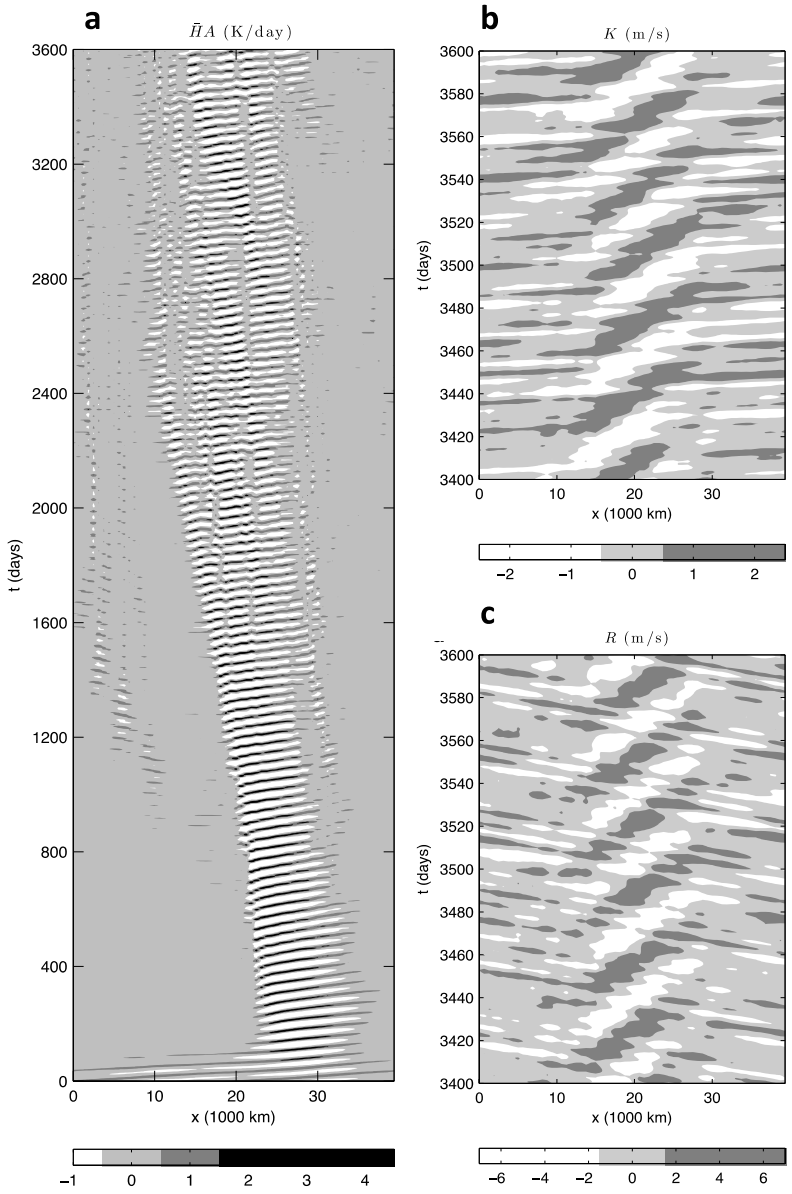

Figure 4 Time-longitude diagrams from nonlinear simulations of the MJO skeleton theory with a warm pool forcing. (a) Total heating field for the total 3600 days duration of the simulation showing regions of active and suppressed MJO within the warm pool in the center of the domain. (b) and (c) contributions from the Kelvin and Rossby wave components to the heating field after 3400 days. Adopted from *Majda and Stechmann* [2011].

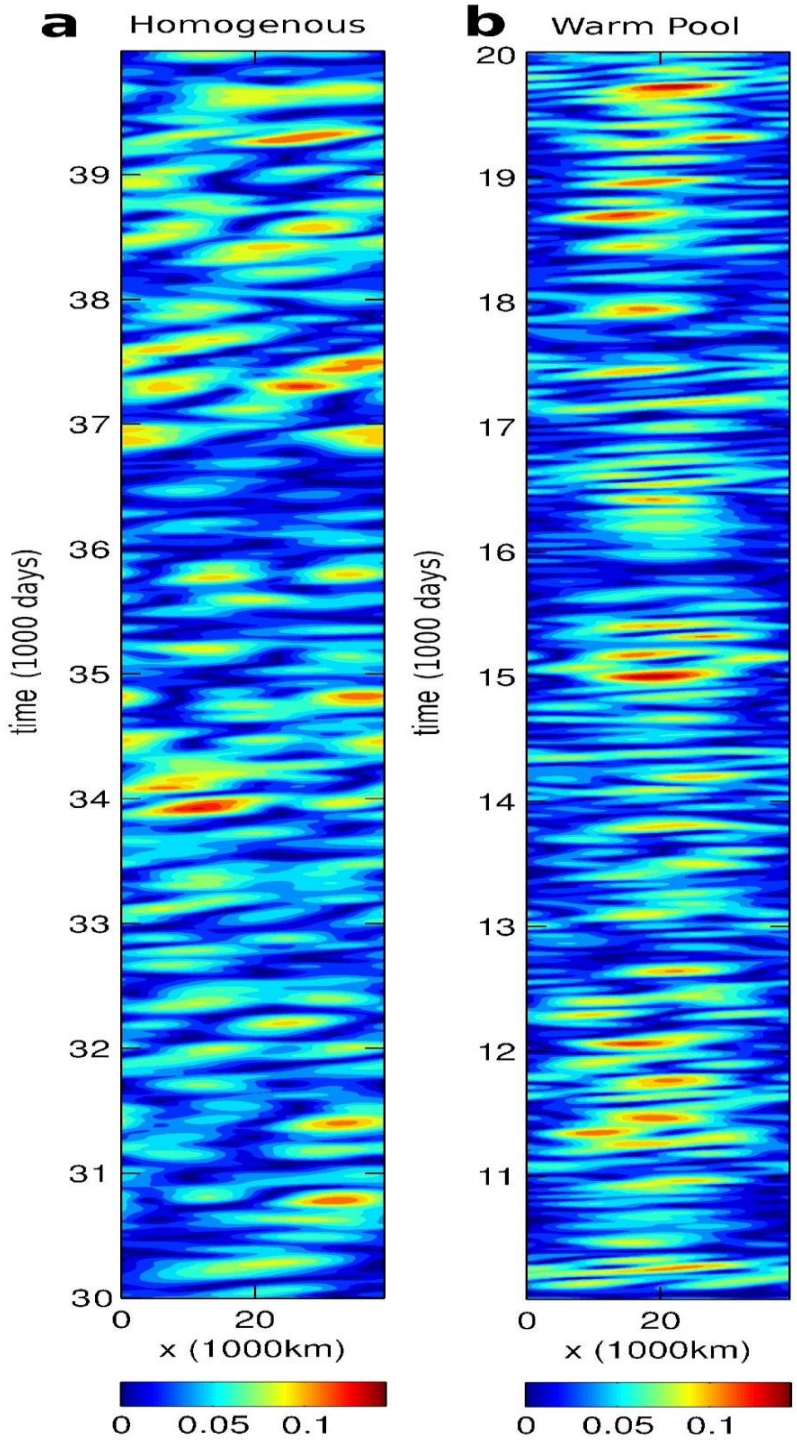

Figure 5 Time-longitude diagrams of the MJO mode for cases of (a) the uniform forcing and (b) the warm pool forcing from numerical simulations using the stochastic skeleton theory. Adopted from *Thual et al.* [2014]

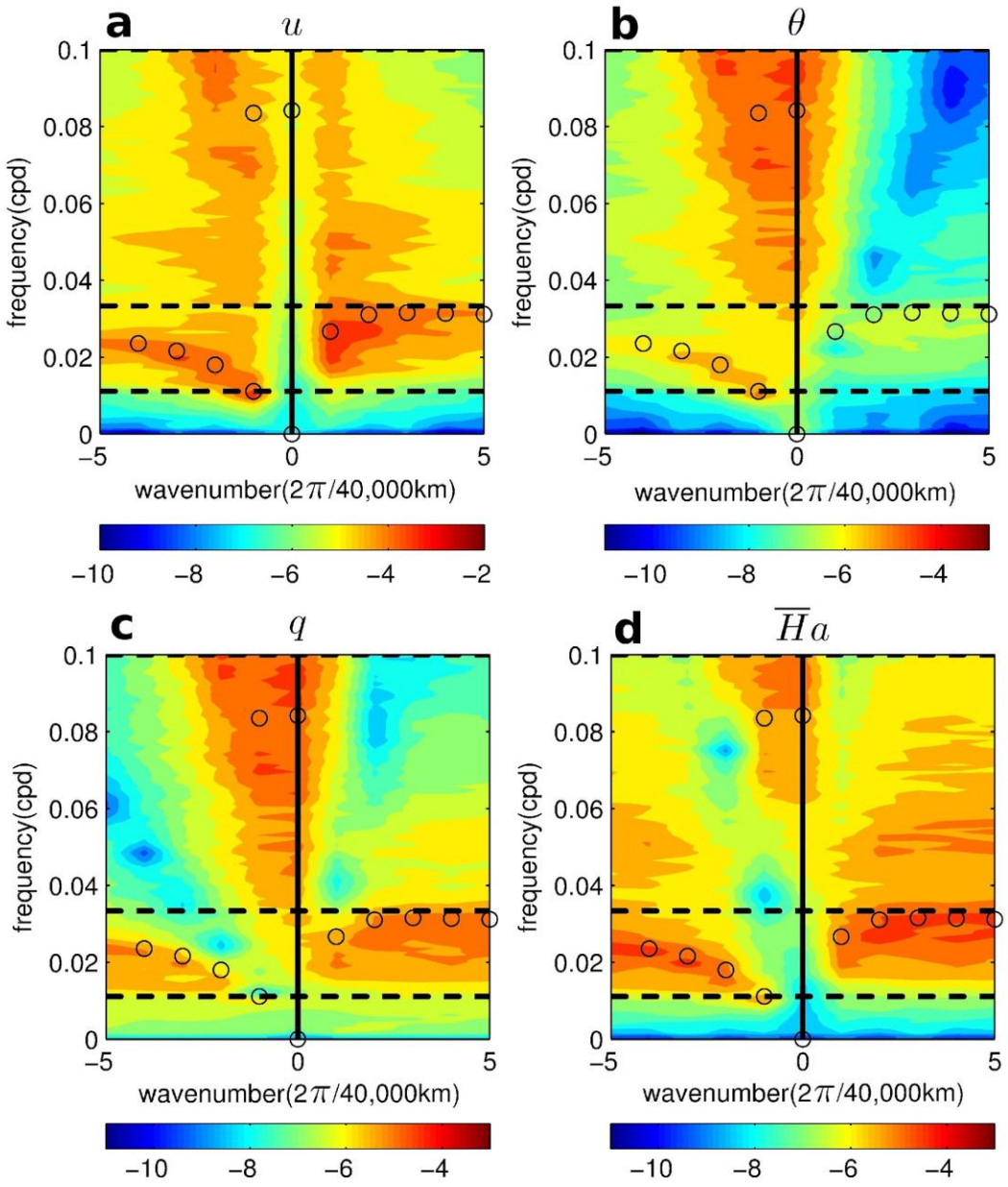

Figure 6 Time-space power spectra for u, θ, q, and a in the warm pool case. The dispersion relations are highlighted with circles. Adopted from *Thual et al*. [2014]

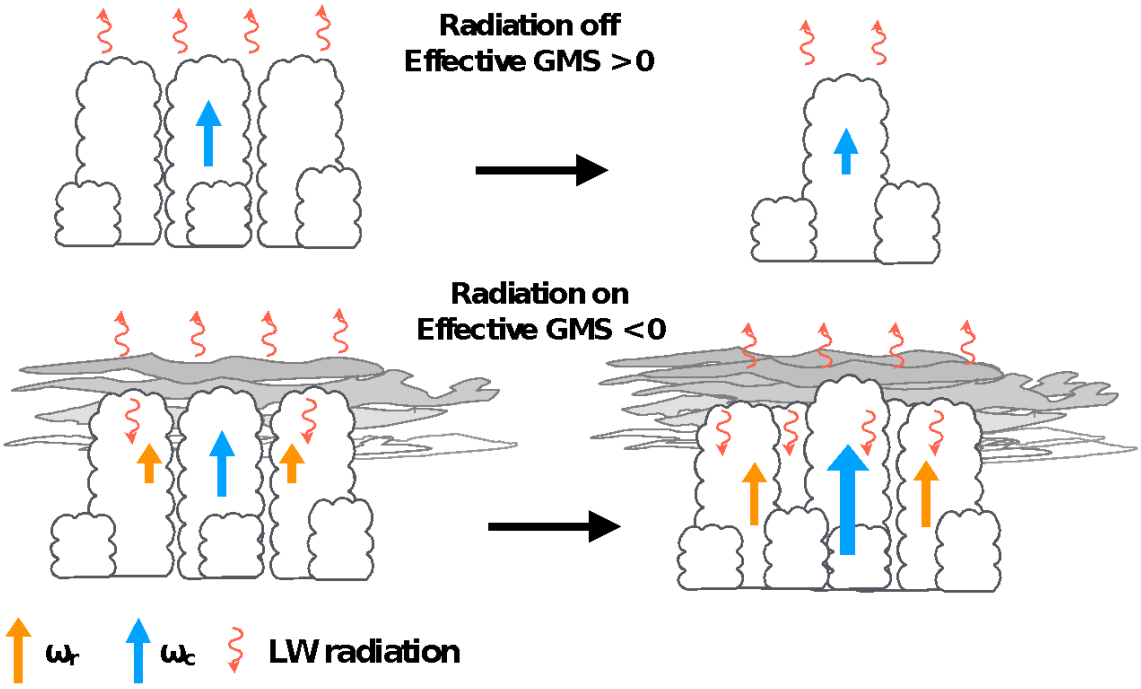

Figure 7 Schematic describing how longwave radiative heating can destabilize an otherwise stable moist column, causing growth of the convective anomalies. In the absence of cloud-radiative interactions (top panel), vertical motions from deep convection (ω_c, blue arrows) would not import enough moisture to compensate for the loss of moisture through condensation. Thus, deep convection would act to dry the column, weakening the intraseasonal precipitation anomalies. When cloud-radiative interactions are present (lower panel), upper level clouds reduce the amount of outgoing longwave radiation, thus heating the column. This heating is balance by anomalous upward motions (ω_r, orange arrows), which imports moisture into the column. These upward motions can cause the net import of moisture to exceed the loss of moisture through condensation, and moisture mode instability ensues.

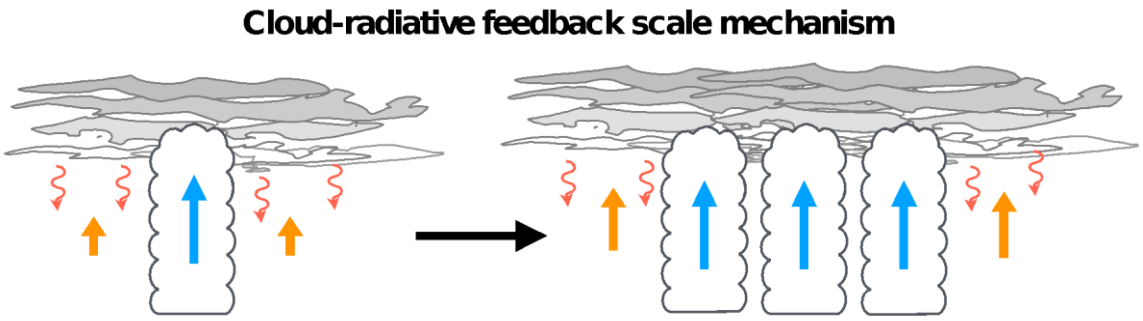

Figure 8 Schematic describing the mechanism in which the interactions between convection and radiation lead to planetary-scale selection. In a moist atmosphere, upper-tropospheric clouds expand far away from a region of precipitation (clouds with blue arrows). This region reduces the outgoing longwave radiation, effectively warming the troposphere. Upward motions (orange arrows) result in order to maintain the WTG balance. These upward motions advect moisture upward and reduce GMS, moistening the troposphere.

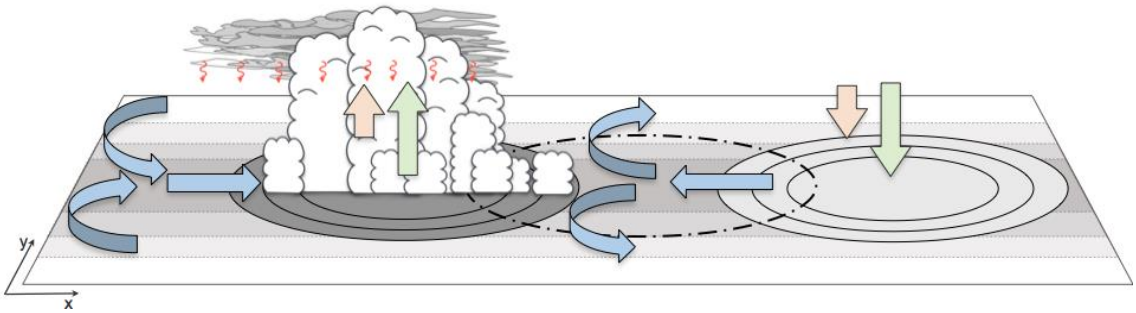

Figure 9 Schematic showing the structure and propagation mechanism of the MJO as interpreted by the moisture-mode theory. Regions of enhanced and suppressed column moisture (dark and light gray-shaded ovals in the plate, respectively) are co-located with enhanced and suppressed convection (green arrows), respectively. Suppression of outgoing longwave radiation (curved arrows) acts to warm the troposphere. This warming is balanced by enhanced vertical motion, which advects moisture upward, maintaining the region of enhanced precipitation (orange arrows). The inverse occurs in the region of suppressed convection. The anomalous heating and associated patterns of divergence lead to planetary wave responses (blue arrows). These modulate the distribution of moisture through horizontal and vertical moisture advection, as well as by modulating the surface latent heat fluxes. This modulation results in a positive moisture tendency (dash-dot line) and as such the precipitation anomalies propagate eastward.

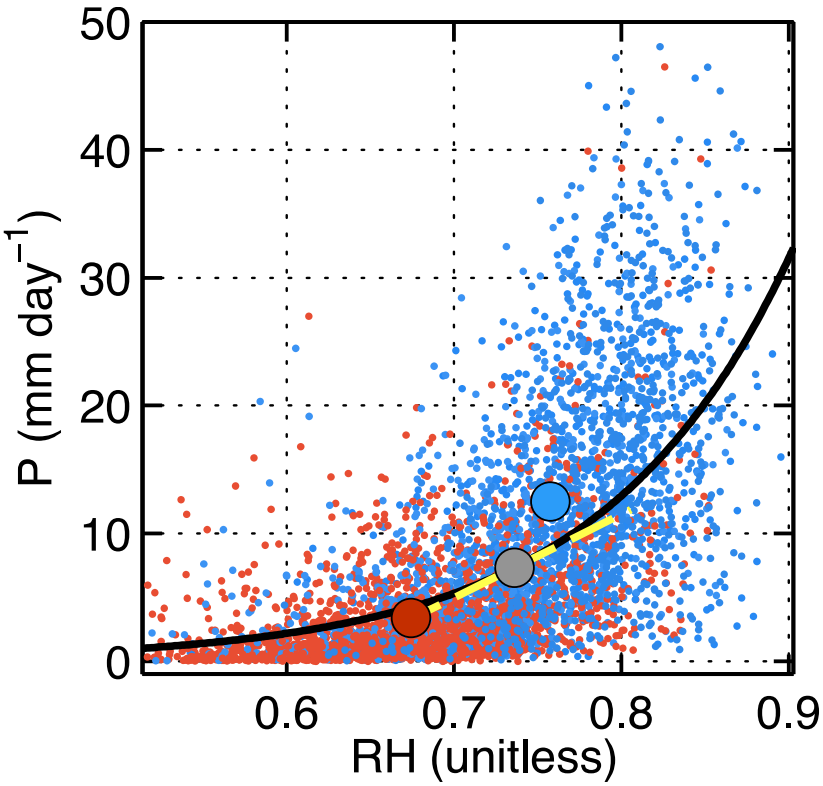

Figure 10 Scatterplot of TRMM 3B42 Precipitation P as a function of ERA-Interim column relative humidity RH averaged over a 5 degree box centered over the equator at 95°E. The black line depicts the nonlinear least squares fit of the points in the scatterplot. The dashed yellow line shows the Taylor series linearization of the exponential fit for a reference relative humidity profile of RH = 0.74, centered on the gray circle. Blue dots correspond to active MJO conditions over the Indian Ocean (Phase 2 of the OLR MJO index, or OMI index of *Kiladis et al.* 2014), red dots correspond to suppressed MJO conditions over the Indian Ocean (Phase 6 of OMI). The large red and blue circles correspond to the centroids of the red and blue cluster of points, respectively.

3049

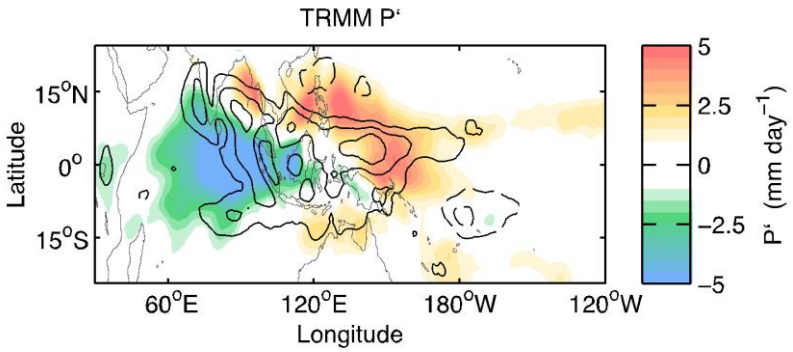

3050

3051 **Figure 11** TRMM 3B42 precipitation (colors, mm day^{-1}) and precipitation tendency
3052 (contours, interval 0.075 mm day^{-2}) for Phase 3 in the OMI of *Kiladis et al.* [2014]. The
3053 anomalies have been smoothed using a 5-point running mean to improve its presentation.

3054

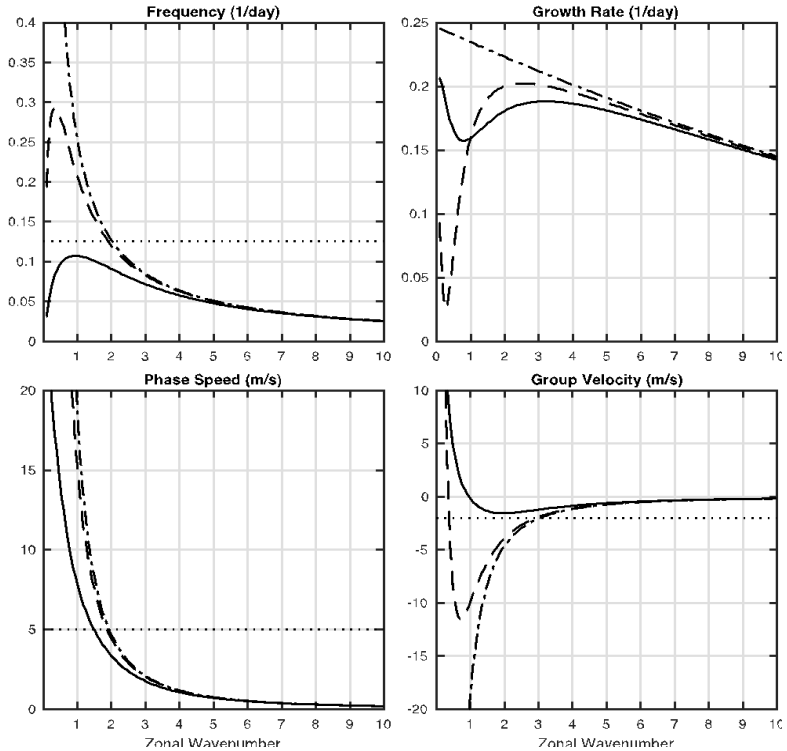

Figure 12 Frequency (top left panel), growth rate (top right), phase speed (bottom left) and group velocity (bottom right) of the moist wave solution obtained by *Adames and Kim* [2016]. The dash-dot line corresponds to the case of no dissipation, while the dashed and solid lines are the cases where the dissipation length scales are 3.6 x 10^7 m and 1.3 x 10^7 m, respectively. For these plots, τ = 12 hours, AKR = 2.5 x 10^{-8} m^{-1}, the NGMS ($\widetilde{M}$) is 0.1, and r_0= 0.2. The dotted lines correspond to a timescale of 50 days in the top-left panel, a phase speed of 5 m s^{-1} in the bottom-left panel, and a group velocity of -2 m s^{-1} in the bottom-right panel.

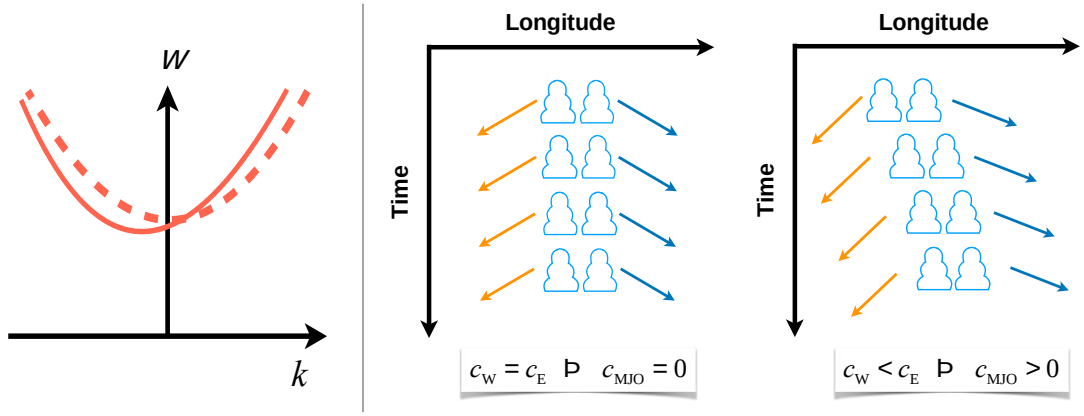

Figure 13 Propagation mechanism of the MJO in the gravity-wave theory. Left: Dispersion relation of inertia-gravity waves. The dashed line represents the dispersion relation symmetric about east and west: $\omega(-k) = \omega(k)$. The solid line represents the dispersion relation with an eastward tilt, as in Earth's tropical atmosphere. Middle: Standing waves when $c_W = c_E$. Right: Eastward propagating wave envelopes when $c_W < c_E$.

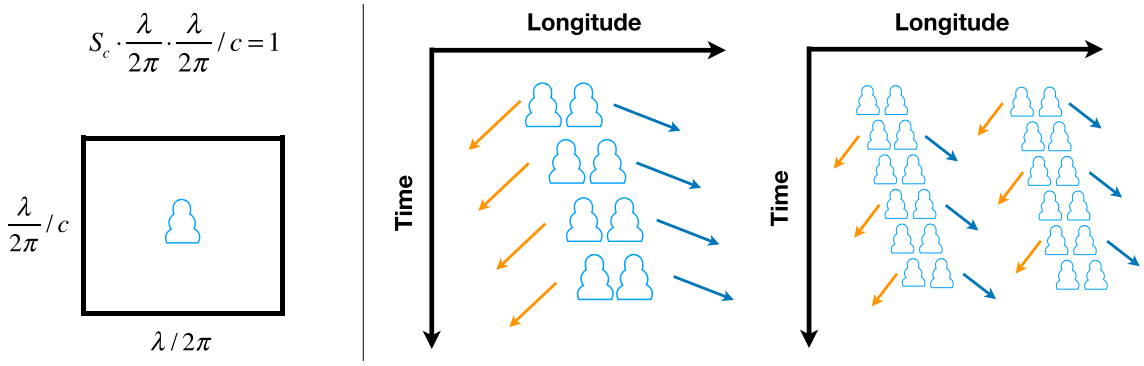

Figure 14 Spatial scale of the MJO in the gravity-wave theory. Left: The time-space area occupied by one convection event. The zonal scale in this plot is analogous to the mean free path of convective storms. Middle: Wavenumber one case: strong storm and fast waves. Right: Wavenumber two case: weak storm and slow waves.

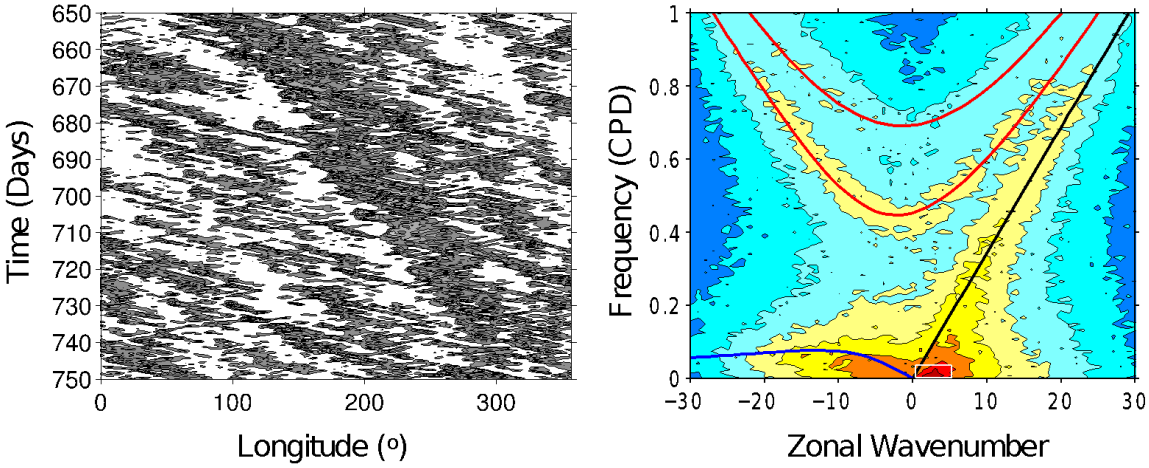

Figure 15 Simulation results of the Yang-Ingersoll model (2D). Left: Time-longitude plot of zonal wind (m/s) averaged over latitudes of -15º to 15º. Black is positive, and white is negative. Right: 2D power spectrum of the symmetric component of zonal wind over latitudes of -15º to 15º. Red represents high spectral density, and blue represents low spectral density. Solid lines are dispersion curves for equatorial waves. The absolute amplitude is not relevant in this model because dynamics is linear. This figure is adopted from *Yang and Ingersoll* [2013].

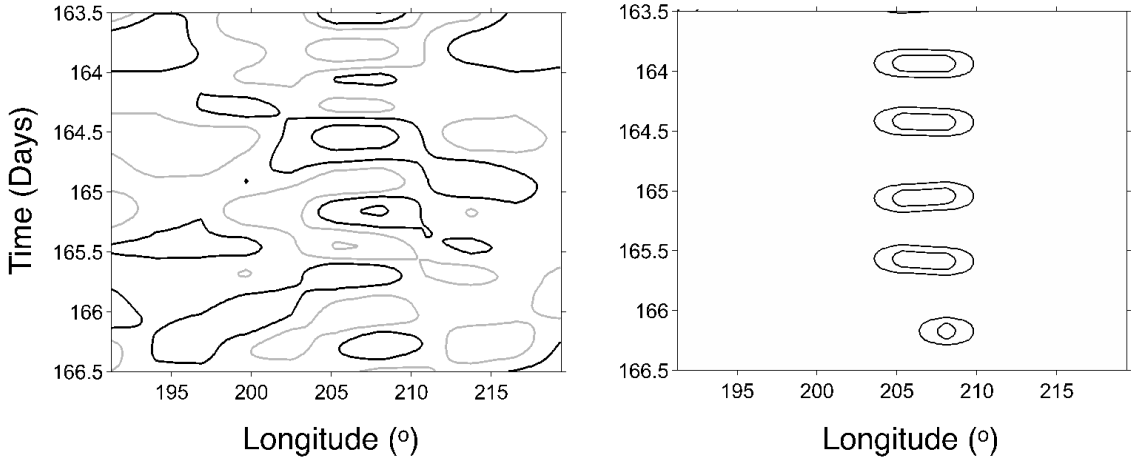

Figure 16 Left: Zoomed-in time-longitude plot of geopotential (m^2s^{-2}). Black is positive, and gray is negative. Right: Zoomed-in time-longitude plot of convective heating (m^2s^{-2}). This figure is adopted from *Yang and Ingersoll* [2013].

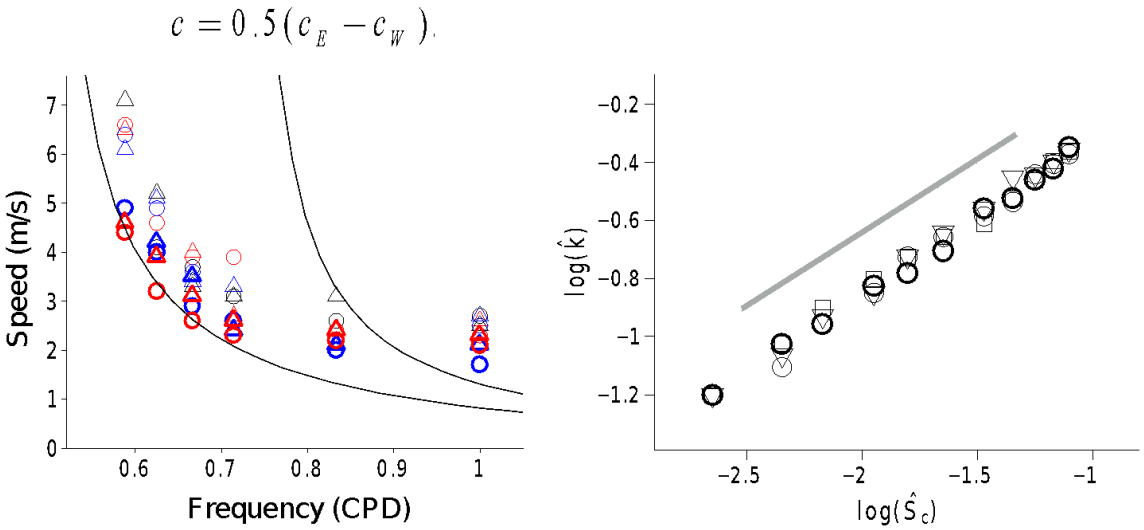

Figure 17 Left: Propagation scaling. All markers are simulation results, and the solid lines are based on Eq. (6.3). Right: Wavenumber scaling. All markers are simulation results with different parameter values. The solid line shows the slope of 0.5 as predicted by Eq. (6.4). This figure is adopted from *Yang and Ingersoll* (2013, 2014).

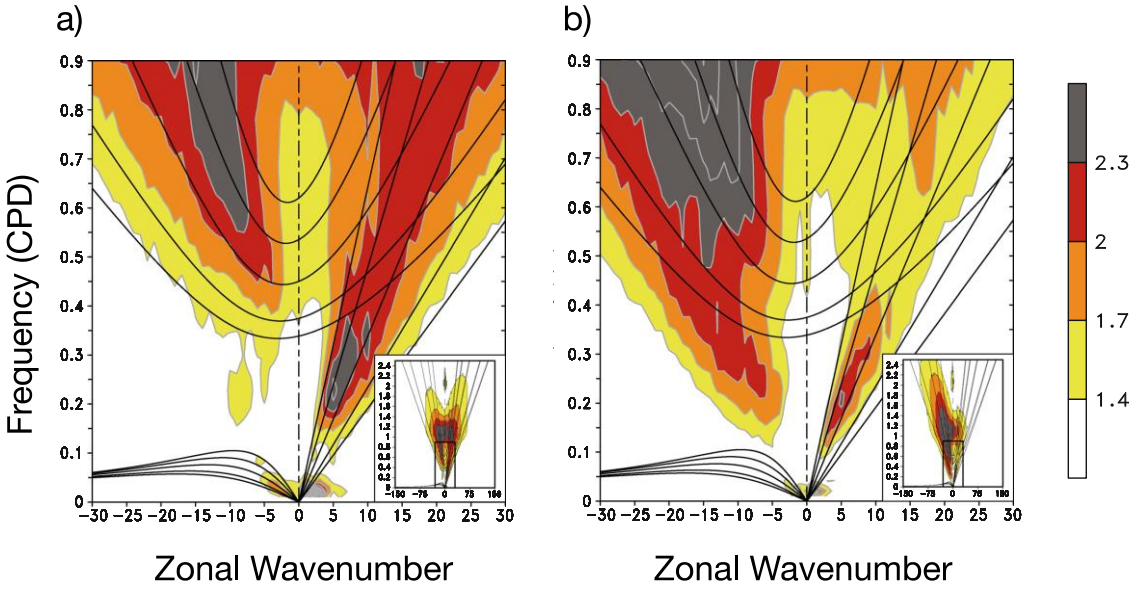

Figure 18 Zonal wavenumber-frequency power spectrum estimates using CLAUS brightness temperature (Tb) for July 1983–June 2006 for the equatorially symmetric components based on the combined Fourier wavelet transform (CFTW) method. (a) The strong MJO season—December, January, and February. (b) The weak MJO season—June, July, and August. This figure is reproduced from *Kikuchi* [2014].

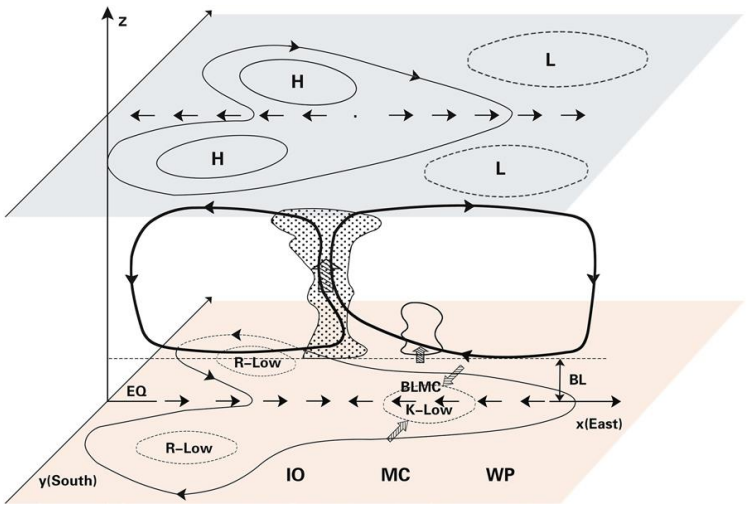

Figure 19 Schematic diagram illustrating the most fundamental three-dimensional structure and essential physics of the MJO in the trio-interaction theory. BLMC represents boundary-layer (BL) moisture convergence, K-Low the low-pressure center of the Kelvin wave, R-Low the low-pressure centers of the Rossby wave, IO the Indian Ocean, MC the Maritime Continent, and WP the western Pacific. Thick lines with arrows represent the zonal-vertical circulation of the MJO, thin lines with arrows the circulation associated with the Rossby wave, and thin straight arrows the circulation associated with the Kelvin wave. Thick hatched arrows represent vertical motions, thin hatched arrows meridional flows in the boundary layer induced by friction acting upon the easterly anomalies of the Kelvin wave. Adopted from *Wang et al.* [2016].

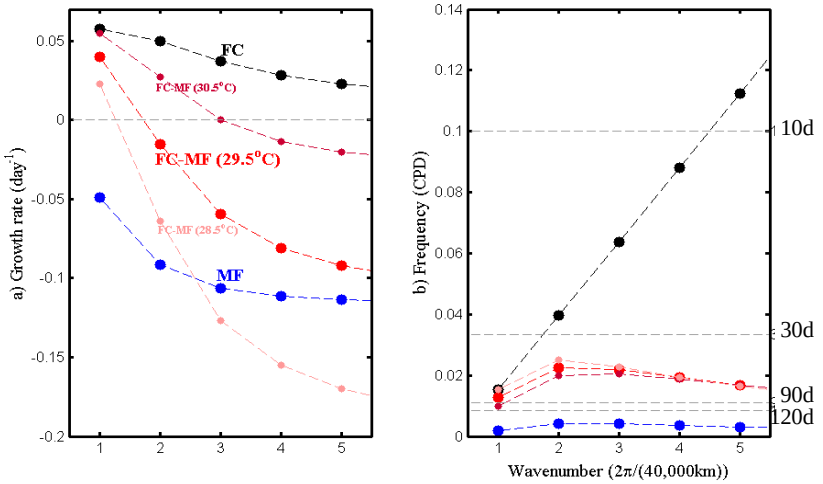

Figure 20 Comparison of (left panel) the growth rate (day^{-1}) and (right) frequency (cycle day^{-1}) as functions of wavenumber obtained from three theoretical models, namely, frictional coupled K-R model (FC; black), moisture-mode model (MF; blue), and the combined FC-MF or trio-interaction model (red). The basic state SST of 29.5^{o}C is uniform. The results from the trio-interaction theory with a warmer SST of 30.5^{o}C and a cooler SST of 28.5^{o}C are also shown for comparison. Adopted from *Liu and Wang* [2017].

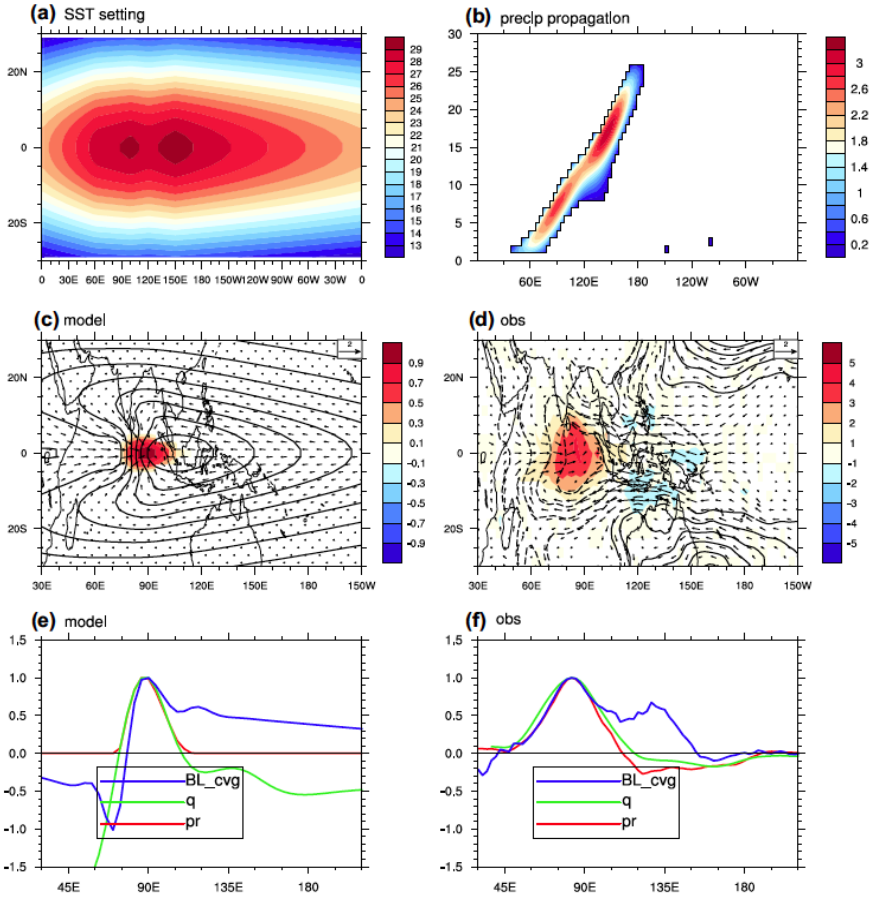

Figure 21 MJO mode simulated using the trio-interaction theory with nonlinear B-M scheme in a varying background SST (°C). (a) Idealized Indo-Pacific warm pool SST configuration. (b) Time-longitude diagram of simulated precipitation rate (mm day^{-1}) along the equator. (c) Simulated normalized low-level (700-hPa) wind (vectors), geopotential height (contours) and precipitation (shading) at day 7. (d) Observed horizontal structures of MJO during November - March, namely, regressions of 700-hPa wind (ms^{-1}, vectors), geopotential height (m, contours), as well as precipitation (mm day^{-1}, shading) with respect to the precipitation index over the eastern Indian Ocean (averaged over 5°S - 5°N; and 70°E - 90°E). (e) Simulated equatorial (averaged between 5°S and 5°N) precipitation (red), column-integrated moisture (green) and BL convergence (blue). (f) Same as (e) except for observations. The observational datasets are ERA-interim and TRMM precipitation from 1998 to 2015. Adopted from *Wang et al.* [2016]

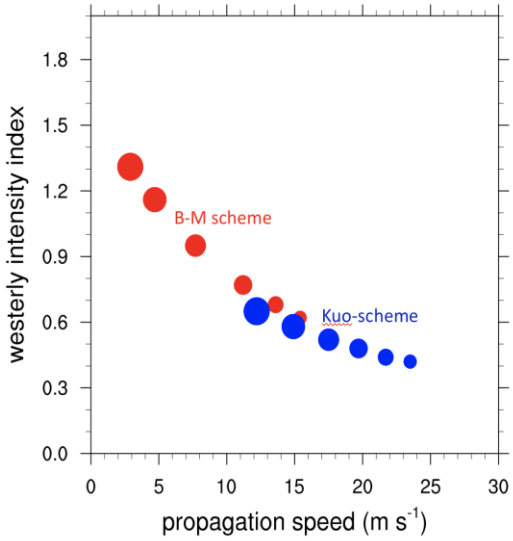

Figure 22 Propagation speed as a function of a westerly intensity index in the trio-interaction theory with the B–M scheme (red dots) and Kuo scheme (blue dots), respectively. The westerly intensity index is defined as the ratio of the maximum MJO westerly versus the maximum MJO easterly speed averaged between 5°S and 5°N (the R-K ratio). The sizes of the dots are proportional to SST, which varies from 27.0 to 29.5 °C, with a 0.5 °C interval. Adopted from *Wang and Chen* [2017]

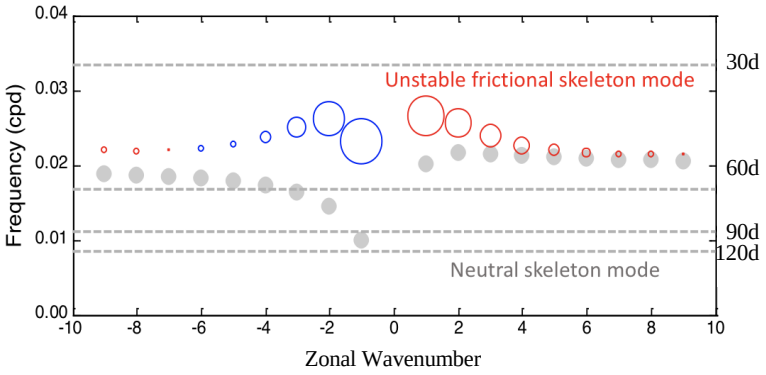

Figure 23 Comparison of results from the skeleton theory (section 4.4) and a frictional skeleton model [*Liu & Wang* 2012] in terms of frequency (period) as a function of wavenumber. Gray dots denote neutral skeleton mode from the skeleton theory without the BL effect. Colored circles denote unstable frictional skeleton mode derived from the frictional skeleton model. Red (Blue) colored circles denote growing (damping) modes. The diameters of the circles represent the magnitude of growth rates with maximum growth rate being 0.11 day^{-1}. Adopted from *Liu and Wang* [2012].

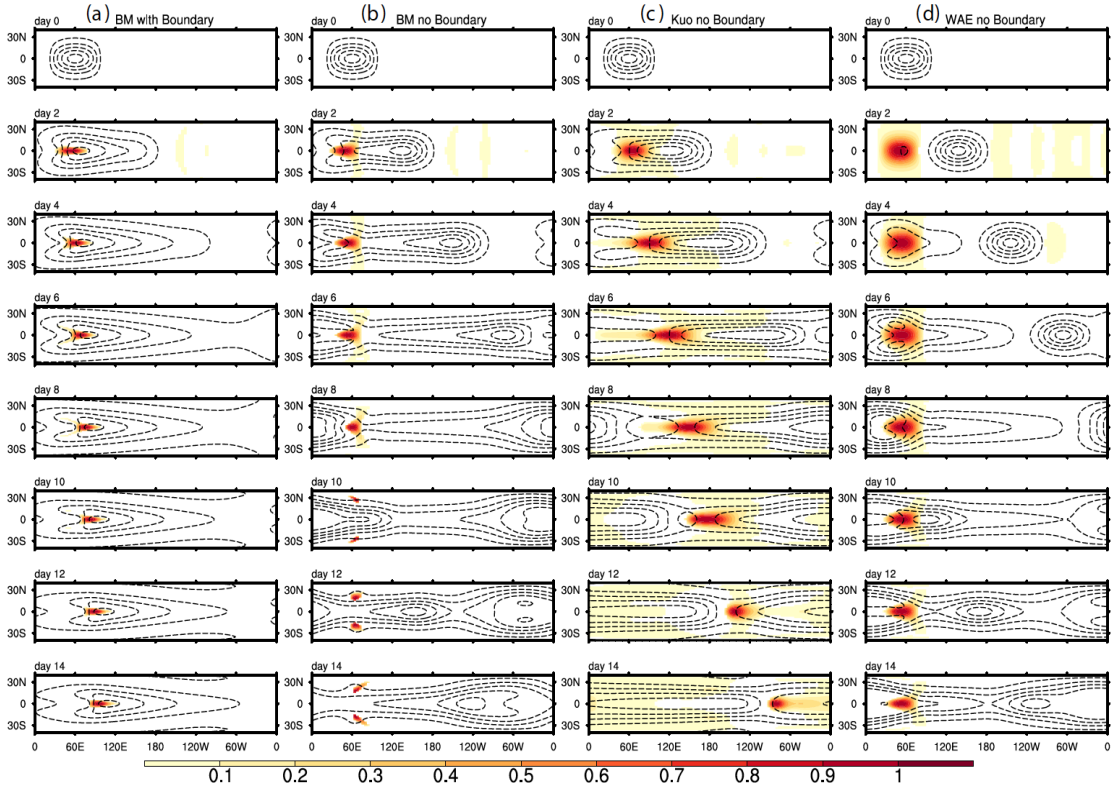

Figure 24 Comparison of the evolution/propagation of the simulated MJO modes using (from left to right): (a) the B-M scheme with BL dynamics, (b) B-M scheme without BL dynamics, (c) Kuo scheme without BL dynamics, and (d) Wave Activity Ensemble scheme without BL dynamics. Sequential maps of precipitation rate (color shading) and lower troposphere geopotential height (contours) are shown. All fields are normalized by their respective maxima (absolute values) at each panel. The contours start from −0.9 with an interval 0.2. The basic state SST is uniform at 29.0 °C. Adopted from *Wang et al.* [2016]

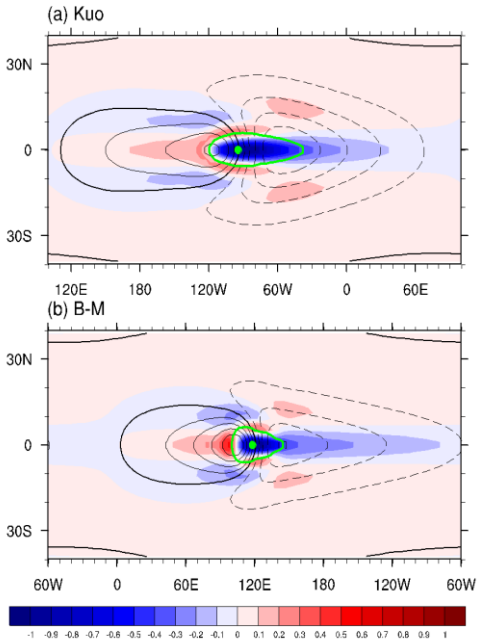

Figure 25 Comparison of horizontal structures of the MJO modes simulated by (a) the Kuo and (b) B–M scheme at day 20. All fields are normalized by their respective maxima (absolute values) at each panel. The green lines outline the region where the normalized precipitation rate is larger than 0.1. The thin solid (dashed) contours indicate positive (negative) lower-tropospheric zonal wind speed with a contour interval of 0.2. The thick black solid line denotes zero contours. The green dot in each panel represents the location of maximum precipitation. Adopted from *Wang and Chen* [2016].

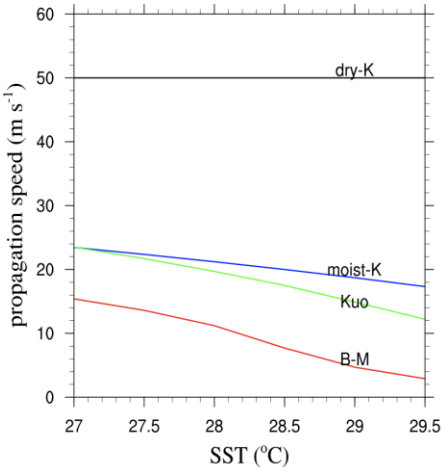

Figure 26 Eastward propagation speed as a function of SST for dry Kelvin wave (dry-K), moist Kelvin wave (moist-K), coupled Kelvin–Rossby waves in simulations using the Kuo scheme and the Betts-Miller (B-M) scheme. Adopted from *Wang and Chen* [2016]